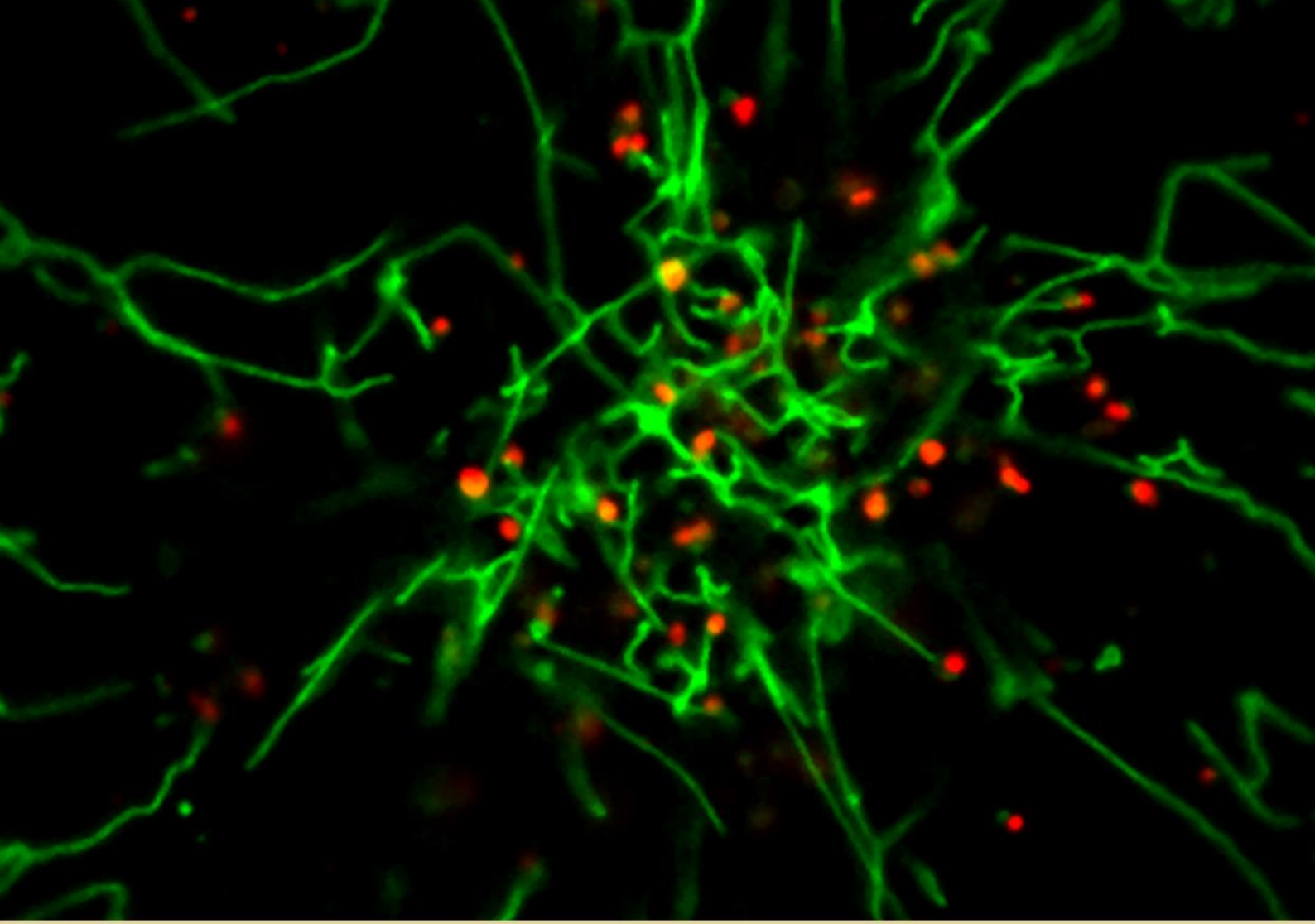

Pedro Filipe Rebelo Guiomar

(RE)DEFINING THE CONCEPT OF "PATHOGENIC MUTATION" TRANSLATIONAL ANALYSIS OF AN UNUSUAL LHON CASE

Dissertação de Mestrado na área científica de Investigação Biomédica,
apresentada à Faculdade de Medicina da Universidade de Coimbra

Junho 2014

· U C ·

Universidade de Coimbra

FMUC FACULDADE DE MEDICINA
UNIVERSIDADE DE COIMBRA

(RE)DEFINING THE CONCEPT OF "PATHOGENIC MUTATION"
TRANSLATIONAL ANALYSIS OF AN UNUSUAL LHON CASE

PEDRO GUIOMAR

Tese de mestrado em Investigação Biomédica

2014

PEDRO FILIPE REBELO GUIOMAR

(RE)DEFINING THE CONCEPT OF "PATHOGENIC MUTATION"
TRANSLATIONAL ANALYSIS OF AN UNUSUAL LHON CASE

Dissertação apresentada à Faculdade de Medicina da Universidade de Coimbra para obtenção do grau de Mestre em Investigação Biomédica.

Orientadora
Doutora Manuela Grazina, Professora Auxiliar, Faculdade de Medicina, Universidade de Coimbra.

Co-orientador
Doutor Henrique Girão, Investigador Auxiliar, Faculdade de Medicina, Universidade de Coimbra.

Pain is inevitable. Suffering is optional.

Haruki Murakami

LIST OF PUBLICATIONS / COMMUNICATIONS

Research paper:

Guiomar P, Simões M, Mendes C, Vaz M, Bacalhau M, Pratas J, Santos M J, Diogo L, Macário M C, Zuzarte M, Rego C, Vieira O, Girão H, Grazina M. Functional genomics analysis of an unusual LHON case suggests intracellular abnormal protein transport (in preparation for submission).

Posters:

Guiomar, P.; Vaz, M.; Bacalhau, M.; Mendes, C.; Simões, M.; Pratas, J.; Santos, M. J.; Silva, E.; Diogo, L.; Girão, H.; Grazina, M. Functional genomics analysis of an unusual LHON case. 5th Annual Meeting of Institute for Biomedical Imaging and Life Sciences (IBILI), Coimbra, 2013.

Guiomar, P.; Vaz, M.; Bacalhau, M.; Mendes, C.; Simões, M.; Pratas, J.; Santos, M. J.; Diogo, L.; Macário, M. C.; Silva, E.; Garcia, P.; Girão, H.; Grazina, M. Functional genomics analysis of an unusual LHON case – Preliminary Results. 10th Portuguese Metabolic Society (SPDM) International Symposium, Cascais, 2014.

FUNDING

The present work was financed by Fundação para a Ciência e a Tecnologia (FCT) – PTDC/DTP-EPI/0929/2012 (Translational Bigenomics Investigation in Leber´s Hereditary Optic Neuropathy: Genotype-Phenotype Correlation. PI – Manuela Grazina) and partially supported by the Strategic Projects PEst-C/SAU/LA0001/2013-2014 (Center for Neuroscience and Cell Biology, University of Coimbra) and by PEst-C/SAU/UI3282/2011-COMPETE (Institute for Biomedical Imaging and Life Sciences, Faculty of Medicine, University of Coimbra).

TABLE OF CONTENTS

ACKNOWLEDGEMENTS

As in biological systems, research exhibits multiple layers of complexity and hence regulation is required. In order to remain in homeostasis it is needed to control diverse processes that occur almost instantaneously. The only way to do that is to keep up with the pace and go along with the stream. So as to contemplate the catalytic activity of the intervening agents that made this work possible, I would like to thank:

- Prof. Manuela Grazina for accepting me in her laboratory as a MSc student, for her orientation, allowing me to learn new concepts and to implement new techniques.
- Prof. Henrique Girão for accepting me in his laboratory, providing materials for microscopy and western blot (PVDF membranes, α-LC3, α-p62 and secondary antibodies) and for transmitting invaluable knowledge.
- Patients and their families for the collaboration in providing samples and information for this study.
- Prof. Otília Vieira for ceding the adenoviral vector of YFP-PH used to study the Golgi apparatus and for the discussion of results.
- Prof. Cristina Rego for the discussions regarding the measurement of the mitochondrial membrane potential and ROS.
- Marta Simões and Cândida Mendes for all the learning moments, for being present in and out of the laboratory, during work hours and later, for all your support and honesty.
- LBG team for introducing me to the techniques performed in the laboratory.
- Teresa Rodrigues, Carla Marques, Tânia Marques and the G(u)IC team for all the cooperation, transference of knowledge and discussions.
- Mónica Zuzarte for the EM study and for the scientific enthusiasm.
- Ana Salomé Pires, Mafalda Laranjo and Margarida Abrantes for providing MitoTracker Green, dihydroethidium and hydrogen peroxide.
- Ana Oliveira, Luana Naia and Tatiana Rosenstock for sparing some time to deepen my practical knowledge on western blot.
- D. Virgínia Fonseca, Vera Oliveira, Susana Bacelar and D. Rosa Cardoso for their friendship and help.
- all my previous professors, for the knowledge they transmitted me, their invaluable lessons and for helping me build my knowledge.
- my family for understanding my goals and for the constant support.
- my parents for their guidance, support and wise teachings.
- everyone that contributed to this work.

ABBREVIATION INDEX

3MA	3-Methyladenine
A	Adenine
Å	Ångström
ADP	Adenosine diphosphate
AMP	Adenine monophosphate
AMPK	Adenine monophosphate kinase
ATP	Adenosine triphosphate
BN-PAGE	Blue native polyacrylamide gel electrophoresis
BSA	Bovine serum albumin
C	Cytosine
CoA	Coenzyme A
COX	Cytochrome c oxidase
CYB	Cytochrome b
Da	Dalton
DNA	Deoxyribonucleic acid
ECL	Enhanced chemiluminescence
EM	Electron microscopy
ER	Endoplasmic reticulum
F_1	Fraction 1
$FADH_2$	Flavin adenine dinucleotide
FMN	Flavin mononucleotide
F_O	Oligomycin-binding fraction
G	Guanine
HBSS	Hank's balanced salt solution
HECT	Homologous to the E6-AP Carboxyl Terminus
ICC	Immunocytochemistry
IF	Immunofluorescence
IMM	Inner mitochondrial membrane
IMS	Intermembrane space
LBG	Laboratory of Biochemical Genetics
LHON	Leber hereditary optic neuropathy
MM	Mitochondrial matrix
MRC	Mitochondrial respiratory chain
mRNA	Messenger RNA
Mrp	Multiple resistance and pH homeostasis protein
MSA	Multiple sequence alignment
mtDNA	Mitochondrial DNA
mTOR	Mammalian target of rapamycin
MTS	Mitochondrial targeting sequence
NADH	Nicotinamide adenine dinucleotide
ND	NADH dehydrogenase
nDNA	Nuclear DNA
np	Nucleotide pair
Nqo	NAD(P)H:quinone oxidoreductase
nsSNP	Non-synonymous SNP
Nuo	NADH-quinone oxidoreductase
OMM	Outer mitochondrial membrane
OSCP	Oligomycin sensibility conferring protein
OxPhos	Oxidative phosphorylation
PBS	Phosphate buffered saline
PCR	Polymerase chain reaction
PFA	Paraformaldehyde
P_i	Inorganic phosphate
PI(3)P	Phosphoinositol 3-phosphate
PI(4)P	Phosphoinositol 4-phosphate
PINK1	PTEN-induced putative kinase protein 1

PVDF	Polyvinylidene fluoride
qPCR	Real-time quantitative PCR
RBR	RING between RING fingers
RFLP	Restriction fragment length polymorphism
RING	Really Interesting New Gene
RNA	Ribonucleic acid
ROS	Reactive oxygen species
rRNA	Ribosomal RNA
S	Sievert
SDS-PAGE	Sodium dodecyl sulphate polyacrylamide gel electrophoresis
SNP	Single nucleotide polymorphism
T	Thymine
TCA	Tricarboxylic acid
TMH	Transmembrane helix
tRNA	Transference RNA
WB	Western blot
yo	Years old

ABSTRACT

Mitochondrial cytopathies are a heterogeneous group of diseases that are characterized by a primary loss of the homeostatic energetic function of the mitochondria. Leber hereditary optic neuropathy (LHON) is a mitochondrial disease resulting from the degeneration of retinal ganglion cells, and represents a major cause of blindness in young males. Besides ocular manifestations, patients may also present neurological findings, being this condition known as LHON-*plus*.

So far, three main sequence variations of the mitochondrial genome (m.11778G>A, m.3460G>A and m.14484T>C) are known to be a primary cause of LHON. These alterations cause single amino acid substitutions at the protein level, affecting three of the seven mitochondrial-encoded subunits of the mitochondrial respiratory chain complex I (ND4 p.R340H, ND1 p.A52T and ND6 p.M64V).

However, the mechanisms underlying the pathogenicity of the above mentioned mutations remain unclear, in addition to the fact that there are families where incomplete “penetrance” is observed.

In 2007, an unusual case was reported by Grazina *et al.*. A 3 years old female patient presented clinical manifestations of LHON-*plus* associated with the m.11778G>A sequence variation, homoplasmic in muscle, lymphocytes and skin-derived fibroblasts. Moreover, 72% of individuals of the maternal lineage are homoplasmic for the same genetic variation but lack the expression of the phenotype.

The aim of this study was to understand the role of the m.11778G>A sequence variation in the molecular mechanism underlying LHON. For that, skin-derived cultured fibroblasts and blood-derived lymphocytes of the aforementioned patient and her mother were studied using a translational approach, resorting to several functional assays aiming to clarify the intracellular impact produced by the presence of that sequence variation.

A preliminary *in silico* study indicated that m.11778G>A is probably a pathogenic mutation, impacting on the function and stability of the complex I subunit ND4. Quantification of the mitochondrial DNA presents reduced number values in the patient under study. Assessment of the mitochondrial respiratory chain (MRC) presented a mild decrease in the activity of complex I during the acute phase of the disease. Also, when cells were subjected to metabolic, complex I failed to maintain its activity.

Protein quantification by western blot and native electrophoresis provided insight on the assembly state of the MRC components, presenting a considerable decrease in the amount of assembled complex III in the patient and her parents’ lymphocytes, and a greater decrease in the amount of complex IV in the patient than that observed in the parents. The affected subunit ND4 was also analysed in primary skin fibroblasts, presenting a decreased quantity in the patient and her mother, compared to controls.

Fluorescence microscopy was used to evaluate the autophagy status in primary skin fibroblasts. An increase on the basal rate of protein ubiquitination was observed by the accumulation of p62 upon pharmacological inhibition of autophagy. Mitochondrial morphology was assessed using transmission electron microscopy and no major modifications were observed. Also, there was a remarkable presence of dictiosomes in the patient. Posterior study of the Golgi apparatus confirmed the abnormal morphology of this intracellular structure in the patient and time lapse imaging suggests defects on the pinching off of vesicles.

This study represents a contribution for the understanding of the role of the m.11778G>A sequence variation in the context of LHON, also providing molecular evidences that this genetic alteration may not be sufficient *per se* to cause the expression of clinical manifestations associated to LHON.

KEYWORDS

Leber Hereditary Optic Neuropathy, Mitochondrial DNA, Mitochondrial Respiratory Chain, Complex I, Functional genomics, Autophagy, Golgi apparatus.

CHAPTER 1

INTRODUCTION

1. INTRODUCTION

1.1. Mitochondria

The fact that we do not understand what we are made of is still one of the existential questions that haunts mankind. Since their discovery, cells have been in the centre of multiple questions and present us with beautiful, complex, intricate and puzzling phenomena. Regardless of the technological and state-of-art knowledge, issues that could be regarded as simple in a first analysis are still to be fully understood.

This section will present the main aspects and roles of mitochondria as an organelle and as part of a larger entity, the cell.

1.1.1. Cellular context

Cells and their organelles can be pictured as a set of reaction vessels that are interconnected and depend mutually to carry out multiple reactions that ultimately result in the execution of a mechanism or process. One of those reaction vessels, which is in turn is itself a complex set of reaction vessels, is the mitochondria, an intracellular organelle ubiquitous to most eukaryotic cells.

It is credible that the self-similarity of this idea of "cell inside a cell" is a hint on the origin of mitochondria. The endosymbiotic theory is pointed as the most probable hypothesis that describes the origin of mitochondria from ancient aerobic bacteria that were engulfed by larger cells and established a symbiotic relationship (Sagan, 1967). One of the main points of the hypothesis is based on the similarities of the mitochondrial components/machinery and that of prokaryotic organisms.

To date, mitochondria have been investigated in the context of different matters and scientific questions. Multiple works contributed to the present knowledge on this organelle and their role in the cell framework.

1.1.2. Structure

Mitochondria are eukaryotic organelles structurally and functionally segmented. The immediate segregation is imposed by the OMM which encloses and individualizes mitochondria from the cytoplasm. Inside this organelle there is another lipid membrane, the IMM which envelopes the MM, the core of the mitochondria. Both OMM and IMM define yet another segment, the IMS.

Each of the aforementioned components has specific characteristics that are responsible for the role they play in the overall mitochondrial function.

To start with, the OMM has integral proteins with aqueous channels – porins – that allow small molecules into and out of the mitochondria by facilitated diffusion. These proteins constitute a coarse selectivity filter avoiding the uncontrolled transit of large molecules (>10 kDa) between mitochondria and cytoplasm. Larger molecules, such as proteins targeted to the mitochondria, are translocated by a complex of membrane proteins that form the Translocase of the Outer Membrane (TOM). Similarly to the OMM, the IMM also has a translocase to import proteins targeted to the MM or the IMM, the Tanslocase of the Inner Membrane (TIM).

In terms of lipid composition, the OMM is similar to other cell membranes (Voet and Voet, 2011).

Unlike the OMM, the IMM has a higher protein-to-lipid ratio. Furthermore, the IMM is characterized by the presence of a special lipid; cardiolipin has a significant representation in this membrane being virtually absent in all the other membranes.

Concerning permeability, the IMM constitutes the specificity filter of the mitochondria harbouring specialized transporters. Moreover, this membrane is only permeable to O_2, CO_2 and H_2O, being impermeable, namely to ATP, ADP, Ca^{2+} and H^+. This selective impermeability to ions, metabolites and other hydrophilic low molecular weight molecules allows the generation of gradients which are partially responsible for the mitochondrial function (Voet and Voet, 2011).

The IMM also differs from the OMM in its morphology. The presence of invaginations, termed cristae, increases the surface-to-volume ratio of this membrane and it has been proposed that the

MRC complexes are located in these portions of the membrane (Gilkerson *et al.*, 2003). Cristae are pleomorphic presenting diverse morphologies ranging from simple tubular shapes to more complex lamellar structures. However, irrespective of their shape, cristae compartmentalize the IMS making the diffusion between intracristae portions less efficient than between intercristae portions; this fact has functional impacts such as the locally increased proton gradient in the former regions. These structures are highly flexible and respond to variation of the MM: cristae collapse when the matrix swells and expand as a response to matrix contraction (Mannella, 2006).

Besides being an intermediary space in terms of the communication between the MM and the cytosol, the IMS contains proteins involved both in the mitochondrial and in the overall cellular functions. Cytochrome c is an example; it functions as a soluble electron carrier of the MRC and as a vital piece in the intrinsic apoptosis pathway. The pH of this reservoir in metabolically active mitochondria is low due to the constant pumping of H^+ from the MM to the IMS by MRC complexes. However, the composition of the IMS in small molecules and ions closely resembles that of cytosol since the OMM is permeable to these components.

The MM is dense and presents high protein content. It is in this reservoir that most of the mitochondrial metabolic processes with overall cellular relevance take place (e.g. TCA cycle, β-oxidation, urea cycle). Furthermore, it is also in the matrix that processes vital to the mitochondrial homeostasis are carried out (e.g. replication of the mitochondrial genome, mtDNA transcription, mitochondrial translation).

1.1.3.Function

Mitochondria are involved in a plethora of cell processes, playing a role in diverse pathways and controlling cell homeostasis.

This section will discuss the mitochondrial function, focusing on energy supply, signalling, cytosolic buffer, metabolic regulation and thermogenesis.

Cells obtain the major part of their energy by catabolic processes; complex compounds are degraded to simpler molecules while chemical bonds are torn apart releasing energy. However, energy needs to be stored so that it can be used by the cellular machinery in the proper timing. The most common form of energy storage is the formation of the highly energetic bond between β- and γ-phosphate groups of ATP.

As efficient reactors, cells rely on tightly controlled biochemical pathways that grant homeostasis. All mechanisms are coordinated and interplay with others so that a complex equilibrium can be achieved. For instance, many catabolic pathways converge and all types of macromolecules (i.e. sugars, lipids, amino acids) are converted in intermediary metabolites that are able to integrate a common pathway – the TCA cycle.

During glycolysis, glucose is converted to pyruvate in the cytosol; this α-ketoacid enters the mitochondria where it is transformed in acetyl-CoA. Mitochondria has a set of enzymes that are able to conclude the oxidation of this compound in aerobic conditions, resulting in the reduction of the electron transporters NAD^+ and FAD^+. The reduced equivalents are then used to fuel the MRC with electrons that are transported from one protein complex to the next which has a lower reduction potential than the previous. During this process, protons are pumped from the MM to the IMS, establishing an electrochemical potential which is used to phosphorylate ADP to ATP. The energy currency is exported from the mitochondria and it is ready to be used in cellular processes.

Despite their contribution to sustaining cell viability, mitochondria are also major players in programmed cell death. The intrinsic pathway of apoptosis integrates stimuli, leading to the modification of the OMM proteome, opening pores in this membrane – mitochondrial permeability transition pore –, which allow the flow of cytochrome c from the IMS to the cytoplasm, where it interacts with other proteins to form the apoptosome, a macromolecular platform for caspase activation. Furthermore, other mitochondrial proteins are released during the process: endonuclease G (cleaves DNA) and SMAC/DIABLO (binds to IAP preventing its anti-apoptotic function).

One of the points that distinguish eukaryotic and prokaryotic cells is the existence of organelles (which are delimited by membranes) in the former species. Hydrophobic bilipid membranes isolate the content of cells in diverse aqueous compartments which present characteristic specializations both in

terms of morphology, composition and physic-chemical environment. Selective storage of compounds is one of those specializations.

Both endoplasmic reticulum and mitochondria can uptake and store calcium ions (Ca^{2+}). In mitochondria, this transient accumulation is due to the influx of Ca^{2+} through the mitochondrial calcium uniporter (MCU) and subsequent efflux via the sodium/calcium exchanger (MNCX). The release of Ca^{2+} is known to trigger signalling cascades that translate into diverse biological functions mainly as a secondary messenger.

The electrochemical gradient established across the IMM is the main motor force that drives the accumulation of cations in the negatively charged MM. The higher the cytosolic Ca^{2+} concentration, the higher the mitochondrial influx rate, and mitochondria continue to function as draining reservoirs until the original cytosolic concentration is reached. The same principle applies when the cytosolic Ca^{2+} concentration decreases below the equilibrium; in this case there is an efflux from the cellular storages in order to restore the equilibrium.

Due to the combined capacity of mitochondria to store Ca^{2+} and their preferential distribution near the nucleus, these organelles can function as protective sinks. This buffer activity avoids fluctuations of osmolarity and Ca^{2+} concentration that may compromise the integrity and function of nucleus. However, it is also important to note that the rapid uptake and slow release of Ca^{2+} also protects the cell from overstimulation of cytosolic Ca^{2+}-dependent signalling pathways. (Ryan and Hoogenraad, 2007)

The enzymatic plethora of mitochondria brings these organelles to the foreground when metabolism is taken into account.

To start with, fatty acids are processed in the mitochondria. The entry can either occur freely if the fatty acid chain has 12 or less carbon atoms; fatty acids with chains longer than 14 carbon atoms (which represent the most common fatty acids obtained through the diet and those released from adipocytes) cannot diffuse freely into mitochondria and require a previous activation by coupling with carnitine to be enzymatically transported to the interior of this organelle. Once inside the mitochondria, fatty acids undergo successive cycles of three enzymatic transformations – β-oxidation – losing two carbon atoms in each cycle as acyl-CoA, which constitutes the acyl-CoA pool together with that formed during glycolysis. Besides, reduced equivalents (i.e. $FADH_2$ and NADH) are produced.

The role of mitochondria in the cellular metabolism extends much further including, for instance, the gluconeogenesis bypass reaction, and the urea cycle.

When the cell's energetic status is fulfilled, the mechanisms that lead to energy production are slowed down. However, there are remarkable exceptions to this regulatory consensus. New-born mammals that lack fur have abundant brown adipose tissue which is responsible to produce heat from substrates arising from catabolic pathways, keeping the new-born warm – nonshivering thermogenesis. Mitochondria from this specialized adipose tissue are globally similar to that of other cells. However the capacity of producing heat is due to a simple modification. Besides being mitochondria-rich, brown adipocytes express the homodimeric uncoupler protein thermogenin (UCP1), which is targeted to the IMM. The mechanism leading to heat production uses the proton gradient formed during aerobic respiration by the MRC, bypassing the energy production process of ATP synthase (which uses the decoupling of the proton gradient to produce ATP). The energy that was stored as a H^+ concentration gradient is directly dissipated by thermogenin (which short-circuits the IMM) and is released as heat instead of being stored in chemical bonds. This scenario also occurs during hibernation; in fact, thermogenin can make up to 15% of the total proteins of mitochondria from brown adipocytes of cold-adapted animals (Voet and Voet, 2011).

1.1.4.Genetics

The discovery of the mitochondrial genome is attributed to Sylvan Nass and Margit Nass who performed electron microscopy studies finding characteristic staining patterns corresponding to DNase-sensitive fibres (Nass and Nass, 1963a; Nass and Nass, 1963b). Posterior studies led to further insights on the mtDNA organization and the machinery associated with its processing as well as its charatcteristic genetic features, which are vital to the understanding of the etiology and pathogenesis of mitochondrial diseases.

The human mitochondrial genome is structurally organized as a double stranded circular DNA molecule with 16568 bp. The strands present an asymmetry of nucleotide representativeness and thus

are differentiated according to their relative molecular weight: the L-strand (5063 kDa), from light, is pyrimidine C/A-rich while the antisense H-strand (5174 kDa), from heavy, is G/T-rich. So far, no histone-like proteins were found associated to mtDNA.

The human mitochondrial genome encodes 37 genes. These are the genes for rRNAs (2 genes), tRNAs (22 genes) and polypeptides (13 genes). All polypeptides encoded by the mtDNA are subunits of the MRC: 7 of complex I (ND1-6 and ND-4L), 1 of complex III (CYB), 3 of complex IV (COX I-III), and 2 of complex V (ATP6 and ATP8). The mammalian mitochondrial genome is devoid of introns and contains only small non-coding regions, making it very compact (Figure 1).

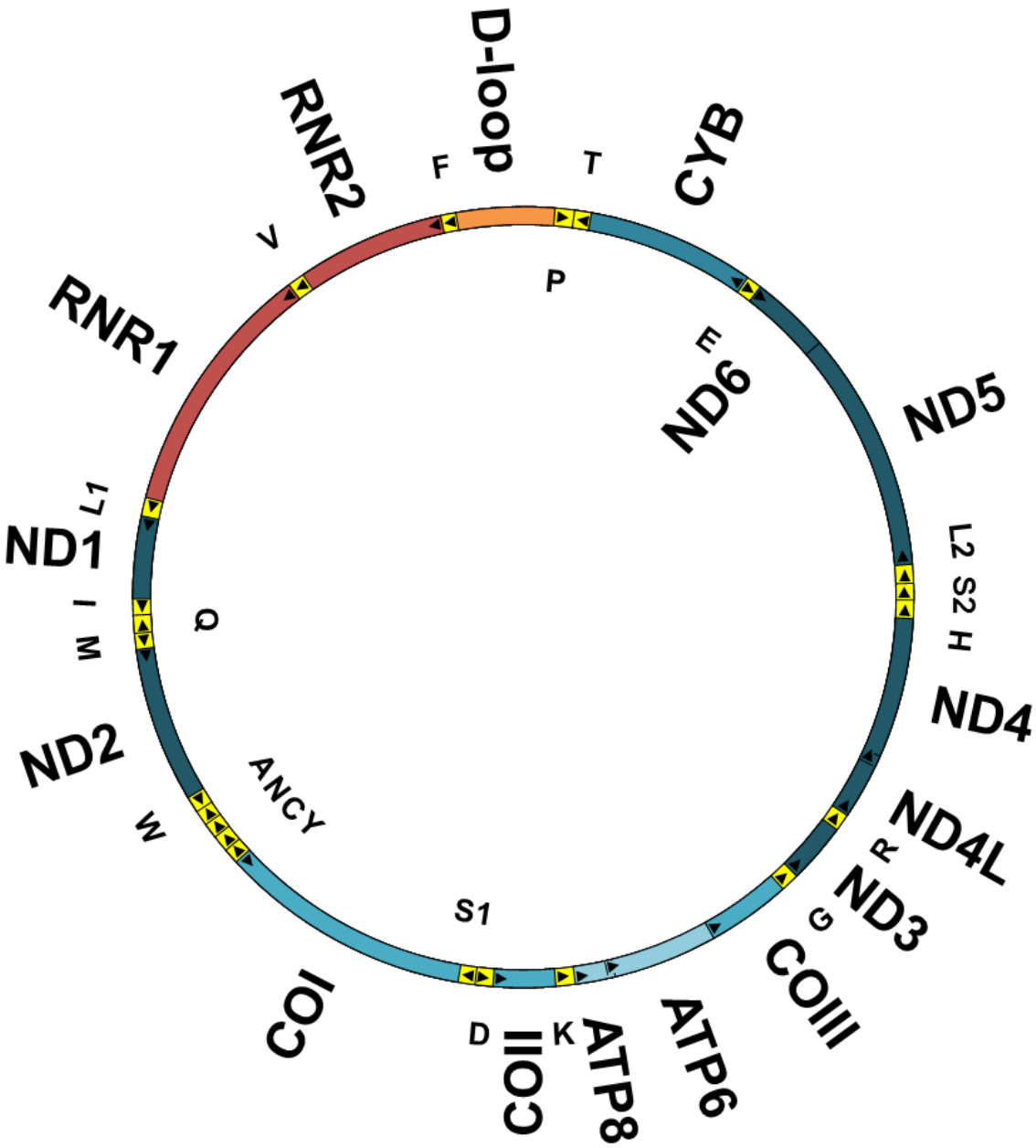

Figure 1 – The human mitochondrial genome. Scheme of the organization of the mitochondrial genome. Each colour represents different classes of genes (orange: D-loop, blue: mRNA, red: rRNA yellow: tRNA). Genes coding subunits of the different MRC complexes are coloured with the same blue hue and are presented in big capital letters. Genes coding tRNAs are represented in small capital letters. Arrowheads indicate the 5'-3' orientation of each gene. Descriptions inside the circle represent genes in which the sense orientation is in the H-strand, while those outside are located in the L-strand. Based on data from (Mitomap).

As any other cellular structure, mitochondria present an intricate and complex system of interactions with other organelles. However, due to the fact that mitochondria have their own genome, the network assumes another dimension. So, mitochondrial and overall cell homeostasis depends on the constant exchange of information and interplay between the two physically segregated genomes of the animal cell – nucleus-mitochondria crosstalk.

Multiple evidence that the nucleus and mitochondria communicate have already been reported. Probably the most striking example is that the mitochondrial proteome is almost entirely encoded by the nuclear genome (Calvo *et al.*, 2006).

The mitochondrial genome has a mutation rate approximately 10–20 times higher compared to that of the nuclear genome (Hofmann and Bauer, 2006). Diverse characteristics of the mtDNA contribute to this fact: (i) location in a region of high ROS production and oxidative damage; (ii) no protective coating histone-like proteins; (iii) very compact structure; (iv) lack of introns or large non-coding regions; (v) low efficiency of the mitochondrial DNA damage response mechanisms (which contributes to the persistence and accumulation of mutations in the mtDNA).

Since there are several mtDNA copies in each mitochondria – copy number –, the effect of the mutation of a single copy may not be expressed. As the number of altered copies in the overall pool of mtDNA molecules – heteroplasmy – increases, the probability of producing an effect on the phenotype also increases. However, in some cases, clinical manifestations correlate with the amount of altered mtDNA copies, which depends on the affected tissue and the pathogenic nature of the mutation, and first occurs upon exceeding a critical threshold level – threshold effect (Hofmann and Bauer, 2006).

Unlike the nuclear genome, mtDNA presents maternal inheritance since the only mitochondria presented in the fertilized egg are those present in the oocyte. Once a heteroplasmic mutation is inherited from the mother, or is acquired during embryogenesis, both normal and mutant copies are randomly distributed throughout mitotic divisions to the resulting cells – mitotic segregation (Hofmann and Bauer, 2006).

1.2. Mitochondrial Respiratory Chain

Energy is involved in every physicochemical process. As reduced size complex multi-segmented reactor chambers, cells also require energy and its transference between different components as work, heat and/or radiation. This fundamental entity is devoid of a material existence *per se*, but can be stored in different forms. Be it the concentration gradient of charged species across an insulating membrane or chemical bonds cells developed mechanisms to exploit diverse energy sources.

As mentioned before, mitochondria are the main location of cellular ATP synthesis from ADP and inorganic phosphate. This occurs due to the special conditions present in these organelles, as proposed by Peter Mitchell in the chemiosmotic theory (Mitchell, 2011). The major contribution of this theory was the identification of the "energy-rich" intermediates that brings the proton gradient and ATP production together. Due to this hypothesis, it is now accepted that electron transport through the MRC and ATP production by oxidative phosphorylation are coupled owing to the impermeability of the IMM which forces H^+ to re-enter the matrix via the ATP synthase, producing ATP from ADP and inorganic phosphate.

This section has the purpose to introduce the concept of MRC, to identify its components and to explain their roles in the global process of OxPhos.

1.2.1. Components

More than one thousand genes are required to maintain mitochondrial homeostasis (Pagliarini *et al.*, 2008). The proteins they encode play very diverse roles in the cellular context, from membrane channels to soluble enzymes, and from biogenic to degradation factors. As mentioned in section 1.1., mitochondria are responsible for many vital processes that must take place to keep the cells in balance with the surrounding environment. In fact, one of the major roles of mitochondria is to maintain the energetic balance.

Mitochondria contribute to the cellular energy pool by producing ATP. In order to do so, mitochondria are equipped with complex machinery that works in a concerted and tightly regulated

fashion. The central piece of mitochondrial energy production comprises five multiprotein complexes that are generally called MRC.

Those complexes are embedded in the IMM and their ultimate goal is to transform reduced equivalents (i.e. NADH, $FADH_2$) produced during catabolic processes into energy equivalents (i.e. ATP). This is achieved by two dependent mechanisms that will be discussed in the next two sections.

The origin and proper function of the MRC results from a complex balance of two information sources – the nuclear and the mitochondrial genomes. This bigenomic cross-talk is strictly necessary since approximately 85% (~70 subunits) of the subunits that compose the MRC are encoded in the nDNA while the remaining (13 subunits) are encoded in the mtDNA (Lloyd and McGeehan, 2013).

The mitochondrial-encoded subunits are highly hydrophobic and are located in the IMM within the membrane-spanning portion of the complexes. Furthermore, these subunits present a remarkable conservation throughout evolution, remaining practically unchanged from the ancient prokaryotic origins. However, the increased complexity and energetic requirements of eukaryotic cells, more specifically, mammalian cells imposed an evolutionary pressure on the MRC resulting in adaptative changes. For instance, complex III and IV present additional subunits that compose a shell surrounding the core mtDNA-encoded subunits, protecting them from chemical damage (e.g. oxidation) while imprinting a regulatory function over these complexes' catalytic function.

Complex I is the largest component of the MRC. It uses the reductive power of NADH to pump H^+ from the MM to the IMS while reducing ubiquinone, a membrane-soluble mobile electron transporter. Due to certain technical constraints, it was not possible to obtain an atomic resolution structure of the mammalian complex I. However, Sazanov and collaborators were successful in producing the crystal structures of the prokaryotic complex I from *Thermus thermophilus* (Baradaran *et al.*, 2013). Regarding the mammalian complex I, cryo-electron microscopy has been the most used technique to determine the global architecture (Clason *et al.*, 2010). Matters regarding complex I will be further presented in section 1.3. .

Unlike the rest of the MRC components, the genetic information for complex II is solely of nuclear origin. This heterotetramer catalyses the electron transfer from succinate (via $FADH_2$) to ubiquinone, but it does not act as a H^+ pump and hence does not contribute to the chemical potential across the IMM. Even though, complex II is an important piece in the metabolic scheme since it bridges the TCA cycle and the MRC (Iverson *et al.*, 2012).

Complex III is the main integration site of MRC since it receives electrons inputted from complexes I and II, via reduced ubiquinone, and then transferred to the soluble mobile transported cytochrome c, which is located in the IMS. This complex is a dimer, each constituted by 11 subunits, one of which (cytochrome b) is encoded by the mtDNA. Cytochrome b is embedded in the IMM and is part of the core of the complex, contributing to its dimerization surface. There are two separate quinone binding sites, one for its oxidation (Q_o) and another for reduction (Q_i). Two electrons originating from the Q_o site follow distinct paths through the complex's prosthetic groups, one of which is delivered to cytochrome c, and the other to the ubiquinone bound at the Q_i site. This cycle – Q-cycle – is coupled to the H^+ pump activity of complex III, and for every ubiquinol molecule oxidized, two H^+ are pumped from the MM to the IMS. For the completion of the Q-cycle, two ubiquinol molecules need to be oxidized at Q_o, producing one ubiquinol at Q_i and pumping four H^+ (Lloyd and McGeehan, 2013).

Complex IV receives electrons from reduced cytochrome c and performs the final electron transfer, reducing molecular oxygen to water while pumping H^+. The complex is composed of 13 subunits, three of which are mtDNA-encoded and form the structural and functional central core.

Inhibitors for each MRC complex are widely known and can act as substrate mimetic compounds or stabilizing agents: rotenone binds to complex I near the ubiquinone binding site, preventing its reduction; malonate ($COO^-CH_2COO^-$) is a competitive inhibitor of complex II since it has a similar structure to the substrate of this complex, succinate ($COO^-CH_2CH_2COO^-$); antimycin A binds to the Q_i site of complex III preventing the electron flow to cytochrome c; cyanide forms a stable coordination complex with the heme groups of complex IV, displacing oxygen and preventing its reduction to water; oligomycin binds to the F_O portion of complex V preventing its rotation and thus its catalytic activity.

As an adjustable system, the MRC is also target for regulatory mechanisms. For instance, the activity of complex IV is rapidly modulated by the ADP/ATP ratio by allosteric effect. If the cytosolic ADP/ATP ratio is high, the affinity of this complex for cytochrome c increases, promoting complex IV

activity (Napiwotzki and Kadenbach, 1998). Also, ATP is able to bind to pockets in the matrix side of complex IV, inhibiting its activity (Arnold and Kadenbach, 1997).

Post-translational modifications such as phosphorylation also play an important role in regulating the activity of the MRC complexes. With the advance of highly sensitive techniques (e.g. mass spectrometry), an increasing number of mitochondrial kinases and phosphatases is being reported, suggesting that phosphorylation may be an important clue to understand the mitochondrial function as well as its regulation. Phosphorylation of subunits of complex I, III, IV and V have already been described, and it is thought that modification of certain residues of complex IV may regulate its activity by controlling its dimerization (Pagliarini and Dixon, 2006).

1.2.2.Electrochemical Potential

There are several aspects that distinguish functional and dysfunctional MRC. Although the presence of the MRC complexes and the required machinery is necessary, it is not sufficient and the correct conditions must be gathered so that the MRC can function properly.

The first crucial aspect to grant MRC function is the presence of substrates for each of the MRC complexes in the adequate compartments. First, reduced equivalents need to be present in the MM since the active site of both complexes I and II are located in this compartment. Secondly, ubiquinone is required in the IMM in order to be reduced by the aforementioned complexes (the ubiquinone binding site is immersed in this membrane) and to transport electrons to complex III. Then, the IMS needs to contain cytochrome c since the binding site for this protein in complexes III and IV is located in this compartment (Nelson and Cox, 2008; Voet and Voet, 2011). Finally, ADP and P_i are required in the MM as substrates for complex V. The ANT (adenine nucleotide translocator) exports ATP from the MM and imports ADP to the MM and the mitochondrial phosphate carrier catalyses the symport of P_i and H^+ into the MM, taking advantage of pH gradient.

Since reduced equivalents cannot pass through the mitochondrial membranes, due to being polar molecules and the lack of specific transporters, there are mechanisms that enable the formation of these species in the MM (e.g. TCA cycle, malate shuttle).

By sequential redox reactions, electrons from reduced equivalents flow through the MRC complexes to the final acceptor, molecular oxygen. This involves conformational changes which lead to the transmission of those electrons to the next acceptor and the transport of H^+ from the MM to the IMS. Complexes I, III and IV contribute to the establishment of the electrochemical gradient across the IMM due to their H^+-pumping activity, which decreases the concentration of this species in the MM, increasing it in the IMS. Since the IMM is impermeable to H^+, the concentration differential is endogenously dissipated by complex V, the mitochondrial phosphate carrier, or thermogenin.

Since a charged species is being selectively segregated in different compartments, two main effects arise: (i) the H^+ is in the basis of the definition of acidity and its segregation originates differences in the pH of those compartments; (ii) since H^+ bears a positive electrical charge, there will also be different charge distribution between the compartments. Therefore, the electrochemical potential can be artificially segregated in pH differential (ΔpH) and membrane potential ($\Delta\Psi_m$).

The establishment of the electrochemical potential is a means to transform energy contained in reduced equivalents so that it can also be used as an energy source/motive force for cellular processes other than OxPhos (e.g. Ca^{2+} transport, ATP/ADP exchange, P_i transport, protein import) (Lloyd and McGeehan, 2013).

1.2.3.Oxidative Phosphorylation

The energy stored as the electrochemical potential is released by dissipating the electrochemical gradient. This may occur via thermogenin, generating heat, or through complex V.

Besides being available to diverse processes, the transformation of energy contained in reduced equivalents into the electrochemical potential precludes the abrupt release of energy as heat if a direct redox reaction occurred instead of sequential reactions. The indirect production of ATP from ADP by oxidation of reduced equivalents is one of the postulates of the chemiosmotic theory (Mitchell, 2011).

Complex V, also termed ATP synthase or ATPase, comprises two physically dissociable subcomplexes, the membrane-associated F_O and the soluble F_1. The F_O subcomplex is composed by ~9 different subunits (a:A6L:b:c_8:d:e_n:f:F6:g_n) arranged in a channel-like structure in the IMM. By its turn, the F_1 subcomplex is located in the MM comprising 6 different subunits (α_3:β_3:γ:δ:ε:OSCP) which contain the ATP, ADP and P_i binding sites and the catalytic sites responsible for ADP phosphorylation (Jonckheere *et al.*, 2012). Protons from the IMS flow through the F_O portion and cause the F_O ring (formed by subunits c) and the F_1 central stalk (subunits γ, δ and ε) to rotate, imposing structural stress on subunits α and β that form the α_3:β_3 hexamer thus promoting changes in their conformation.

1.3. Complex I

The diverse cellular mechanisms have been co-evolving, strengthening their interplay and their role within the cell. This co-evolution is not only directed by environmental interactions but also by the multiple cross-talks that coordinate cell functions. For instance, in order to produce a certain action, mechanisms related to a certain triggering event have to evoke and convey a message that the integrator part understands and, in turn, this unit has to initiate the corresponding function by means of a compatible interaction with the effector.

Considering the mechanisms that lead to energy production, glucose must be processed to pyruvate through several enzymatic-catalysed transformations; pyruvate is transported by specialized proteins into the mitochondria, where it is further processed in order to allow the phosphorylation of ADP, producing ATP. So, a tight correlation of each cellular component is vital to ensure that cells are able to perform their processes.

The MRC is not an exception. Complex I can withdraw electrons from NADH upon oxidation of this dinucleotide to NAD^+ while complex II oxidizes succinate to fumarate to input electrons into the MRC via $FADH_2$ oxidation.

The course of evolution is clear in this cellular subsystem. One can observe the increase in the complexity of the proteins that comprise the MRC from simpler to more complex organisms.

This section focuses on one MRC complex which is still not completely understood, being one of the targets for this study.

1.3.1. Structure

In genomic terms, the 45 protein subunits that make up eukaryotic complex I are coded by genes scattered throughout the nuclear and mitochondrial genomes, unlike the prokaryotic equivalent which is coded in operons (e.g. *NQO1-14* in *Thermus thermophilus*) (Yano *et al.*, 1997). The mtDNA encodes the ND subunits (ND1-6 and ND4L), which constitute the membrane-embedded part of complex I. These peptides are synthesized by mitochondrial ribosomes and, due to their highly hydrophobic character, they are integrated in the IMM. It is possible that the proximity between genome and target compartment of the encoded protein avoids off-target events during their allocation since the nearer hydrophobic medium is the IMM. On the other hand, subunits encoded in the nuclear genome are translated in the cytoplasm and imported into the mitochondria. This transport is selective due to the presence of specific localization signals that target their recipients to the target compartment (Nelson and Cox, 2008; Voet and Voet, 2011).

In the context of proteomics, complex I is a membrane-bound assembly with a combined mass of approximately 550 kDa (*Escherichia coli*) or ~1 MDa (human and bovine) (Efremov *et al.*, 2010), with a non-covalently bound FMN, eight iron-sulphur (Fe-S) clusteres and a ubiquinone molecule. Its characteristic L-shape (Figure 1) corresponds to the membrane-embedded moiety and to a peripheral arm extending 100 Å into the MM, which is composed of hydrophilic subunits (Hirst *et al.*, 2003).

While the bacterial (*Escherichia coli*) complex I comprises 14 proteins (Efremov *et al.*, 2010), bovine complex I is composed of at least 45 proteins (Hirst *et al.*, 2003; Carroll *et al.*, 2006). However, the 14 proteins of the prokaryotic complex are conserved from bacteria to humans and compose the core subunits of the mammalian complex I.

Figure 2 – *Thermus thermophilus* entire complex I. The atomic resolution structure is represented as cartoons. Different subunits are represented in different colours. The membrane-embedded subunits are coloured blue (Nqo12/ND5), green (Nqo13/ND4), yellow (Nqo14/ND2), orange (Nqo7/ND3, Nqo11/ND4L, Nqo10/ND6) and red (Nqo8/ND1). (PDB 3M9S (Efremov *et al.*, 2010)).

Two striking features can be observed in the membrane domain of complex I. The first is the similarity of the three most distal subunits, and the other is the long helix parallel to the plane of the membrane.

The distal segment of the membrane portion is composed by subunits ND5, ND4 and ND2, which are related to each other and to the Mrp Na^+/H^+ antiporter family. Furthermore, each of these three subunits presents two "broken" helixes, which is also indicative of H^+-translocase activity. Subunit ND5 is the most distal and presents an extended C-terminal relative to the other two; this extension forms a long helical segment which interacts with ND4 and ND2, suggesting a mechanical control of the overall conformational changes of the membrane domain by a cooperative mechanism (Bridges *et al.*, 2011).

The membrane portion of complex I interacts with the soluble portion predominantly via ND1, although subunits ND3 and ND4L may also be involved in this connection.

Dissociation of complex I can be accomplished *in vitro* using chaotropic agents, producing four types of subcomplexes (Carroll *et al.*, 2006): subcomplex Iλ is composed by 15 predominantly hydrophilic subunits corresponding to the peripheral arm (7 of which are core subunits) and contains all redox cofactors known in complex I plus the NADH binding site; subcomplex Iα, formed by Iλ plus Iγ, includes eight other subunits presenting a total of 9-10 predicted transmembrane helixes (five of them in ND6), thus embedding the additional part of this subcomplex in the IMM; subcomplex Iβ, constituted by 13 subunits and having a total of approximately 36 predicted transmembrane helixes (30 of them in ND4 and ND5) is the most hydrophobic corresponds to the majority of the membrane-embedded arm of complex I (Table 1; Figure 3 A) (Hirst *et al.*, 2003; Carroll *et al.*, 2003).

Among the 15 subunits that constitute subcomplex Iλ, only B16.6 has a predicted transmembrane helix. Adding to this, the presence of low levels of B14.7 (also presenting potential transmembrane helices) explains why this predominantly hydrophilic subcomplex tends to aggregate in the absence of detergent, once isolated (Fearnley *et al.*, 2001; Hirst *et al.*, 2003). Furthermore, this subunit, also known as Gene associated with retinoic and interferon-induced mortality 19 protein (GRIM-19), as well as SDAP (also known as mitochondrial acyl carrier protein) are examples of proteins which have a described function but their role as part of complex I is yet to be clarified.

Complex I subunits share sequence similarity across species, even between prokaryotes and eukaryotes (Table 2). However, the latter present additional subunits that may be related to fine regulation of its catalytic activity.

Table 1 – Subunit composition of the three main bovine complex I subcomplexes. Parentheses denote subunits detected at trace levels (adapted from Hirst et al., 2003; Carroll *et al.*, 2003).

Iα	Iλ	Iβ
75 kDa	75 kDa	AGGG
51 kDa	51 kDa	ASHI
49 kDa	49 kDa	ESSS
30 kDa	30 kDa	MNLL
24 kDa	24 kDa	PDSW
PSST	PSST	SDAP
TYKY	TYKY	SGDH
18 kDa	18 kDa	B22
13 kDa	13 kDa	B18
10 kDa	10 kDa	B17
B17.2	B17.2	(B15)
B16.6	B16.6	(B14.5b)
B14.7	(B14.7)	B12
B14.5a	B14.5a	ND4
B13	B13	ND5
B8	B8	
(42 kDa)		
39 kDa		
15 kDa		
MWFE		
PGIV		
SDAP		
(B15)		
B14		
B9		
ND6		

Table 2 – Interspecies correspondence of complex I subunits. *Ec – Escherichia coli*; *Tt – Thermus thermophiles*; *Bt – Bos taurus*; *Hs – Homo sapiens* (adapted from Hirst et al., 2003).

Ec	*Tt*	*Bt*	*Hs*
NuoG	Nqo3	75 kDa	NDUFS1
NuoF	Nqo1	51 kDa	NDUFV1
NuoD	Nqo4	49 kDa	NDUFS2
NuoC	Nqo5	30 kDa	NDUFS3
NuoE	Nqo2	24 kDa	NDUFV2
NuoB	Nqo6	PSST	NDUFS7
NuoI	Nqo9	TYKY	NDUFS8
		42 kDa	NDUFA10
		39 kDa	NDUFA9
		18 kDa	NDUFS4
		15 kDa	NDUFS5
		13 kDa	NDUFS6
		10 kDa	NDUFV3
		AGGG	NDUFB2
		ASHI	NDUFB8
		ESSS	NDUFB11
		KFYI	NDUFC1
		MLRQ	NDUFA4
		MNLL	NDUFB1
		MWFE	NDUFA1
		PDSW	NDUFB10
		PGIV	NDUFA8
		SDAP	NDUFAB1
		SGDH	NDUFB5
		B22	NDUFB9
		B18	NDUFB7
		B17.2	NDUFA12
		B17	NDUFB6
		B16.6	NDUFA13
		B15	NDUFB4
		B14.7	NDUFA11
		B14.5a	NDUFA7
		B14.5b	NDUFC2
		B14	NDUFA6
		B13	NDUFA5
		B12	NDUFB3
		B9	NDUFA3
		B8	NDUFA2
NuoH	Nqo8	ND1	ND1
NuoN	Nqo14	ND2	ND2
NuoA	Nqo7	ND3	ND3
NuoM	Nqo13	ND4	ND4
NuoK	Nqo11	ND4L	ND4L
NuoL	Nqo12	ND5	ND5
NuoJ	Nqo10	ND6	ND6

The structural similarities presented by complex I of different species are a strong indicator of other shared characteristics, as presented in section 1.3.2. .

1.3.2.Function

Both bacterial and mitochondrial complex I present three main catalytic functions: dehydrogenase, hydrogenase and proton translocator. These are essential for the function of the complex. The dehydrogenase module is responsible for the oxidation of NADH. The resulting electrons are shuttled via cofactors to the hydrogenase unit, which carries out the reduction of ubiquinone to ubiquinol using the shuttled electrons and protons from the MM. Finally, these exergonic redox reactions are in concert with the endergonic translocation of protons from the MM (N-side) to the IMS (P-side); this is the responsibility of the proton translocation module, which is composed of several transmembrane proteins. The overall catalysed reaction is represented in Eq. 1.

$$NADH + 5\ H^+_N + Q \longrightarrow NAD^+ + 4\ H^+_P + QH_2 \qquad \text{Eq. 1}$$

Besides having the same functional properties, there are also structural similarities. Since both complexes catalyse the same reaction and all bacterial subunits of complex I have analogues in the mitochondrial enzyme (Table 2) the former can be considered as the minimal enzyme and is often used to study its mitochondrial counterpart.

Concerning its catalytic activity, complex I can also be subdivided according to the activity of the subunits: the membrane portion is responsible for the H^+ translocase activity (Figure 3 B yellow); the interconnecting region between the membrane and the soluble portions is the hydrogenation module, being responsible for the reduction of ubiquinol (Figure 3 B blue); the distal segment of the soluble portion is responsible for the dehydrogenase activity by which NADH is oxidized (Fig 3 B red).

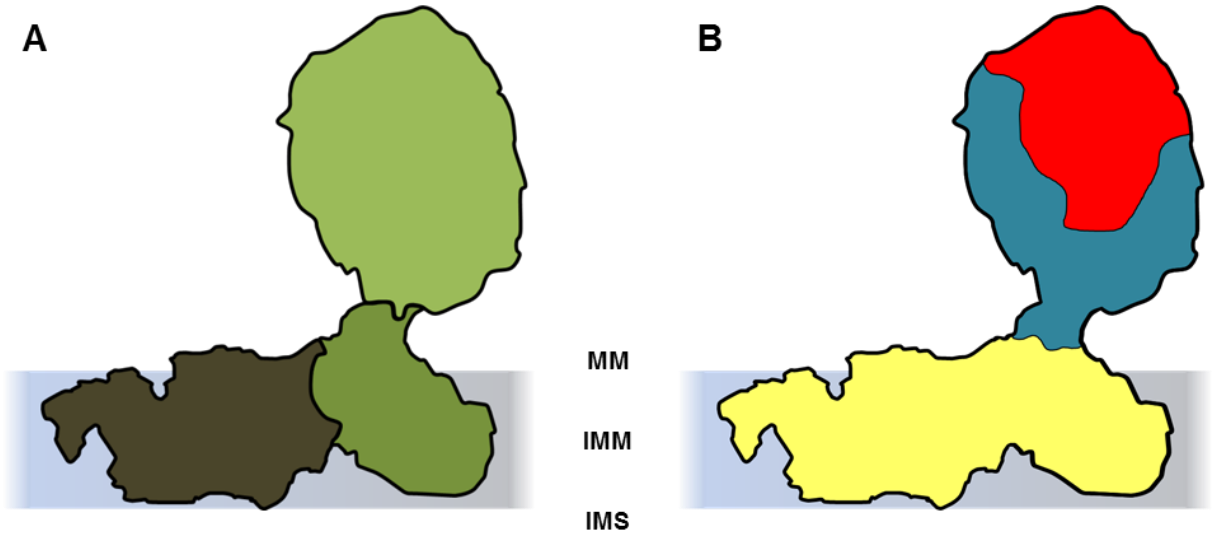

Figure 3 – Structural and functional subdivisions of the *Homo sapiens* complex I. (**A**) Structural subdivision of complex I. Subcomplex Iβ: dark green. Subcomplex Iγ: green. Subcomplex Iλ: light green. Adapted from (Ugalde *et al.*, 2004). (**B**) Functional subdivision of complex I. H^+-translocation / P-module: yellow. Hydrogenase / Q-module: blue. Dehydrogenase / N-module: red. Adapted from (Dieteren *et al.*, 2012).

1.3.3.Challenges

Studies involving complex I are more challenging as the level of detail needed increases. The existence of highly hydrophobic subunits composing a membrane-integrated moiety, the considerably high molecular weight, the high number of subunits and their low number of repetition (i.e. complex I is possibly a pentatetracontamer) represent major obstacles that difficult the generation of atomic resolution structures by means of protein crystallization followed by X-ray diffraction. These techniques have been evolving and are constantly proving their value. Although complex structures as ribosomes, large assemblies as virus capsids, and membrane proteins have been resolved, complex I still gathers the most puzzling drawbacks and no crystal structure of eukaryotic complex I is available.

The only structures with atomic resolution that have been attained so far are those of the prokaryotic minimal enzyme from *Escherichia coli* and *Thermus thermophilus*.

Stepping back, other techniques can be used to study complex I in a coarser fashion. For example, crosslinking agents have been employed to fix interacting subunits and determine the protein-protein interactions that hold the complex together and are responsible for all its functions (Patel *et al.*, 1988; Patel and Ragan, 1988; Cleeter *et al.*, 1985).

Depending on the nature of the assays, different requirements must be met in order to produce valid results. For instance, molecular, proteomic and structural studies require that complex I is available in significant quantities and/or can be isolated with high purity levels. If processing of complex I prior to its analysis is required (e.g. enzymatic digestion and dissociation), it is necessary to ensure the reproducibility of the procedure.

Moreover, the subunit interactions are not completely resolved and further studies need to be conducted in order to determine the architecture of complex I in finer detail.

1.4. Supercomplexes

The evolution of biological systems is shaped by many variables such as environmental conditions and access to nutritional sources. However, the diversity created by the evolutionary processes have one ultimate goal, adaptation. This means that systems tend to modify their components so that maximum efficiency can be achieved considering the present variables.

Adaptation is present in every level of the biological systems. A good example is the modification of the shape of anatomical pieces of birds, such as beaks, is a macroscopic manifestation of adaptation to their diet. Since Darwin's report on the morphological variation of beaks in finches (Darwin, 1988), new techniques have been discovered enabling the explanation of that observation at the molecular level (Abzhanov *et al.*, 2004).

One of the major goals for evolution at the microscale is efficiency. Variations in the genetic code are selected in a way that the coded proteins perform their function in a more efficient way. Enzymes are shaped so that the reaction they catalyse has the maximum yield possible taking into account the microenvironmental conditions. When comparing enzymes of organisms which habitat presents different conditions (e.g. temperature, pressure, presence and concentration of certain elements), an evolutionary strategy can be noticed. As an example, the differences in the DNA polymerases of thermophiles shift the maximum activity to higher temperatures.

Other strategies involve the modification of interactions established between macromolecules. Metabolic pathways are complex networks of simple molecules and enzymes that catalyse reactions that lead to the transformation of the former. Although all reactions are interconnected, some of them bring that tie to another level. The majority of enzymes release the products of the reaction they catalyse into the surrounding medium. Those compounds can act as substrates to other enzymes that will further transform them. In this process, there is a step where a reaction intermediate is diffused into the turmoil of the Brownian motions of medium components and, in order to continue the processing pathway, the released molecule needs to collide with the next enzyme. There are enzymes that restrict the loss of the compounds they transform by associating to other enzymes that take part in the transformation pathway. An example of such systems is the pyruvate dehydrogenase complex. This stable multienzyme complex is composed by three enzymes (pyruvate dehydrogenase, dihydrolipoyl transacetylase and dihydrolipoyl dehydrogenase) in close proximity so that the product of one enzymatic reaction can be directly conveyed to the next where it will act as substrate – substrate channelling. Mechanistically and kinetically, this process presents several advantages: (i) prevent the loss of intermediates by diffusion; (ii) decrease the transit time of intermediates; (iii) protect labile intermediates from the aqueous external environment; (iv) limit the routing of compounds to competing pathways; (v) prevent the buildup of intermediates; (vi) overcome unfavourable equilibria (Miles *et al.*, 1999; Huang *et al.*, 2001).

In the light of the exposed matters, when considering the flow of metabolites through the MRC it seems plausible to hypothesize the existence of assemblies between complexes. Accordingly, (i) the electron flow from reduced equivalents to oxygen would be more efficient, (ii) the electron transport would be independent of the diffusion of intermediate species, (iii) since ubiquinol would be

channelled, less reduced species would be available to non-specifically produce radical species such as reactive oxygen species.

Diverse techniques proved the existence of assemblies of MRC complexes, more specifically between complex I, complex III and complex IV in a ratio of 1:2:0, 1:2:1 and 1:2:2. So far, the technique most commonly used to study these supercomplexes is native electrophoresis which allows the separation of proteins according to their mass and shape, keeping them in their native state which preserves structure, function and interactions (Lenaz *et al.*, 2010; Schägger and Pfeiffer, 2001).

Using three independent methods, Schägger and Pfeiffer determined the ratio of oxidative phosphorylation complexes. Besides updating the previous information on this matter using modern technology, the study also focuses in the stoichiometric parameters of supercomplexes. Results show that almost all complex I (~90%) is bound with complex III forming supercomplexes; on the other side, only ~60% of total complex III participate in supercomplexes leaving approximately one third in the free state (Schägger and Pfeiffer, 2001).

One of the factors that determine the formation of supercomplexes from isolated complexes is the phospholipid milieu. Due to its characteristics and location, the IMM is not commonly target of drastic modifications in terms of lipid quantities. However, the lipid composition may be more critical for the correct function and structure of mitochondria. This biological membrane is highly enriched in cardiolipin, a diphosphatidylglycerol lipid which is ideally inexistent in other biological membranes other than the IMM. At physiological pH, cardiolipin bears a single negative charge (pK_{a2} = 8.0). The protonated phosphate group forms a hydrogen bond with the hydroxyl group of the central glycerol moiety, which in turn establishes an interaction of the same type with the negatively charged phosphate. This creates a bicyclic resonance form that delocalizes the negative charge. Moreover, the capacity to uptake one proton and to stabilize the protonated form grants this lipid with a buffering capacity – proton trap. Cardiolipin-binding sites have been detected in subunits of the MRC complexes, strongly suggesting a functional role for this lipid. Due to the capacity to uptake a proton, cardiolipin can function as a buffer. This function is especially relevant when taking into account local pH variations due to proton transport across the IMM catalysed by MRC complexes. Moreover, since cardiolipin can diffuse across the IMM, the proton transport is facilitated by the presence of cardiolipin-binding sites in proteins that catalyse proton transport across the membrane (Haines and Dencher, 2002). Also, cardiolipin is important to stabilize supercomplexes (Pfeiffer *et al.*, 2003). Posterior studies focused in the supercomplexes of Barth syndrome patients harbouring a mutation in the *TAZ* gene, which codes an enzyme involved in the cardiolipin biosynthetic pathway showing that complex IV readily dissociates from supercomplex $I_1III_2IV_1$, and that complex I and III establish less stable interactions as seen by the decreased amounts of supercomplex I_1III_2 (McKenzie *et al.*, 2006; Lenaz *et al.*, 2010).

After the discovery of the MRC complexes, it was postulated that the overall respiratory function is the result of both (i) intracomplex electron transfer in solid state between fixed redox centres, and (ii) intercomplex electron transfer ensured by rapid diffusion of mobile species. Posterior studies showing that the IMM is fluid, thus enabling the free lateral diffusion of the MRC complexes, led to the publication of the Random Collision Model of Electron Transfer by Hackenbrock and collaborators. This hypothesis is based on five postulates: (i) all redox components diffuse laterally in an independent mode; (ii) cytochrome c diffuses in three dimensions; (iii) the electron transport kinetics depends on the rate of diffusion; (iv) electron transport is a multicollisional, obstructed, long-range diffusional process; (v) the overall electron transport kinetics is dependent on the diffusion rate of the redox components. Additionally, it rejects the notion that permanent or transient aggregates of redox components anchored to the membrane are necessary to the normal respiratory function (Hackenbrock *et al.*, 1986). According to this view, the MRC is in organized in a liquid state where molecules are randomly distributed in the plane of the IMM and diffuse freely mainly in a lateral fashion, being the diffusion rate of ubiquinone and cytochrome c higher than that of the large complexes. On the other hand, the components of the MRC can be envisaged as a solid-state assembly where complexes associate permanently or transiently, forming clusters which turnover presents slower kinetics than the electron transfer process (Lenaz and Genova *et al.*, 2007). This hypothesis – Solid State Electron Channelling – was initially propsed by Chance and Williams (Chance and Williams, 1955). Structural evidence of the existence of aggregates of respiratory complexes (Schägger and Pfeiffer, 2001) brought this model back to scientific debate (Lenaz and Genova *et al.*, 2007).

There is a growing number of studies performed in complex III mutants where a severe decrease in the supercomplex stability is observed. Moreover, in more drastic cases where complex III is absent, complex I is less stable and combined complex I and III deficiencies are observed (Blakely *et al.*, 2005; Acín-Pérez *et al.*, 2004). Similar evidences impute to complex III (Blakely *et al.*, 2005), and to a lesser extent to complex IV (Diaz *et al.*, 2006), roles in the stabilization and assembly of complex I (Lenaz *et al.*, 2010).

1.5. Degradation Pathways

The major accomplishment of the father of modern Chemistry, Antoine Lavoisier, is the condensation of centuries of intensive alchemical work under a simple formulation, the Principle of Mass Conservation: the mass and energy of a closed system remain constant over time. Ultimately, the principle can be rearranged in the famous maxim "nothing is created, nothing is destroyed, everything is transformed". Although during Lavoisier's lifetime little was known on the cell mechanisms, his principle can be applied to large and complex chemical reactors such as cells.

Cellular mechanisms are tightly regulated and no matter is created nor destroyed: only transformations occur. In order to survive, certain processes need to be maintained, requiring building blocks (e.g. amino acids, lipids, sugars). When in an adverse environment cells adapt by decomposing some of their structures in order to obtain those building blocks and proceed with the vital processes. Sometimes similar decomposing pathways are employed to destroy defective components which are potentially hazardous to the cell, producing building blocks that can be reused.

In this section diverse degradation pathways, their mechanisms and biological relevance will be presented, focusing on protein degradation pathways.

1.5.1. Ubiquitin-Proteasome System

Cells have developed specialized strategies to degrade different types of proteins, some of which are very selective, requiring a tag to identify the components that are targeted to destruction. One of those mechanisms is the Ubiquitin-Proteasome System (UPS).

This mechanism mobilizes very diverse components both in their size and complexity, being ubiquitin the simpler (8 kDa, monomeric) and the 26S proteasome the more complex (2 MDa, pseudoheptameric).

Ubiquitiin is the first intervenient in the UPS. It is a small protein which C-terminal carboxyl group can be covalently coupled to lysine residues in target proteins as an ATP-dependent post-translational modification. Furthermore, ubiquitin has itself lysine residues capable of undergoing coupling with the C-terminal diglycine moiety of other ubiquitin molecules, forming poly-ubiquitin chains. Different poly-ubiquitin chains are involved in diverse processes; for instance, while linear poly-K48 ubiquitin chain of at least four ubiquitin moieties are required to target a protein to proteasomal degradation, poly-K63 ubiquitin and monoubiquitination are mainly involved in endocytosis (Wilkinson, 1997; Voet and Voet, 2011).

A set of diverse enzymes is required to modify target proteins with ubiquitin units. These enzymes can be segregated in three classes according to the reaction they catalyse: Ubiquitin-Activating Enzyme (E1), Ubiquitin-Conjugating Enzyme (E2), and Ubiquitin-Protein Ligase (E3). The E1 adenylates the C-terminal residue of ubiquitin and then forms a thioester bond with a cysteine residue of the enzyme, transporting it to an E2, which receives the activated ubiquitin molecules by trans-thiolation. Finally, the E3 couples the ubiquitin molecule to the ε-amino group of a target lysine residue on the substrate, forming an isopeptide bind. The E3 binds simultaneously the E2 and the target protein and thus is the component which is primarily responsible for the specificity of the ubiquitination process. Moreover, the interplay between E2 and E3 enzymes further increases the specificity of this mechanism by making ubiquitination a combinatorial process (Voet and Voet, 2011).

There are two mechanistically distinct classes of E3 ligases: RING E3 transfer ubiquitin directly from the E2 to the target protein; HECT E3 transfer ubiquitin from the E2 to themselves, forming an intermediary E3~Ub thioester, before modifying the substrate. A newly reported E3 class carries out

protein ubiquitination using a hybrid mechanism involving RING-mediated formation of a E3~Ub intermediary; this class is termed RING-in-between-RING(IBR)-RING (RBR) E3 ligases. The RBR E3 ligases present a RING domain (RING1) which transfers ubiquitin from the E2 to a catalytic cysteine residue of another RING domain (RING2), from which ubiquitin is finally transferred to the substrate (Wauer and Komander, 2013).

The ultimate component of the UPS is the proteasome. It is a very large hollow cylindrical multi-protein complex that can be structurally divided in two regulatory particles (19S) and one core complex (20S); these three components associate and form the conventional eukaryotic 26S proteasome. In functional terms, the 19S regulatory particle can be further divided into lid (presents deubiquitinating activity) and base (binds poly-ubiquitin chains and has ATPase activity); on the other hand, the 20S core complex is formed by four heptameric rings composed of two functionally distinct subunits – α (structural and selectivity role) and β (proteolytic activity) – forming the catalytic chamber (Voet and Voet, 2011; Nelson and Cox, 2008).

Once the poly-ubiquitin chains are recognized the regulatory particles, they are cleaved and ATPases in the base unfold the target protein, which is channelled to the pore formed by the α subunits of the core complex. The substrate is hydrolysed by the β subunits and the resulting peptides exit the catalytic chamber. The ubiquitin molecules that were once tagging the protein targeted for decomposition are early removed by the lid avoiding their degradation and thereby enabling their reutilization, precluding unnecessary material and energetic expenditures.

1.5.2.Lysosomal Proteolytic Pathways

As in other mechanisms, eukaryotic cells present optional routes for protein degradation. They do not rely solely in the proteasome to eliminate proteins and other of their constituents.

Lysosomes are spherical organelles that contain hydrolytic enzymes, thus making them important players in degradation pathways, being able to digest virtually all cell components to simpler forms.

The lumen of lysosomes presents a remarkable low pH (pH ~5) when compared to the cytosol (pH ~7), this contributes to the denaturation of substrates, granting access to their core structures. Since lysosomal enzymes present optimal activity at low pH, once in the cytosol, the relatively high pH renders them almost inactive. So, the main function of this chemical difference is to prevent cellular autolysis in case of disruption of the lysosomal membrane. Furthermore, in order to restrict the range of lysosomal hydrolases, the luminal portions of lysosomal membrane proteins are highly glycosylated decreasing the accessibility of the enzymes to the lysosomal membrane.

The main responsible for the acidic pH of lysosomes is the H^+-pump activity of V-type ATPases present in the lysosomal membrane. These pumps actively transport H^+ from the cytosol to the lumen of lysosomes decreasing the pH (Lodish *et al.*, 2003).

Lysosomes can degrade both exogenous (e.g. phagocytosed bacteria) and endogenous components (e.g. aged or defective organelles). However, the mechanisms involved in the targeting of substrates to lysosomes differ according to their provenience: endocytosis and autophagy, respectively (Lodish *et al.*, 2003).

The concept of autophagy comprises three catabolic processes: (i) macroautophagy, characterized by the formation of phagophores, engulfment of large volumes of cytoplasm and fusion of the resulting autophagosomes with lysosomes; (ii) microautophagy, which involves invagination of the lysosomal membrane and direct uptake of cytoplasmic material, and; (iii) chaperone-mediated autophagy (CMA), which requires the action of chaperones that recognize specific sequences in the target proteins, directing them to specific channel receptors in the lysosomal membrane (Wilkinson, 1997; Lodish *et al.*, 2003).

Unlike the UPS, which is usually involved in the turnover of short-lived proteins, macroautophagy is commonly responsible for the degradation of long-lived physically large and chemically diverse cell components (i.e. protein aggregates, whole organelles, cytosolic pathogens) (Randow and Youle, 2014; Fader and Colombo, 2009). However, there are striking resemblances between both degradation systems that further corroborate their tight cross-regulation as discussed below.

The energetic state of the cell, nutrient deprivation and lack of growth factors are major triggers of macroautophagy in most cells. The AMP/ATP ratio, free amino acid levels, and growth factors produce different impacts on the cellular mechanisms; however, the signalling pathways they trigger converge in two protein complexes that direct the cell response, mTORC1 and mTORC2.

Amino acid levels are directly sensed by Rag GTPases. Upon starvation, low free amino acid levels switch the Rag heterodimer to its active state (RagA/RagB:GTP-RagC/RagD:GDP) which is then able to interact with Raptor thus recruiting mTORC1 to the surface of late endosomes and lysosomes, where Rags reside. This clustering enables mTORC1 to interact with the GTPase Rheb which is essential to activate this mTOR complex. By its turn, Rheb is negatively regulated by the TSC1-TSC2 complex, which integrates stimuli such as energetic stress (via AMPK), hypoxia (via HIF1α) and growth factors (via Ras and via PI3K).

Downstream effects of mTORC1 activation include stimulation of mRNA translation to proteins, ribosome biogenesis, mitochondrial biogenesis (via the transcriptional master regulator PGC1α), and inhibition of autophagy. Since mTORC1 activity culminates in the enhancement of processes that demand large quantities of energy it is necessary to ensure that the appropriate conditions are present enabling cells to withstand such demands. Growth factor signalling cascades also impact on mTORC2. Although the activity and regulation of this complex is not as well characterized as mTORC1, it is known that mTORC2 activation leads to cell survival, cell-cycle progression, anabolism and enhanced cytoskeleton dynamics (Figure 4). Key regulators coordinate the activity of mTORC1 and mTORC2; these components (e.g. Akt, PDK1, TSC1-TSC2, S6K) constitute feed-back loops which ensure that the activity of mTOR complexes is not overwhelming (Zoncu *et al.*, 2011; Sparks and Guertin, 2010; Dodson *et al.*, 2013).

During starvation, the lack of growth factors, the relatively low levels of nutrients (i.e. glucose, amino acids) and the consequent imbalance between energy expenditure and nutrient intake convey inhibitory signals to mTORC1 which acts by inhibiting processes that require great amounts of energy, such as biosynthesis, and upregulating macroautophagy in order to redirect basic units from existing cell components to vital processes. Inhibition of mTORC1 also impacts on mitochondria at three levels: (i) halt mitochondria biogenesis; (ii) destroy a subset of existing mitochondria; (iii) increasing the efficiency of existing mitochondria by releasing the inhibition of 4E-BP1 (Zoncu *et al.*, 2011).

Starvation-induced macroautophagy is nonselective, degrading random cytosolic components to their basic units which can then be directed to vital processes. In contrast, selective macroautophagy targets specific cytosolic components and plays diverse roles in cell homeostasis: turnover of cell components, degradation of dysfunctional/damaged proteins and organelles, and destruction of cytosolic pathogens. Specificity is a key feature in homeostatic macroautophagy, which is achieved by: (i) presence of certain signals (often termed "eat me" signals) in the materials to be degraded; (ii) existence of receptors for those signals in macroautophagic structures; (iii) although not strictly necessary, adapter proteins are found to play an important role in bringing the two previous components physically together.

Upon induction of macroautophagy, diverse signalling pathways converge in the activation of the Atg1 kinase complex which is composed by the Atg1 mammalian homologue ULK1, Atg13, Atg101 and FIP200. The translocation of the Atg1 complex to the ER recruits the class III PI3K complex I. This complex contains regulatory subunits as well as a targeting subunit (Atg14L) which directs it to the ER. Furthermore, the class III PI3K complex I also incorporates the phosphoinositide 3-kinase Vps34 which generates a PI(3)P-rich pool in the ER, also called omegasome, allowing the recruitment of further macroautophagy machinery (e.g. DFCP1 and WIPI2). DFCP1 translocates into the omegasome by directly binding PI(3)P, initiating the formation of the phagophore. Then, two ubiquitin-like protein conjugation systems act to expand the omegasome into a phagophore. Atg12 has a ubiquitin-like dynamic; it is bound to the E1-like Atg7, transferred to the E2-like Atg10 and finally to the E3-like Atg5. This final step creates an isopeptide bond between the C-terminal glycine residue of Atg12 and a lysine residue of Atg5, forming the Atg12–Atg5 conjugate. This conjugate forms a stable complex with Atg16 which is recruited to the autophagic membrane. The other ubiquitin-like system beguins with the cleavage of the C-terminal of the Atg8 mammalian homologue LC3 by Atg4, generating the cleaved form LC3-I. Then, ubiquitin-like LC3-I is activated by the E1-like activity of Atg7 and conjugated to the E2-like Atg3 by a thioester bond. The Atg3–LC3-I conjugate is targeted to the autophagic membrane via hydrophobic interactions with the Atg3-binding surface of Atg12. This brings LC3-I to close proximity with the lipids of the membrane and, due to the E3-like activity of the Atg12–Atg5:Atg16L complex, LC3-I is transferred to a PE molecule, originating the C-terminal

lipidated form, LC3-II. Polyubiquitinated proteins are recognized by receptors such as p62, which functions as an adaptor, bridging autophagosomes and their cargo. Maturation of the autophagosome results in the complete closure of the phagophore and cleavage of the lipidated C-terminal LC3-II exposed to the cytosol in the autophagosome outer membrane, releasing LC3-I and PE (which remains in the membrane). Finally, the outer membrane of the mature autophagosome is decorated with class III PI3K complex II and the whole structure fuses with lysosomes. Once the autophagic cargo is delivered to the lysosome it is degraded to simpler molecules by the diverse hydrolases present in this organelle. The resulting products are transported to the cytosol by permeases present in the lysosomal membrane, and can thus be recycled (Figure 5) (Noda *et al.*, 2013; Klionsky and Deretic, 2010). Besides this hypothesis, there are others that consider the contribution of further biological membranes other than the ER for the phagophore formation (e.g. plasma membrane and Golgi apparatus).

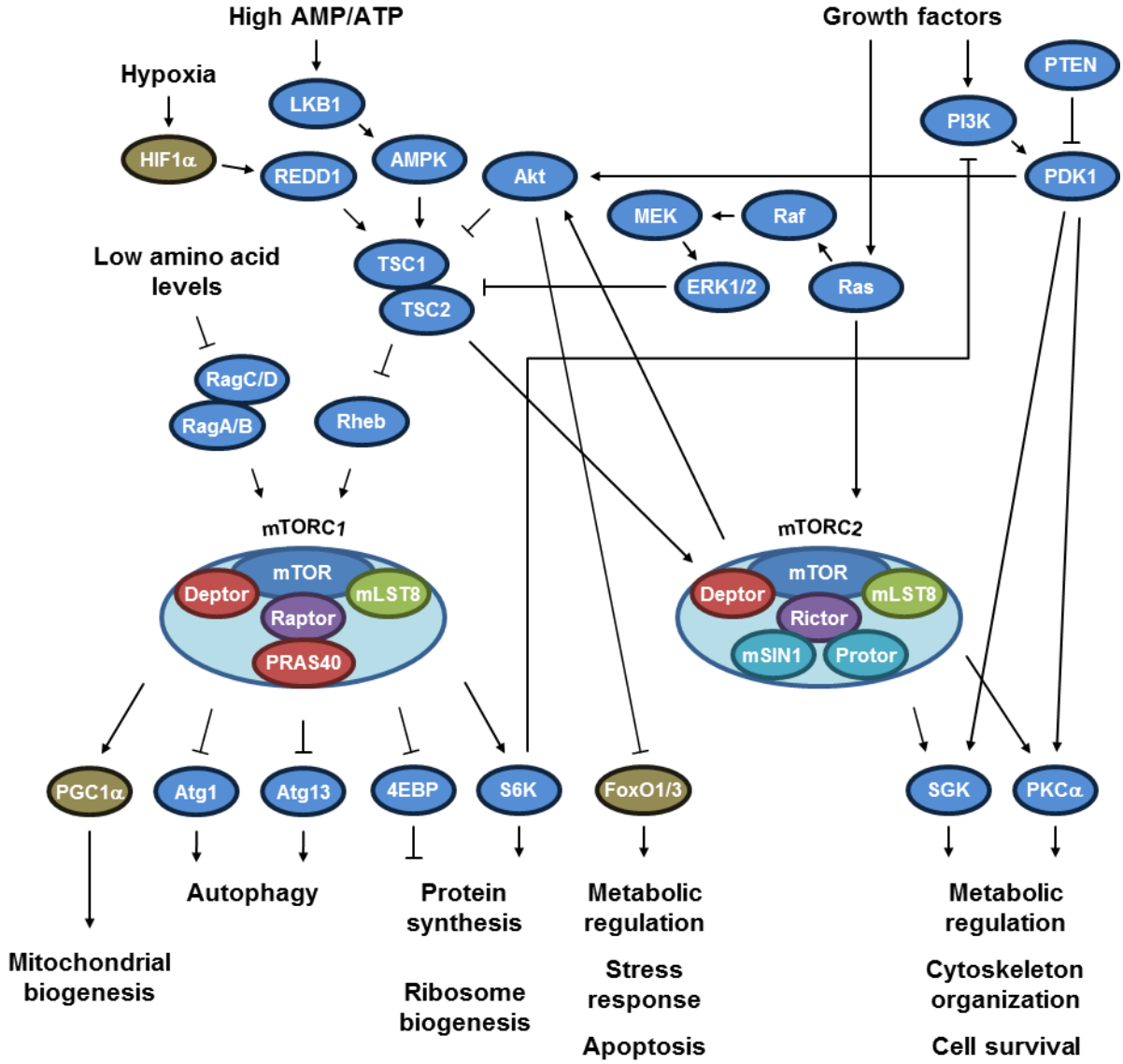

Figure 4 – The mTOR signalling pathway. mTORC1 integrates signals from diverse sources, including oxygen, energy, nutrient status and growth factors; these signals are integrated by the TSC1-TSC2 complex which in turn finely tune Rheb, which is essential to mTORC1 full activation. Signals regarding the amino acid levels are relayed into the pathway via the GTPase complex RagA/B-RagC/D. mTORC2 is mainly regulated by signals coming from growth factor-mediated cascades such as the Ras-Raf and PI3K pathways. Several molecules up- and downstream of mTOR complexes act as regulators of this pathway. Components of the mTOR complexes that negatively regulate them are coloured red while positive regulators are coloured green; mTORC1 and mTORC2 specific components are coloured violet. Transcription factors are coloured brown. Adapted from (Zoncu *et al.*, 2011; Sparks and Guertin, 2010).

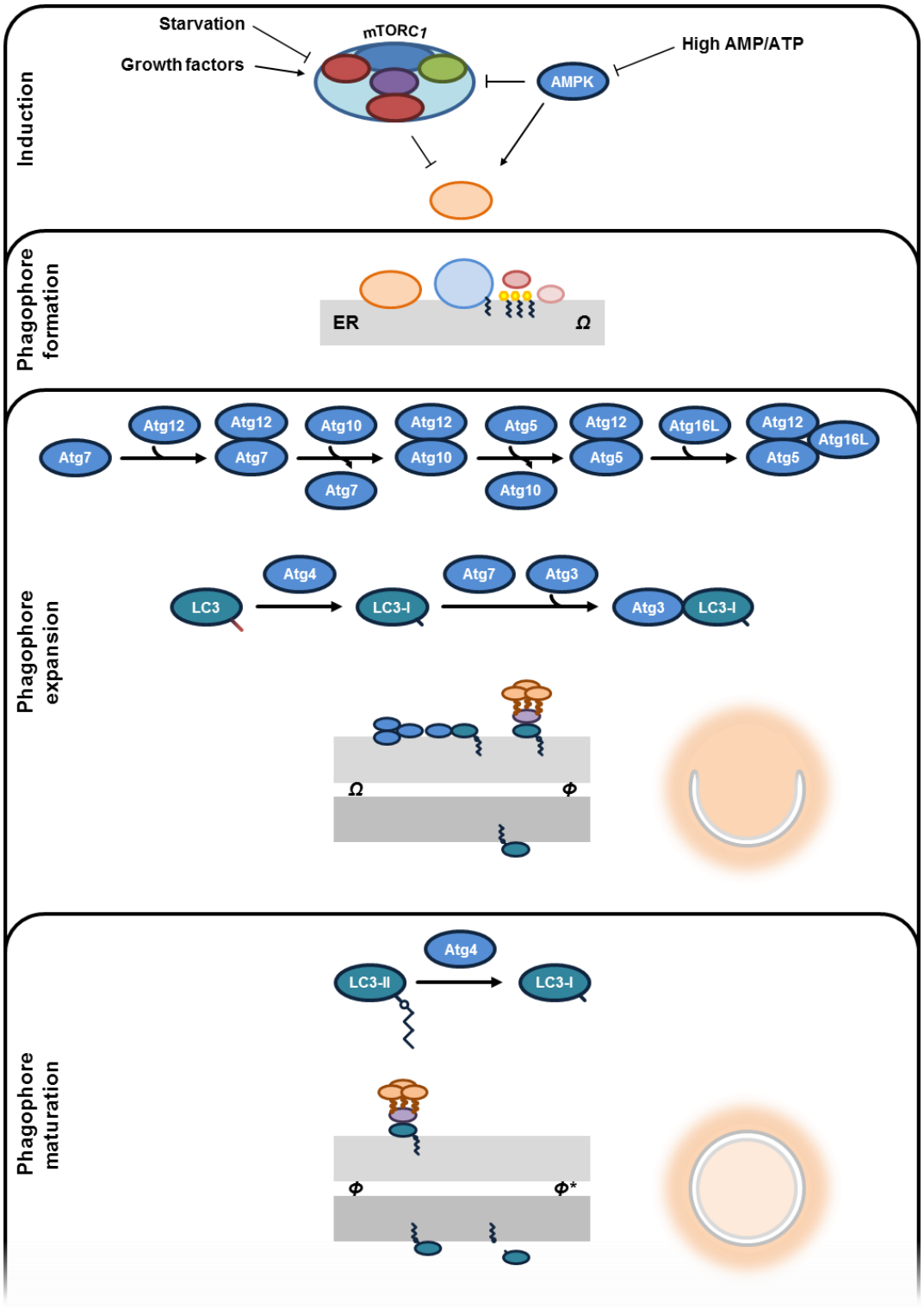
Induction
Starvation
Growth factors
mTORC1
AMPK
High AMP/ATP
Phagophore formation
ER
Ω
Phagophore expansion
Atg7
Atg12
Atg10
Atg5
Atg16L
LC3
Atg4
LC3-I
Atg3
Ω
Φ
Phagophore maturation
LC3-II
Φ
Φ*

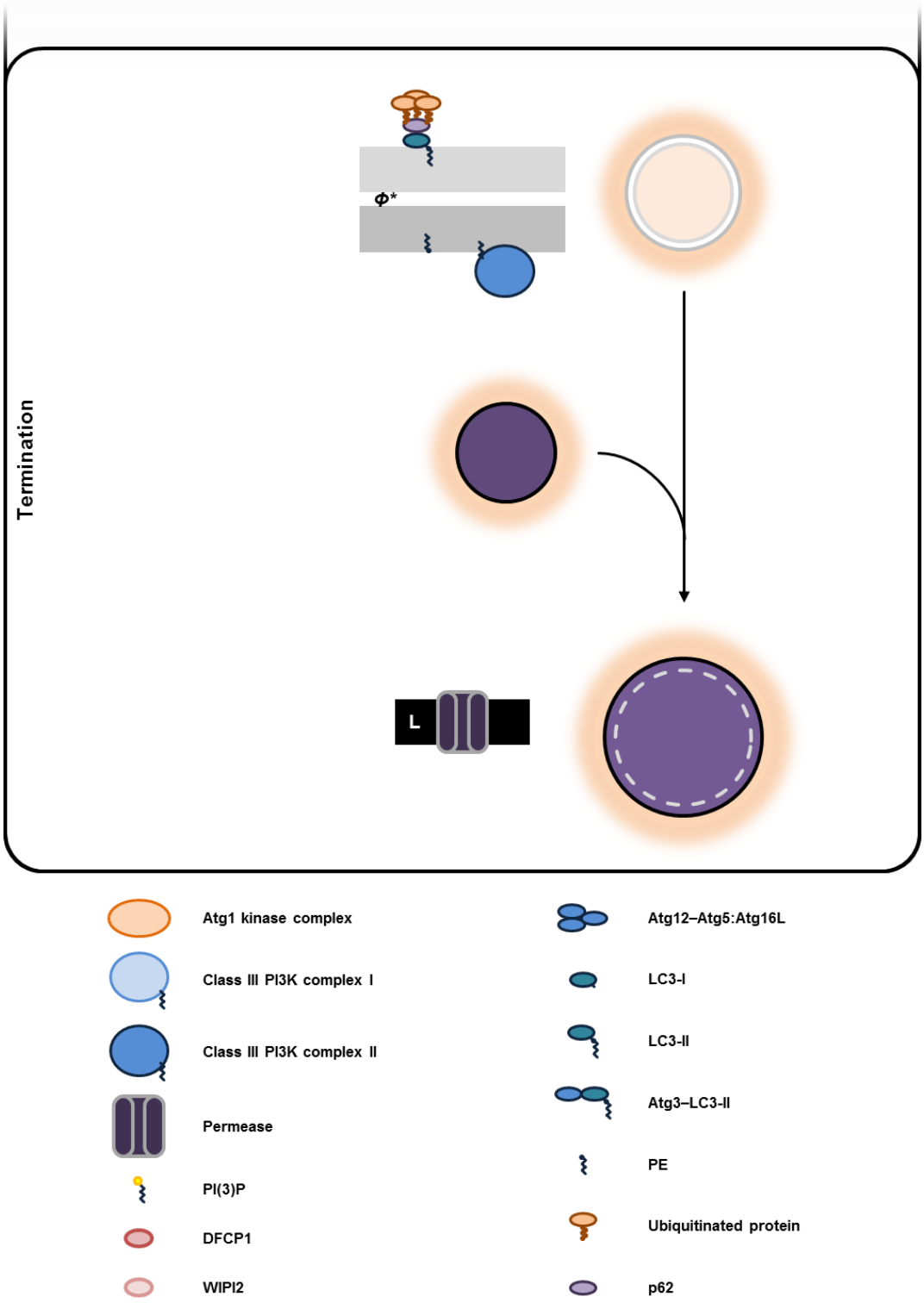

Figure 5 – The autophagy pathway. Diverse signals convey cellular adaptations which induce autophagy by Atg1 kinase complex activation. This complex localizes to the ER membrane and recruits the class III PI3K complex I. This complex is the main component involved in the formation of the omegasome (Ω) by enriching the PI(3)P pool of the ER membrane and thus recruiting additional cell machinery. Upon formation of the Atg3–LC3-I conjugate and its Atg5–Atg12:Atg16L complex-mediated recruitment to the omegasome, LC3-I is lipidated to the membrane bound form LC3-II, which can collect cargo by interacting with adaptor proteins such as p62. During autophagosome (Φ) maturation, the autophagic membrane closes, segregating the cargo inside. After LC3-II being removed from the outer membrane of the autophagosome, the mature structure fuses lysosomes in order to degrade its cargo and recycling the constituents while regulating the material and energetic status of the cell. Adapted from (Klionsky and Deretic, 2010).

1.5.3.Mitophagy

Cells are highly organized structures and their components and pathways are tightly regulated. In homeostatic conditions, both material and energy waste tend to be minimized. That is, cells do not engage in processes that will lead to unfruitful usage of their resources.

Besides being the main location of production of energy equivalents, mitochondria present a high maintenance cost for the cell requiring, for example, specialized protein and antioxidant machinery. Regulated degradation of cellular structures such as mitochondria plays a role in providing material and energetic support to cells during starvation – macroautophagic degradation of mitochondria.

Besides these roles, selective degradation of mitochondria is responsible for the homeostatic clearance of these organelles in certain cells and the quality-control preventing collateral damage to cell structures – mitophagy. (Randow and Youle, 2014).

The mitochondrial quality-control involves the coordination of mitochondrial clues with nuclear-encoded proteins and diverse cell machinery in order to maximize ATP production with minimal adverse effects such as increased ROS production.

PINK1 (PTEN-induced putative kinase) (Figure 6 A, B) is a mitochondrial protein encoded in the nuclear genome. Upon translation, PINK1 is targeted to mitochondria by its MTS. In healthy mitochondria, PINK1 is imported to the IMM by the TOM/TIM system. Once in the IMM, the mitochondrial protease MPP cleaves the MTS. PINK1 is further processed by another protease, PARL, and ultimately degraded.

The mitochondrial membrane potential is essential for many processes occurring in this organelle; one of those processes is the import of some proteins via TIM complex. Damaged mitochondria (which often present a decreased or null membrane potential) cannot deliver PINK1 to its final destination since its import is potential membrane-dependent. However, PINK1 can still be imported into the OMM via TOM complex. In this compartment, neither MPP nor PARL can exert their proteolytic activity and thus PINK1 is not cleaved or degraded (Ashrafi and Schuarz, 2013; Koh and Chung, 2012).

Note that PINK1 is constantly being targeted to mitochondria; however, according to the quality state of mitochondria, it is directed to distinct compartments where is performs differently. In healthy mitochondria, PINK1 is imported to the IMM and is quickly degraded, presenting a fast turnover. On the other hand, in damaged mitochondria, import to the IMM is disabled and PINK1 is directed to the OMM where it accumulates, exhibiting a slower turnover.

This differential dynamics depending on the mitochondrial membrane potential makes PINK1 the main mitochondrial damage/stress sensor, eliciting signalling pathways involving a cytosolic E3 ubiquitin-ligase, Parkin.

Parkin is a RBR E3 ligase presenting a N-terminal UBL domain, a RING0 (also termed UPD, Unique Parkin Domain), and a C-terminal RBR domain comprising RING1, IBR, and RING2 (Figure 6 C, D) (Wauer and Komander, 2013).

Parkin is found in the cytosol mostly in an autoinhibited state where its N-terminal UBL domain binds the C-terminal RBR domain. Upon interaction with PINK1 via RING0, the UBL domain of Parkin is phosphorylated releasing this inhibition (Wauer and Komander, 2013).

The PINK1/Parkin pathway is not completely defined and requires deeper clarification. It is accepted that (i) PINK1 kinase activity is required for Parkin recruitment to the mitochondria, (ii) PINK1 phosphorylates substrates intended to be recognized by Parkin for ubiquitination, and (iii) Parkin-mediated ubiquitination modulates diverse aspects of mitochondrial dynamics. However, the intermediates and signalling pathways involved in this mechanism are still not fully understood. Several models have been proposed based on diverse experimental findings which enrich the picture of this pathway (Figure 7).

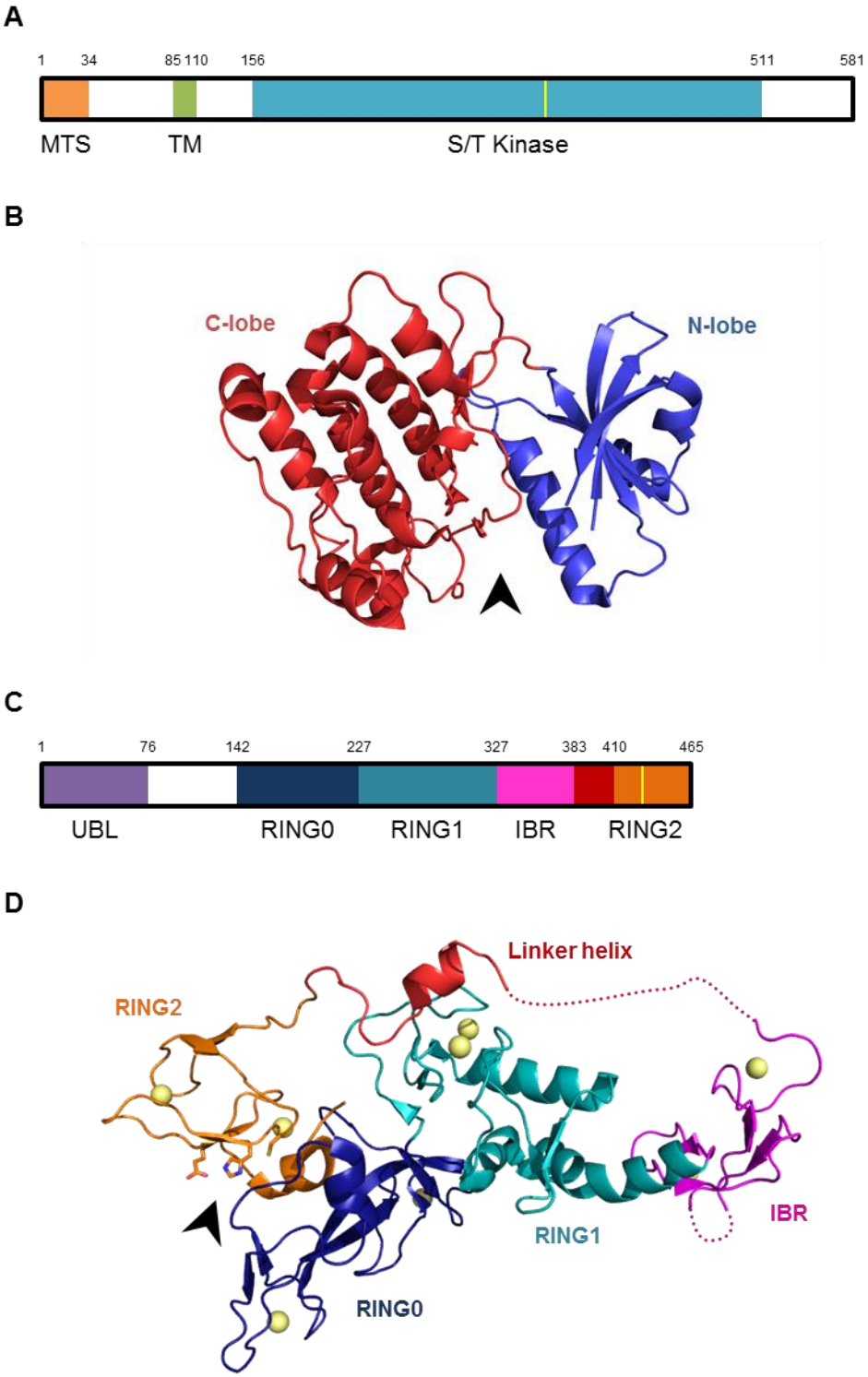

Figure 6 – Structural organization of the proteins involved in mitophagy. (**A**) Domain organization of PINK1. The aspartate catalytic residue (D362) is located by a yellow line. MTS: mitochondrial targeting sequence; TM: transmembrane region; S/T Kinase: serine/threonine kinase domain. (**B**) Model of PINK1 (PDB 2V7O (Rellos *et al.*, 2010)). Since no crystal structure of PINK1 is available, a structural homologue (human CaMKIIδ) is presented, which models the kinase domain of PINK1. The N-lobe is coloured blue while the C-lobe is coloured red. The ATP binding site and the catalytic site are located in the cleft formed between the two lobes (arrowhead). (**C**) Domain organization of Parkin The catalytic cysteine residue (C431) is located by a yellow line. UBL: ubiquitin-like domain; IBR: in between RING domain. (**D**) Crystal structure of Parkin. (PDB 4I1H (Riley *et al.*, 2013)). The crystal structure depicts the fragment 141-465. RING0 is coloured blue, RING1 is coloured teal, IBR is coloured pink, the linker helix that connects the IBR to RING2 is coloured red, and RING 2 is coloured orange. Zinc ions are depicted as yellow spheres. The sidechain of catalytic residues (C431, H433, E444) of the active site (arrowhead) are shown. Adapted from (Trempe and Fon, 2013) and (Wauer and Komander, 2013).

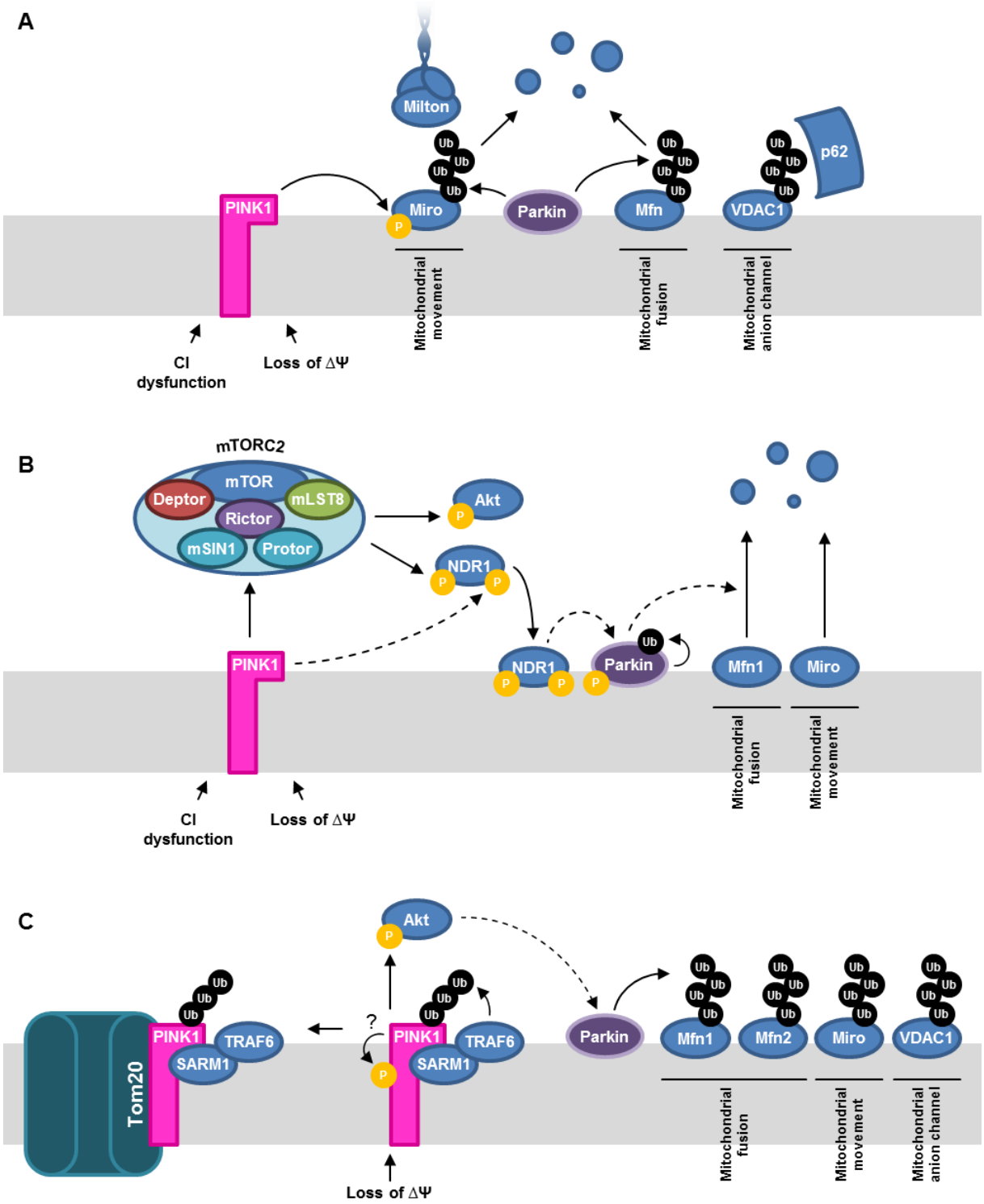

Figure 7 – Mechanistic models of mitophagy. (**A**) The model proposed by Koh and Chung (Koh and Chung, 2012) supports that PINK1 phosphorylates mitochondrial proteins such as Miro. This post-translational modification is then recognized by the E3 Parkin which ubiquitinates modified proteins, targeting them to proteasomal destruction. (**B**) Wu *et al.* (Wu *et al.*, 2013) suggest that PINK1 acts through protein kinases which trigger signalling cascades that result in mTORC2-dependent and mTORC2-independent NDR1 phosphorylation. This modification leads to parkin recruitment to the mitochondria, exerting its ubiquitinating activity on itself and on other proteins. (**C**) Murata *et al.* proposed a model where PINK1 is stabilized in the OMM by interaction with other proteins. TRAF6, which is recruited by SARM1, decorates PINK1 with poly-K63 ubiquitin chains further stabilizing PINK1 and preventing its translocation to the IMM. This association also promotes the interaction between PINK1 and Tom20 on depolarized mitochondria. Parkin recruitment is dependent on Akt activation which is caused by PINK1. The autophosphorylation activity of PINK1 may be involved in the mechanism.

Besides the loss of the mitochondrial membrane potential, complex I dysfunction has been reported as another main trigger of mitophagy (Wu *et al.*, 2013; Hoepken *et al.*, 2007; Koh and Chung, 2012). Complex I is involved in the establishment of the electrochemical gradient across the IMM and hence is necessary but not essential to maintain the mitochondrial membrane potential. Complex I mutations may lead to impaired transport of H^+ and decrease the membrane potential; however, mitochondria and the MRC are very dynamic entities and, as a consequence of complex I dysfunction, the quantity and/or activity of other complexes (namely complex II) may be increased to supress the diminished function of the defective component.

Moreover, complex I is the main source of mitochondrial ROS, especially when it is not completely functional either by usage of inhibitors (e.g. rotenone, paraquat, MPTP or as consequence of mutations. So, complex I is often correlated with increased oxidative damage, which may by itself be a cause of mitochondrial damage and trigger mitophagy.

1.6. LHON

Mitochondrial cytopathies form a heterogeneous group of multisystem disorders which are related by the main role of mitochondria in the pathogenic mechanism. The main affected tissues (i.e. nervous system, muscle and liver) are those which are more dependent on the mitochondrial function, namely for ATP production. These disorders can be caused by diverse types of mutations, both in the mitochondrial genome and/or the nuclear genome. Furthermore, the clinical manifestations are diverse owing to the non-uniform distribution of mitochondria in different tissues (mitotic segregation), different levels of altered mtDNA copies (heteroplasmy). Routine laboratorial tests that can be used to diagnose LHON involve biochemical, but mainly genetic and proteomic studies including analysis of the MRC activity, amino acid profile and DNA sequencing.

LHON is a maternally inherited disorder of the optic nerves, causing painless acute or subacute onset of bilateral loss of vision, being one of the most common causes of blindness in young males (Phasukkijwatana *et al.*, 2010).

This pathology was first described by the german ophthalmologist Theodor Leber in 1871 (Leber, 1871) and since then, several studies have been performed in order to reach a better understanding of its mechanism.

At the molecular level, several mutations in the mitochondrial genome have been identified as the pathogenic cause of the disease, from which three are the most frequent – m.11778G>A, m.3460G>A and 14484T>C –, that translate into missense mutations in three different subunits of the MRC complex I – ND4 p.R340H, ND1 p.A52T and ND6 p.M64V, respectively (Carelli *et al.*, 2002; Giordano *et al.*, 2013; Phasukkijwatana *et al.*, 2010).

Besides genetic factors, several environmental factors have also been indicated as potential triggers for LHON. Alcohol and tobacco are the leading potential factors that determine the non-genetic susceptibility to LHON (Carelli *et al.*, 2002).

The clinical manifestations of LHON include fundus changes such as telangiectatic microangiopathy which may precede the onset of visual loss. At fundus examination, the main features are the early drop out of the papillo-macular bundle, the oedematous appearance of the adjacent nerve fibre layer and the enlarged and tortuous peripapillar vessels. Upon examination of the visual field, cecocentral scotoma is usually detected with variable degrees of preservation of peripheral vision. Furthermore, the visual loss is often bilateral and asynchronous with a lag time of weeks to months between maximum optic atrophy of both eyes. Athough rare, recovery cases have been reported; if this does not occur, the visual loss stabilizes one year after the onset, leaving a typical pale optic disc more marked on the temporal side (Nikoskelainen *et al.*, 1994; Carelli *et al.*, 2002; Giordano *et al.*, 2013).

Concerning the histopathology, LHON is characterized by a severe loss of retinal ganglion cells (RGCs) caused by a degenerative process, and variable degrees of myelination in degenerating axons, containing swollen mitochondria, mainly in the central portion of the optic nerve (Carelli *et al.*, 2002).

The initial non-myelinated part of the optic nerve is rich in mitochondria, presenting an intense COX staining. When axons begin to be myelinated, the number of mitochondria sharply decreases, as observed by the COX-negative staining of this region. This asymmetry may translate the energetic needs of these different regions. Transmitting action potentials across unmyelinated axons is highly energy demanding while saltatory conduction in myelinated axons is faster and requires less energy. The small calibre fibres of the optic nerve, mostly belonging to the papillo-macular bundle, responsible for central vision, have a low volume to surface ratio, meaning that the energy demand is high while the energy source is limited. Moreover, the thickness of the myelin sheath is low and the firing rate of these neurons is high, further increasing the need for energy supply and are thus the fibres in the most disadvantageous energetic conditions among those that constitute the optic nerve (Carelli *et al.*, 2002).

Clinical manifestations of LHON such as disc swelling and microangiopathy show that the unmyelinated portion of the papillo-macular bundle is likely to be involved in the pathogenic mechanism. In fact, this is the most sensitive part of the fibre since the energy requirements are high in this region in order to sustain the propagation of action potentials, as mentioned before. Considering that mutations causing LHON correlate with energy depletion due to impairment of the MRC, it is reasonable to state that neurons composing the papillo-macular bundle, more specifically, their unmyelinated region, are particularly affected in LHON patients (Carelli *et al.*, 2002).

Electron microscopy studies performed on optic nerves of LHON patients show an unusual accumulation of mitochondria and other cell components as well as cytoskeleton changes in the myelinated portion of the nerve. This has been correlated with a deficient axonal transport. Since motor proteins (i.e. kinesins and dyneins) require ATP hydrolysis to perform their function, axonal transport may be impaired in neurons presenting energy deficits. However, the energy-depletion model is not satisfactory to explain the LHON phenotype since it does not explain why RGCs are the primary highly energy-demanding cells being affected. Other factors such as ROS production and oxidative stress must also be considered since they may arise from mutations which render complex I less efficient, and may cause severe damage to cell components that lead to cell degeneration and death (Carelli *et al.*, 2002).

Modification of the myelin sheath has also been reported in optic nerves from LHON patients. Demyelination is common, being a hallmark of the degenerative process. However, remyelination is also observed, mainly in patients harbouring the m.14484T>C mutation which presents a higher chance of visual recovery. The hypothesis of LHON as a myelin pathology is not to disregard since a subset of LHON patients also presents more diverse neurological symptoms (such as widespread myelin pathology in the central nervous system). These cases are known as LHON-*plus* and resemble the clinical presentation of multiple sclerosis (Carelli *et al.*, 2002).

Currently, LHON is characterized by incomplete "penetrance" since multiple cases have been reported where not all homoplasmic carriers of LHON mutations present manifestations of the disease. So, it can be concluded that the mutations in the mitochondrial genome are necessary but not sufficient to cause optic atrophy, and other factors must play a significant role in the etiopathogeny (Giordano *et al.*, 2013; Phasukkijwatana *et al.*, 2010).

To date, LHON is not fully understood and many questions still lack an explanation. These include: (i) incomplete "penetrance"; (ii) gender bias; (iii) age of onset; (iv) cell type specificity; (v) sequential loss of vision in both eyes; (vi) spontaneous recovery in some patients.

CHAPTER 2

AIMS

2. AIMS

LHON is one of the most common mitochondrial cytopathies and besides presenting typical clinical manifestations, the pathogenic mechanisms underlying the disease are still poorly understood. Being the most complex component of the MRC, complex I is still object of many studies and discoveries regarding both its structure and function are invaluable to understand not only LHON but also other mitochondrial cytopathies and even to provide deeper knowledge on the function of the MRC.

The herein presented work aimed to step forward in the understanding of the molecular mechanisms of LHON, providing new knowledge on the MRC to basic researchers, and additional diagnosis tools to clinicians. Ultimately, this work opens new paths on the identification of pharmacological targets to ameliorate the symptoms of LHON patients accordingly to the cellular phenotype.

More specifically, the aims of this work were:

- Evaluate the impact of the m.11778G>A mutation on the cellular function and homeostasis mainly in terms of mitochondria-related processes.
- Carry out a proteomics study to quantify ND4 and the relative ratios of MRC complexes.
- Study the assembly of complex I.
- Analyse the status of the autophagy pathway.

CHAPTER 3

PATIENTS AND METHODS

3. PATIENTS AND METHODS

3.1. Patients and Samples

Biological samples (skin biopsies and/or peripheral blood) were collected from the individuals investigated in the present study during diagnostic investigation of a patient with LHON-*plus*, at the LBG. The proband is a Portuguese female patient followed in the Metabolic Diseases Unit of the Hospital Pediátrico de Coimbra and presently, since the age of 18 years old, in the Neurology Department of the Centro Hospitalar e Universitário de Coimbra. This patient was diagnosed with LHON-*plus* at the age of 3 years old and the case was previously reported (Grazina *et al.*, 2007). A skin biopsy was collected at that age and a new skin biopsy was performed at the age of 20 years old, in the context of a medical intervention. Blood samples were also obtained at the same age.
Skin biopsies and/or peripheral blood from healthy Portuguese individuals without clinical evidence of a mitochondrial disorder, collected in the context of other medical interventions, were used as control samples in the experiments. The biochemical and genetic screening of the control samples was carried out by spectrophotometric bioanalytical evaluation, and DNA automated sequencing or PCR-RFLP to check for cellular and molecular indicators of mitochondrial cytopathies.
Data concerning the characterization of the samples is presented in Table 3.
All samples were obtained following informed consent; all ethical, social and legal issues as privacy and data protection were also taken into account throughout the entire study. This study was approved by the Ethics Committee of the Faculty of Medicine, University of Coimbra.
To the date of execution of this work, it was not possible to obtain further samples of skin fibroblasts.

Table 3 – Characterization of the samples used in this study.

Sample	Tissue	Gender	Age at collection / yo
Patient-3yo	Blood	F	3
Patient-3yo	Skin biopsy	F	3
Patient-20yo	Blood	F	20
Patient-20yo	Skin biopsy	F	20
Mother	Blood	F	40
Mother	Skin biopsy	F	40
Father	Blood	M	42
Control 1	Skin biopsy	F	11
Control 2	Skin biopsy	F	12
Control 3	Skin biopsy	F	16
Control 4	Blood	F	38
Control 5	Blood	F	23
Control 6	Blood	F	10
Control 7	Blood	F	42

3.2. Materials and Methods

3.2.1. Biological samples

Isolation of lymphocytes from peripheral blood
Peripheral blood samples (9 mL) were collected by venipuncture to sterile tubes containing EDTA. The blood was diluted 1:1 in PBS and carefully laid on top of 10 mL of Ficoll-Paque (GE Healthcare Life Sciences) using a syringe with needle. Following centrifugation at 800 g for 10 min at room temperature, the buffy coat was collected and washed with PBS. Lymphocytes were pelleted by centrifugation. After resuspension of the obtained pellet in 50-200 µL of PBS, the cell suspension was stored at -80 ºC.

Culture of human primary fibroblasts
Skin biopsies were collected in the hospital under local anaesthesia and immediately placed in sterile Mg^{2+}/Ca^{2+}-free HBSS. Following the reception of skin biopsies, they were processed in sterile conditions. Fibroblasts were grown in complete medium: Ham's F-10 (Gibco, Life Technologies)

supplemented with 20% fetal bovine serum (Gibco, Life Technologies), 4 mM GlutaMAX (Gibco, Life Technologies), 2.5 mM sodium pyruvate (Gibco, Life Technologies), 65 µg mL^{-1} uridine (Sigma-Aldrich, 250 U mL^{-1} penicillin (Gibco, Life Technologies), 250 µg mL^{-1} streptomycin (Gibco, Life Technologies), 250 µg mL^{-1} kanamycin (Sigma-Aldrich), 2.5 µg mL^{-1} amphotericin B (Gibco, Life Technologies), 2% Ultroser G (Gibco, Life Technologies). Incubation took place at 37 ºC, 5% CO_2 and adequate humidity levels in appropriate flasks. When confluent, cells were passaged using 0.05% trypsin. Culture medium was renewed twice a week. Fibroblasts were used for the described techniques only upon reaching confluence. All handling was performed in aseptic conditions in a laminar flow cabinet using sterile instruments and reagents.

3.2.2.Genetic analysis

Total DNA extraction
Total DNA was extracted from lymphocytes, fibroblasts and muscle using the phenol-chloroform method according to standard protocols (Sambrook *et al.*, 1987; Moore *et al.*, 1997, prior to this work, at LBG.

PCR-RFLP
Total DNA was amplified by PCR using a protocol optimized at the LBG. Briefly, total DNA was added to the PCR master mix containing 200 µM of each dNTP (GE Healthcare Life Sciences), 1 U of recombinant Taq DNA polymerase (GE Healthcare Life Sciences), 1x Taq polymerase buffer and each primer (forward and reverse). In order to confirm the presence of the amplification product, the mix was run on an agarose gel stained with ethidium bromide. This procedure was followed by RFLP analysis with endonuclease *Mae III* (Roche) according to the manufacturer's indications. Finally, the products were run on an agarose gel stained with ethidium bromide. Detection of bands was carried out using the ChemiDoc XRS+ Imaging System (Bio-Rad).

mtDNA copy number analysis
Total DNA from fibroblasts and lymphocytes was used to determine the mitochondrial DNA content by real-time PCR (qPCR) according to previously described protocols (Venegas *et al.*, 2011). The qPCR reactions for each locus (*TRNL1* and *B2M*) were performed in triplicate. The intensity of the SYBR Green fluorescence signals were detected using a 7500 Fast Real-Time PCR System (Applied Biosystems) and the results were analysed using the corresponding software (7500 Fast Software v2.0.4.). Quantification of the mtDNA copy number is obtained using the $2^{-\Delta\Delta C_t}$ method, where $\Delta\Delta C_t = \Delta C_t^{Sample} - \Delta C_t^{Control}$ and $\Delta C_t = C_t^{TRNL1} - C_t^{B2M}$.

3.2.3.Protein analysis

Spectrophotometric bioanalytical evaluation
Human primary fibroblasts were pelleted from six T_{25} culture flasks and washed twice with PBS prior to resuspension in the same buffer and storage at -80 ºC for 8 days. Ended this standardized period of time, samples (fibroblasts from cell culture or lymphocytes isolated from peripheral blood samples) were subjected to two freeze-thaw cycles. The spectrophotometric determination of the catalytic activity of the MRC complexes and segments was performed as described elsewhere using a SLM AMINCO DW2000 UV-VIS spectrophotometer (Grazina, 2012). The reactions used in the previously described assays are presented below (Eq. 2 – 13; the species whose absorbance is being measured are represented in bold). The enzymatic activities of all respiratory complexes and segments were normalized for total protein mass, determined by the Bradford method (Bradford, 1976), and citrate synthase activity to correct for variations in mitochondrial content (Trounce *et al.*, 1996). All measurements were performed at 37 ºC using a temperature-controlled cuvette jacket.

Complex I
NADH + H^+ + Q ⟶ NAD^+ + QH_2 Eq. 2

Complex II
Succinate + Q ⟶ Fumarate + QH_2 Eq. 3
QH_2+**DCPIP^{Ox}** ⟶ Q + $DCPIP^{Red}$ Eq. 4

Complex III

QH_2 + Cyt c^{Ox} ⟶ Q + **Cyt c^{Red}** Eq. 5

Complex IV

Cyt c^{Red} + O_2 ⟶ Cyt c^{Ox} + H_2O Eq. 6

Complex V

Mg[ATP] ⟶ Mg[ADP] + P_i Eq. 7

Mg[ADP] + Phosphoenolpyruvate ⟶ Mg[ATP] +Pyruvate Eq. 8

Pyruvate+ **NADH** + H^+ ⟶ Lactate + NAD^+ Eq. 9

Segment I+III

NADH + H^+ + Cyt c^{Ox} ⟶ NAD^+ + **Cyt c^{Red}** Eq. 10

Segment II+III

Succinate + Cyt c^{Ox} ⟶ Fumarate + **Cyt c^{Red}** Eq. 11

Citrate synthase

Oxaloacetate + Acetyl-S-CoA ⟶ Citrate + CoA-S^- Eq. 12

CoA-S^- + DTNB ⟶ CoA-S-S-Nitrobenzoate + **Thionitrobenzoate** Eq. 13

Preparation of mitochondria-rich fractions from cultured cells

Human primary fibroblasts were grown to confluence, as described above. After being washed and scraped from the culture flasks, cells were homogenized at 4 ºC using a glass/Teflon homogenizer in isolation buffer (20 mM HEPES, 10 mM KCl, 1.5 mM $MgCl_2$, 250 mM sucrose, 1 mM EDTA, 1 mM EGTA, pH 7.4) containing protease inhibitors (1 mM DTT, 1 µg mL^{-1} chymostatin, 1 µg mL^{-1} leupeptin, 1 µg mL^{-1} antipain, 1 µg mL^{-1} pepstatin A and 0.1 mM PMSF). The lysate was centrifuged at 700 g for 12 min at 4 ºC in order to sediment mainly cell debris and nuclei. The supernatant was then centrifuged at 12000 g for 20 min at 4 ºC to obtain the mitochondrial pellet, which was solubilized (10 mM Tris-acetate, pH 8.0, 5 mM $CaCl_2$, 0.5% nonidet P-40, 1 mM DTT, 1 µg mL^{-1} chymostatin, 1 µg mL^{-1} leupeptin, 1 µg mL^{-1} antipain, 1 µg mL^{-1} pepstatin A and 0.1 mM PMSF) prior to being stored at -80 ºC.

Denaturing electrophoresis

Samples were analysed by SDS-PAGE according to the method previously described (Schägger, 2006). Total protein content of mitochondria-enriched fractions was quantified using the Bradford method (Bradford, 1976). Volumes were adjusted according to the total protein concentration of each sample and then mixed with reducing Laemmli sample buffer 4x (Laemmli, 1970); this mixture was incubated for 5 min at 95 ºC and loaded into polyacrylamide gels (4-20% Mini-PROTEAN TGX Precast gel, Bio-Rad). Each lane of the gel was loaded with 30 µg of total protein.

Western blot

Proteins were transferred from polyacrylamide gels to a PVDF membrane (Hybond P 0.45 µm, Amersham) for 90 min at 100 V, at 4ºC. Blocking was carried out using 5% skimmed milk in TBS-T (50 mM Tris, 150 mM NaCl, 0.1% Tween-20) for 1 h at room temperature. Afterwards, the membranes were incubated with the primary antibody solution (overnight, 4ºC). After washing the membranes in TBS-T, they were incubated with secondary antibody solution (90 min, room temperature). Afterwards, membranes were incubated with chemiluminescence substrate (Clarity Western ECL Substrate, Bio-Rad) and detection was carried out using the VersaDoc Imaging System 3000 (Bio-Rad). Information concerning antibodies is presented in Table 4.

Table 4 – List of antibodies used in this study.

Immunogen	Host species	Clonality	Conjugate	Supplier	Clone
Citrate Synthase	Rb	m	-	Abcam	EPR8067
OxPhos cocktail	Ms	m	-	Abcam	ab110411
ND4	Ms	p	-	Abnova	A01
LC3	Rb	p	-	Pierce	16930
p62	Ms	p	-	Millipore	11C9.2
Ms	Gt	p	HRP	Bio-Rad	
Ms	Gt	p	AF633	Bio-Rad	
Rb	Gt	p	HRP	Bio-Rad	
Rb	Gt	p	AF568	Bio-Rad	

Native electrophoresis

Samples were processed according to the protocol described elsewhere (Wittig *et al.*, 2006; Wittig *et al.*, 2007). Volumes of isolated lymphocytes containing equal amounts of total protein were solubilized. Firstly, mitochondria were sedimented by centrifugation at 20000 g for 10 min at 4 ºC. After discarding the supernatant, samples were vortexed with 10 µL μg^{-1} of buffer (50 mM Tris-glycine, 50 mM NaCl, 2 mM 6-aminohexanoic acid, 1 mM EDTA, pH 7.0) and solubilised by incubation with a detergent (digitonin or DDM) for 10 min at 4 ºC. Following centrifugation at 20000 g for 20 min at 4 ºC, supernatants were supplemented with 50% glycerol and Coomassie Blue G-250 suspension (5% Coomassie Blue G-250, 500 mM 6-aminohexanoic acid). One anode buffer (25 mM Tris-glycine, pH 7.0) and two cathode buffers were used; deep blue cathode buffer B (7.5 mM Tris-glycine, 50 mM tricine, 0.02% Coomassie Blue G-250, pH 7.0) was replaced by blue cathode buffer B/10 (7.5 mM Tris-glycine, 50 mM tricine, 0.002% Coomassie Blue G-250, pH 7.0) when the running front reached 1/3 of the total running length. A molecular weight marker (NativeMARK Unstained Protein Standard, Life Technologies) and samples were loaded into polyacrylamide gels (4-20% Mini-PROTEAN TGX Precast gel, Bio-Rad) and run at 80 V at 4 ºC.

Polyacrylamide gel staining

Polyacrylamide gels were stained using standard protocols (Schägger, 2006). Polyacrylamide gels were first incubated in fixing solution (50% methanol, 10% acetic acid, 100 nM ammonium acetate) for 15-30 min, stained (0.025% Coomassie Blue G, 10% acetic acid) for 30-60 min and destained (10% acetic acid) twice for 15-60 min. Images were obtained by epi-illumination with white light.

3.2.4.Microscopy tools

Immunocytochemistry

Primary human fibroblasts were cultured in plastic dishes containing glass coverslips until confluent. Cells were then subjected to different treatments for two hours (no treatment, 3MA, serum-free medium, serum-free medium plus 3MA); after one hour of treatment the cells were inspected to assess the necessity to stop the treatments. Following, MitoTracker Green (1:10000 in HBSS; Invitrogen) incubation was carried out for 30 min to stain mitochondria. After washing with HBSS, cells were fixed with 4% PFA for 10 min after which they were further washed in PBS to remove the excess PFA. Permeabilization of cell membranes was performed using 0.2% Triton X-100 in PBS. Coverslips were washed and then blocked with 2% BSA for 20 min at room temperature. Primary antibody solutions were prepared in 0.05% BSA and incubated for 1 h at room temperature. Following washing, the secondary antibody solution was prepared in 0.05% BSA and incubated for 1 h at room temperature. After the final washing, coverslips were mounted on glass slides using Mowiol (Sigma-Aldrich). Information concerning antibodies is presented in Table 4.

Adenoviral infection

The generation of the recombinant plasmids and adenovirus used for expression of YFP-PH were described previously (Vieira *et al.*, 2005). Human primary fibroblasts were cultured on 35 mm µ-dishes (Ibidi LLC, Verona, WI). Once cells reach the desired confluence, the culture medium was removed and adenoviral transfection was carried out in Opti-MEM (Life Technologies) for 1 h at 37 ºC. After this time cells were incubated in culture medium overnight before being imaged.

Confocal microscopy
Immunostained cells were imaged using an inverted microscope (Leica SP5II AOBS, Leica). For live imaging experiments, cells were imaged with the same microscope using a stage heater regulated at 37 ºC and an incubation chamber with an atmosphere of 5% CO_2.

Electron microscopy
Cultured cells were fixed for 5 min with 5% glutaraldehyde in 0.1 M cacodylate buffer (pH 7.2) plus one drop of calcium chloride for every 5 mL of solution. Then, cells were scraped from the flasks, centrifuged and additionally fixed for 2 h with 2.5% glutaraldehyde in the same buffer. After washing, pellets were treated with 1% osmium tetroxide in cacodylate buffer for 1 h. After incubating overnight at 4 ºC with fresh cacodylate buffer, pellets were washed with 0.05 M cacodylate buffer and once with water for 10 min each. Contrasting was performed with 2% uranyl acetate for 1h in the dark. After three washing steps with water, samples were dehydrated by incubation in acetone solutions with crescent concentration (30%, 50%, 70%, 80%, 90%, 95%, 100%), 10 min each. Then pellets were impregnated using solutions with crescent resin:acetone ratios (1:2, 1:1, 1:0), 1.5 h each. Inclusion in resin blocks was carried out by polymerizing the absolute resin solution at 60 ºC for 24 h. Thin sections were obtained and deposited in carbon-coated cupper grids. Additional contrasting was obtained with lead citrate. The final product was observed under the Tecnai G2 Spirit (FEI) transmission electron microscope and images were acquired using the software AnalySIS 3.2.

3.2.5. Computational tools

***In silico* tools**
The *in silico* tools used in this work are summarized in Table 5.

Table 5 – List of *in silico* tools used in this study.

Tool	Purpose	Reference
Clustal W2	MSA	Larkin *et al.*, 2007
Clustal O	MSA	Sievers *et al.*, 2011
TM-Coffee	MSA/Structure prediction	Notredame *et al.*, 2000
SIFT	Functional prediction	Ng and Henikoff, 2003
PolyPhen-2 v2.2.2	Functional prediction	Adzhubei *et al.*, 2010
PROVEAN v1.1	Functional prediction	Choi *et al.*, 2012
MutationAssessor release 2	Functional prediction	Reva *et al.*, 2011
PANTHER PSEC	Functional prediction	Thomas *et al.*, 2003
MutPred	Functional prediction	Li *et al.*, 2009
SNPs&GO	Functional prediction	Calabrese *et al.*, 2009
SOSUI	Structure prediction	Hirokawa *et al.*, 1998
DAS	Structure prediction	Cserzö *et al.*, 1997
SPLIT	Structure prediction	Jurietić *et al.*, 2002
DPM	Structure prediction	Deléage and Roux, 1987
DSC	Structure prediction	King and Sternberg, 1996
GORI	Structure prediction	Garnier *et al.*, 1978
GORIII	Structure prediction	Gibrat *et al.*, 1987
GORIV	Structure prediction	Garnier *et al*, 1996
HNN	Structure prediction	Guermeur *et al.*, 1999
PHD	Structure prediction	Rost and Sander *et al.*, 1993
PREDATOR	Structure prediction	Frishman and Argos *et al.*, 1996
SIMPA96	Structure prediction	Levin, 1997
SOPM	Structure prediction	Geourjon and Deléage, 1994
SOPMA	Structure prediction	Geourjon and Deléage, 1995
MLRC	Structure prediction	Guermeur *et al.*, 1999
YASPIN	Structure prediction	Lin *et al.*, 2005
HMMTOP	Structure prediction	Tusnády and Simon, 2001
TMMOD	Structure prediction	Kahsay *et al.*, 2005
Phobius	Structure prediction	Käll *et al.*, 2004
SPOCTOPUS	Structure prediction	Viklund *et al.*, 2008
TOPCONS	Structure prediction	Bernsel *et al.*, 2009
PSIPRED	Structure prediction	Jones, 1999
I-TASSER	Structure prediction	Roy *et al.*, 2010
ConSurf	Structure prediction	Celniker *et al.*, 2013
MTDB	MtDNA database	Ingman and Gyllensten, 2006
PDB	Structure database	Bernstein *et al.*, 1977
UniProt	Protein database	UniProt Consortium, 2014

Image analysis
Images from confocal microscopy, electron microscopy and ECL revelation of western blots were processed with ImageJ.

Statistical analysis
Statistical analysis of the results (Mann-Whitney test) was performed using GraphPad Prism version 6.00 for Windows, GraphPad Software, San Diego California USA, www.graphpad.com. Significance is considered when $p<0.05$. Results of the statistical significance between sample and respective control is represented as * for $0.050 \geq p > 0.010$, ** for $0.010 \geq p > 0.001$ and *** for $p \leq 0.001$.

CHAPTER 4

RESULTS AND DISCUSSION

4. RESULTS AND DISCUSSION

4.1. *In silico* study of the m.11778G>A sequence variation

Technology has empowered many scientific breakthroughs with the advent of new possibilities, higher levels of detail, more precise determinations and faster processing times. Creation of complex networks of cell components from experimental data is a relevant source of information to understand cell processes. Sharing that information is now possible by diverse means and is an invaluable help to communicate and facilitate the access of data around the world.

A plethora of *in silico* tools is being created. Some of them have the purpose to analyse the impact of protein alterations in the overall cell context, using different methods and data. A commonly used tool to determine the importance of a residue in the protein function or structure is MSA, which provides clues on the evolutionary conservation of given residues.

Proteins which are crucial for the existence of cells and their correct function are preserved almost unaltered across evolution (e.g. tubulin and histones). Likewise, residues that are crucial for protein function are kept intact throughout evolution. This observation is further corroborated by selection mechanisms: if a conserved residue is mutated, the protein is likely to be dysfunctional and the survival of the cell (and of the entire organism) may be compromised. Thus, the possible sequence variations of a certain protein that are observed correspond to those which are not incompatible with life. Variations which give rise to disease are still observed, although at a relatively low frequency (for a general case).

In order to inspect the conservation of the mtDNA 11778 np and the ND4 Arg^{340} residue, homologue sequences from diverse species were aligned (Figure 8).

The prokaryotes *Escherichia coli* and *Thermus thermophilus* were included in this evolutionary study mainly because they will be used as models for the human complex I (section 4.2.).

Evolutionary conservation shows that both mtDNA 11778 np and the ND4 Arg^{340} residue are highly conserved throughout different eukaryotes (15/15). Besides np 11778, np 11777 is also conserved (15C /15) while np 11779 presents a lower conservation index (5C, 5T, 4A, 1G /15). This variation does not have impact at the protein level since the third base of the codon is less specific than the first and the second base in terms of codification for a given amino acid. In this case, the mitochondrial codons for arginine are CGN, withdrawing relevance from np 11779 since np 11777 and 11778 are the ones which define the information for Arg^{340} in ND4. Furthermore, conservation of the nucleotide sequences (Figure 8 A) is in accordance with the possible bacterial origin of mitochondria.

So, it can be concluded from this analysis that modifications in the mtDNA at position 11778 are probably associated to ND4 dysfunction.

Evolutionary conservation is one of the most used parameters to infer on the pathogenicity of a sequence variation. However, exceptions exist and one must be cautious when generalizing conclusions obtained from particular cases. For instance, the majority of disease-associated residues in membrane subunits of complex I are not highly conserved. Due to the critical role of this complex and the system where it is inserted, it is highly probable that mutations of residues that are critical for structure and/or activity do not present as diseases since they may not be well tolerated. Furthermore, if mutations in these residues occur, they are more probable to be observed in heteroplasmy/heterozygosity, since non-mutated proteins can rescue the deleterious effect of the mutation.

A

H. sapiens	1009	A	C	T	C	A	C	A	G	T	C	**G**	C	A	T	C	A	T	A	A	T	C	1029
P. paniscus	1009	A	C	C	C	A	C	A	G	T	C	**G**	C	A	T	C	A	T	A	A	T	T	1029
P. troglodytes	1009	A	C	C	C	A	C	A	G	T	C	**G**	C	A	T	C	A	T	A	A	T	T	1029
P. pygmaeus	1009	A	C	C	C	A	C	A	G	C	C	**G**	C	A	T	C	A	T	A	A	T	C	1029
M. mulatta	1009	A	C	C	C	A	C	A	G	C	C	**G**	T	A	C	C	A	T	A	C	T	A	1029
B. taurus	1009	A	T	C	C	A	C	A	G	C	C	**G**	A	A	C	C	A	T	A	A	T	T	1029
S. scrofa	1009	G	T	A	C	A	C	A	G	C	C	**G**	A	A	C	C	A	T	A	A	T	C	1029
C. lupus familiaris	1009	A	T	C	C	A	T	A	G	C	C	**G**	T	A	C	T	A	T	A	A	T	T	1029
M. musculus	1009	A	T	C	C	A	C	A	G	C	C	**G**	T	A	C	T	A	T	A	A	T	C	1029
R. norvegicus	1009	A	T	T	C	A	C	A	G	C	C	**G**	A	A	C	T	A	T	A	A	T	T	1029
C. porcellus	1009	A	T	T	C	A	C	A	G	C	C	**G**	T	A	C	T	A	T	A	A	T	T	1029
G. gallus	1009	A	C	A	C	A	C	A	G	C	C	**G**	C	A	T	T	C	T	T	A	T	C	1029
D. rerio	1012	A	C	T	C	A	T	A	G	C	C	**G**	G	A	C	C	A	T	A	A	T	C	1032
D. melanogaster	974	C	T	T	G	G	A	A	G	T	C	**G**	A	A	G	A	A	T	A	T	T	A	994
C. elegans	893	C	T	-	G	G	G	A	G	G	C	**G**	T	A	T	A	A	T	-	T	T	A	913
E. coli	1096	A	T	C	C	A	T	A	C	C	C	**G**	C	G	A	C	A	T	-	G	C	G	1116
T. thermophilus	1006	A	C	G	G	G	C	A	C	C	C	**T**	G	G	A	G	A	T	C	G	G	G	1026
							*		*								*						

B

H. sapiens	330	A	N	S	N	Y	E	R	T	H	S	**R**	I	M	I	L	S	Q	G	L	Q	T	350
P. paniscus	330	A	N	S	N	Y	E	R	T	H	S	**R**	I	M	I	L	S	Q	G	L	Q	T	350
P. troglodytes	330	A	N	S	N	Y	E	R	T	H	S	**R**	I	M	I	L	S	Q	G	L	Q	T	350
P. pygmaeus	330	A	N	S	N	Y	E	R	T	H	S	**R**	I	M	I	L	S	Q	G	L	Q	T	350
M. mulatta	330	A	N	S	N	Y	E	R	T	H	S	**R**	T	M	L	L	S	R	G	L	Q	I	350
B. taurus	330	A	N	S	N	Y	E	R	I	H	S	**R**	T	M	I	L	A	R	G	L	Q	T	350
S. scrofa	330	A	N	T	N	Y	E	R	V	H	S	**R**	T	M	I	L	A	R	G	L	Q	T	350
C. lupus familiaris	330	A	N	S	N	Y	E	R	I	H	S	**R**	T	M	I	L	A	R	G	L	Q	T	350
M. musculus	330	A	N	S	N	Y	E	R	I	H	S	**R**	T	M	I	M	A	R	G	L	Q	M	350
R. norvegicus	330	A	N	T	N	Y	E	R	I	H	S	**R**	T	M	I	M	A	R	G	L	Q	M	350
C. porcellus	330	A	N	S	N	Y	E	R	I	H	S	**R**	T	M	I	L	A	R	G	L	Q	T	350
G. gallus	330	A	N	T	N	Y	E	R	T	H	S	**R**	I	L	I	L	T	R	G	L	Q	P	350
D. rerio	331	A	N	T	S	Y	E	R	T	H	S	**R**	T	M	I	L	A	R	G	L	Q	M	351
D. melanogaster	318	A	N	V	S	Y	E	R	L	G	S	**R**	S	M	L	I	N	K	G	L	L	N	338
C. elegans	291	I	G	E	F	Y	H	T	S	G	S	**R**	M	I	Y	F	M	S	S	F	F	S	311
E. coli	359	C	G	Q	L	Y	E	R	I	H	T	**R**	D	M	R	M	M	G	G	L	W	S	379
T. thermophilus	329	A	G	R	L	Y	E	R	T	G	T	**L**	E	I	G	R	Y	R	G	L	A	Q	349
				.		*	.			:		:				.	:						

Figure 8 – Evolutionary study of m.11778G>A and ND4 p.340. (**A**) Alignment of the mtDNA highlighting the evolutionary conservation of position 11778. Sequences were obtained from the NCBI Nucleotide database (**B**) Evolutionary conservation of the ND4 protein for residue 340. Sequences were obtained from the NCBI Protein database. DNA and protein sequences were aligned with ClustalW2; consensus coherence was determined by the alignment algorithm and is presented in the bottom of each alignment panel.

The number of servers for prediction of diverse biological parameters is growing both in number and diversity. For instance, nsSNPs, which lead to an amino acid substitution, can be analysed in terms of their impact on cell homeostasis, this is, their pathogenic potential. This prediction compares the function of the altered protein and the wild-type. According to the server, different parameters can be used to reach a pathogenicity score; examples of those parameters are evolutionary conservation and structural information (when available).

In order to assess the pathogenic potential of the m.11778G>A sequence variation as the ND4 p.R340H amino acid substitution, diverse servers were used to produce *in silico* predictions.

SIFT (Sorting Intolerant From Tolerant) uses sequence homology to predict the impact of an amino acid substitution in the function of a given protein and, hence, potentially giving rise to an altered phenotype. The prediction method used by SIFT considers that conserved amino acids are the most critical for protein function and modifications in those are very likely to be deleterious. Furthermore, the method is flexible and contemplates the characteristics of amino acids. For example, if a position in the alignment contains only one amino acid, changes to any other amino acid will be predicted as deleterious; however, if a position contains diverse amino acids that share a certain characteristic (e.g. polarity, size), changes to amino acids with the same characteristics will be classified as tolerated while changes to amino acids with distinct characteristics will be predicted as affecting the function of the protein (Ng and Henikoff, 2003).

After imputing a protein sequence, SIFT searches for proteins what are related to the query and aligns the set of sequences. Then, based on the produced alignment, SIFT calculates the probability that the selected amino acid at the specified position is tolerated (given that the most frequent amino acid at the same position is classified as tolerated). If the final score is inferior to a certain cutoff (0.05), the substitution is considered deleterious (Ng and Henikoff, 2003).

PolyPhen-2 (Polymorphism Phenotyping v2) also uses information from sequence alignments; however, this algorithm makes use of additional structural properties (e.g. accessible surface area of amino acid residue) to predict the pathogenicity of single amino acid substitutions. After imputing a sequence and the desired variations, the algorithm gathers similar sequences to the query by homology search and performs an initial MSA; then, this alignment is refined and clustered, providing sufficient data to output the results as scores. This prediction algorithm also uses information from annotation and structure. Two datasets were used to train this algorithm: HumDiv (contains all damaging alleles with known effects on the function of proteins causing Mendelian diseases) and HumVar (contains all human disease-causing mutations from UniProtKB together with common human nsSNPs without annotated involvement in disease, which were considered as non-damaging). The first set is used to diagnose Mendelian diseases, enabling the segregation of mutations with drastic effects from common variations and mildly damaging alleles. The second set is used to evaluate rare alleles at loci that may be disease-related, where even mildly deleterious variations must be treated as damaging (Adzhubei *et al.*, 2013; Adzhubei *et al.*, 2010; Ramensky *et al.*, 2002).

Unlike most pathogenicity prediction servers, PROVEAN (Protein Variation Effect Analyzer) accounts for all classes of protein sequence variations (i.e. single amino acid substitution, insertion, deletion and multiple substitutions). The algorithm uses MSA of proteins that present sequence similarity with the query. These sequences are provided by two different datasets, Human Polymorphisms and Disease Mutations (for single substitutions) and UniProtKB/Swiss-Prot (for insertions, deletions and multiple substitutions). In order to provide a clear output, the algorithm uses a threshold (-2.282) which confers the highest balanced accuracy (Choi et al., 2012).

Servers that use evolutionary conservation via MSA (e.g. SIFT, PolyPhen-2, Mutation Assessor) may present different predictions despite using the same methodology. Besides additional contributions from other classes of data, this variation can be explained by distinct algorithmic and processing of the results arising from the alignment. Moreover, the method and databases used to fetch related sequences and the alignment algorithm also contribute to the variation.

PANTHER PSEC (position specific evolutionary conservation) also relies on sequence similarity. However, this algorithm uses this type of data in a different fashion. The first step of the algorithm is to find similar sequences and align them. Then, the same is done for the altered protein sequence. The differences in the alignments of both wild-type and mutant sequences are quantified and presented as a score which in turn can be transposed to the probability of the substitution being deleterious, $P_{deleterious}$; the more negative the alignment score difference, the higher $P_{deleterious}$. The cutoff for segregation of deleterious and neutral mutations is -3, which corresponds to $P_{deleterious} = 0.5$ (Thomas *et al.*, 2003).

The aforementioned pathogenicity prediction servers were applied to the mutation which is central to this work. Results are presented below (Table 6, Figure 9) followed by some comments.

Table 6 – *In silico* pathogenicity prediction. Results from predictions concerning the pathogenicity of the single amino acid substitution ND4 p.R340H.

Algorithm	Prediction	Score	Range [a]
SIFT	Affects protein function	0.00	1 – 0
PolyPhen-2	Probably damaging	0.999	0 – 1
PROVEAN	Deleterious	-4.741	2 – -10 [b]
Mutation Assessor	High functional impact	4.605	-3 – 5
PANTHER PSEC		-4.29846	0 – -10
MutPred		0.866	0 – 1
SNPs&GO	Disease	0.771	0 – 1

[a] The values are presented in crescent order of pathogenicity.
[b] Values outside this range are permitted.

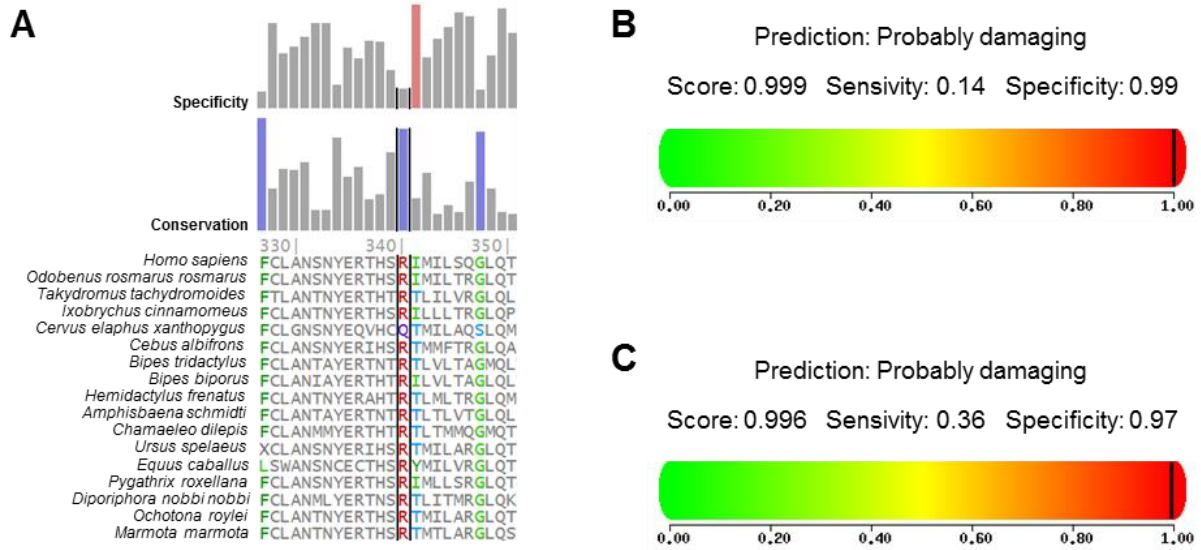

Figure 9 – Prediction of the pathogenicity of the ND4 p.R340H single amino acid substitution. (**A**) MutationAssessor (Reva *et al.*, 2011) non-redundant MSA results highlighting the evolutionary conservation of residue 340 across diverse species. Specificity: conservation within a subfamily and variation between subfamilies. Conservation: conservation across the entire family. Pathogenicity prediction results from PolyPhen-2: (**B**) HumDiv; (**C**) HumVar. Sensitivity: true positive rate .Specificity: true negative rate.

SIFT predicts that the arginine to histidine substitution in the ND4 sequence affects protein function despite the database used to search for related sequences for the alignment. The score of this prediction is 0.00, which is explained by the fact that the only tolerated amino acid at position 340 is arginine, being the other nineteen proteinogenic amino acids non-tolerated. PolyPhen-2 classifies the variation as probably damaging (HumDiv 0.999; HumVar 0.996). PROVEAN considers the substitution to be deleterious with a score of -4.741. PANTHER PSEC outputs a score of -4.29846 and a corresponding probability of the substitution being deleterious of 0.78558. MutPred provides information on overall modifications caused by the single amino acid substitution, such as loss of disorder (P = 0.0484), loss of solvent accessibility (P = 0.0576), gain of helix (P = 0.1736), loss of phosphorylation at S339 (P = 0.1879) and loss of loop (P = 0.2237).

Altogether, these predictions corroborate the role of the m.11778G>A sequence variation in pathogenic processes, linking it to protein dysfunction.

Despite these results, the wild-type and mutated residues share some physicochemical properties. This is corroborated by the low Grantham score (29 in a range of 5 – 215) (Grantham, 1974). So, there must be other factors that contribute to the defunctionalisation caused by the m.11778G>A variation at the protein level.

4.2. Analysis of the structural impact of m.11778G>A

Despite all prediction tools and pathogenicity assessors, basic biochemistry knowledge is invaluable when evaluating the impact of protein modifications. The understanding of how the properties of amino acids shape proteins and coordinate their function and interaction is of utmost importance to analyse the role of single amino acid substitutions.

In the case of the m.11778G>A sequence modification modifies residue Arg^{340} of the ND4 subunit of complex I to a histidine residue. Since, at physiological pH, arginine is a positively charged amino acid and histidine is neutral, the R340H substitution can disrupt intra- and inter-molecular interactions such as salt bridges and hydrogen bonds with neighbour acidic residues or H^+ acceptor groups. The reduction of the side chain size may also impart to the altered interactions.

However, in order to understand the effect of the local changes produced by the substitution, it is necessary to understand the spatial context of the altered residue.

As mentioned in section 1.3.1, there is no atomic-resolution structure of the human complex I available. While precluding the analysis of the human complex and imposing special caution on the conclusions made using non-human structures, the use of homologue complexes is the best opportunity to study complex I at the atomic scale (Figure 10).

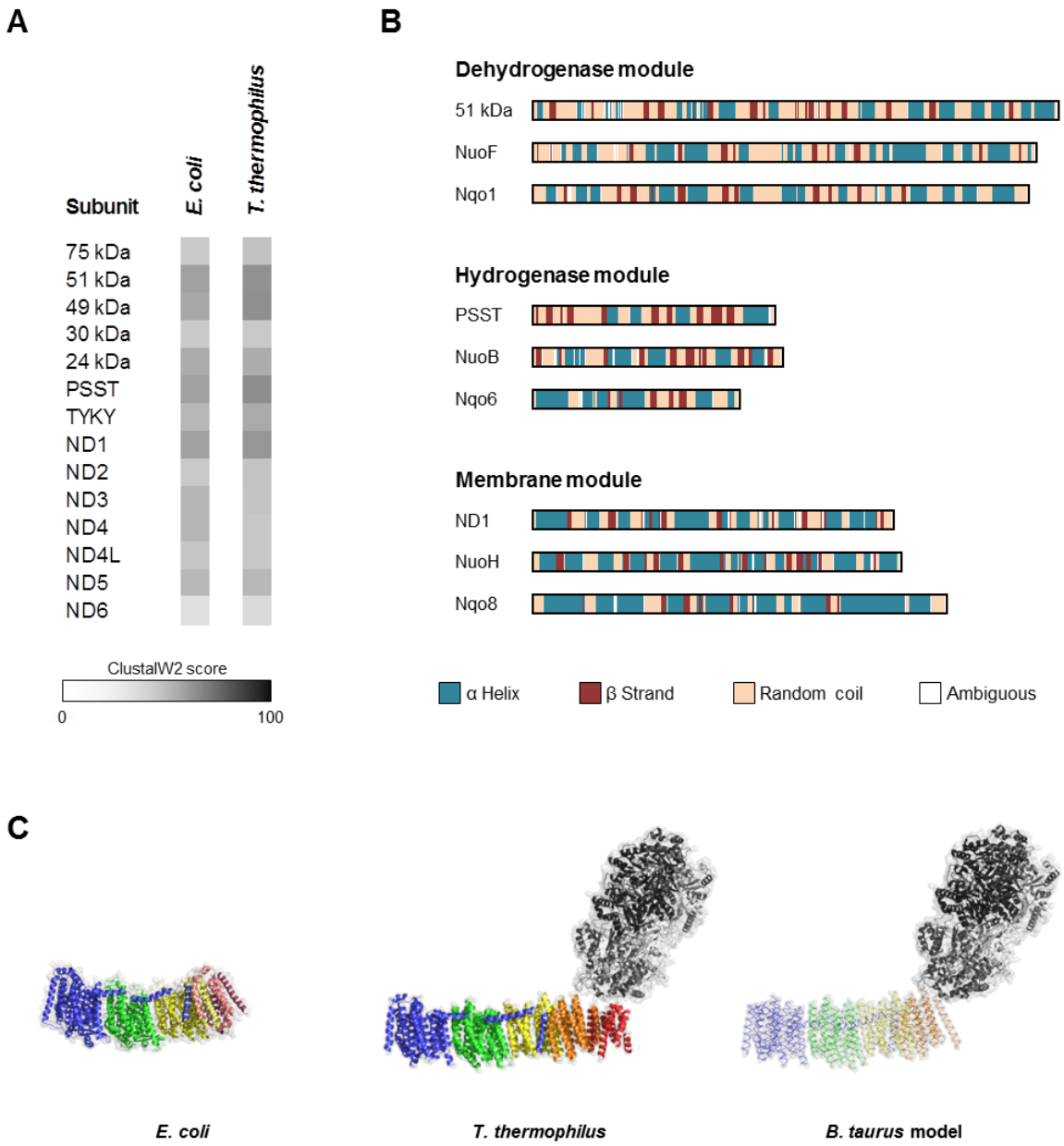

Figure 10 – Conservation of the primary, secondary, and quaternary structures of complex I. (**A**) The primary structure of the *Escherichia coli* and *Thermus thermophilus* complex I subunits were compared to their *Homo sapiens* homologues by sequence alignment using ClustalW2. Sequences were obtained from UniProt. ClustalW2 scores are presented as grayscale. (**B**) The secondary structure of representative complex I subunits of *Homo sapiens* (top), *Escherichia coli* (middle) and *Thermus thermophilus* (bottom) was predicted from their primary structure using diverse algorithms (see Figure 13). (**C**) The quaternary structure of complex I from *Escherichia coli* (left; PDB 3RKO (Efremov and Sazanov, 2011)) and *Thermus thermophilus* (centre; PDB 3M9S (Efremov *et al.*, 2010)) is presented from atomic-resolution data while *Bos taurus* complex I is presented as a model fitted from cryo-EM data (right; PDB 2YYB (Tomoike *et al.*, 2009)). Only the membrane portion of *Escherichia coli* complex I is available.

Primary sequences of the complex I subunits present low similarity, which is expected since a comparison between very distinct species is being established. However, differences are attenuated in the secondary structure prediction with shared motifs. Finally, the arrangement of the subunits in the quaternary structure of the organisms is maintained with the L-shape being a transversal feature across the analysed species.

In order to further investigate the similarity of ND4 primary structure with the species which atomic-resolution structure of complex I is available, sequence alignment was performed using diverse servers.

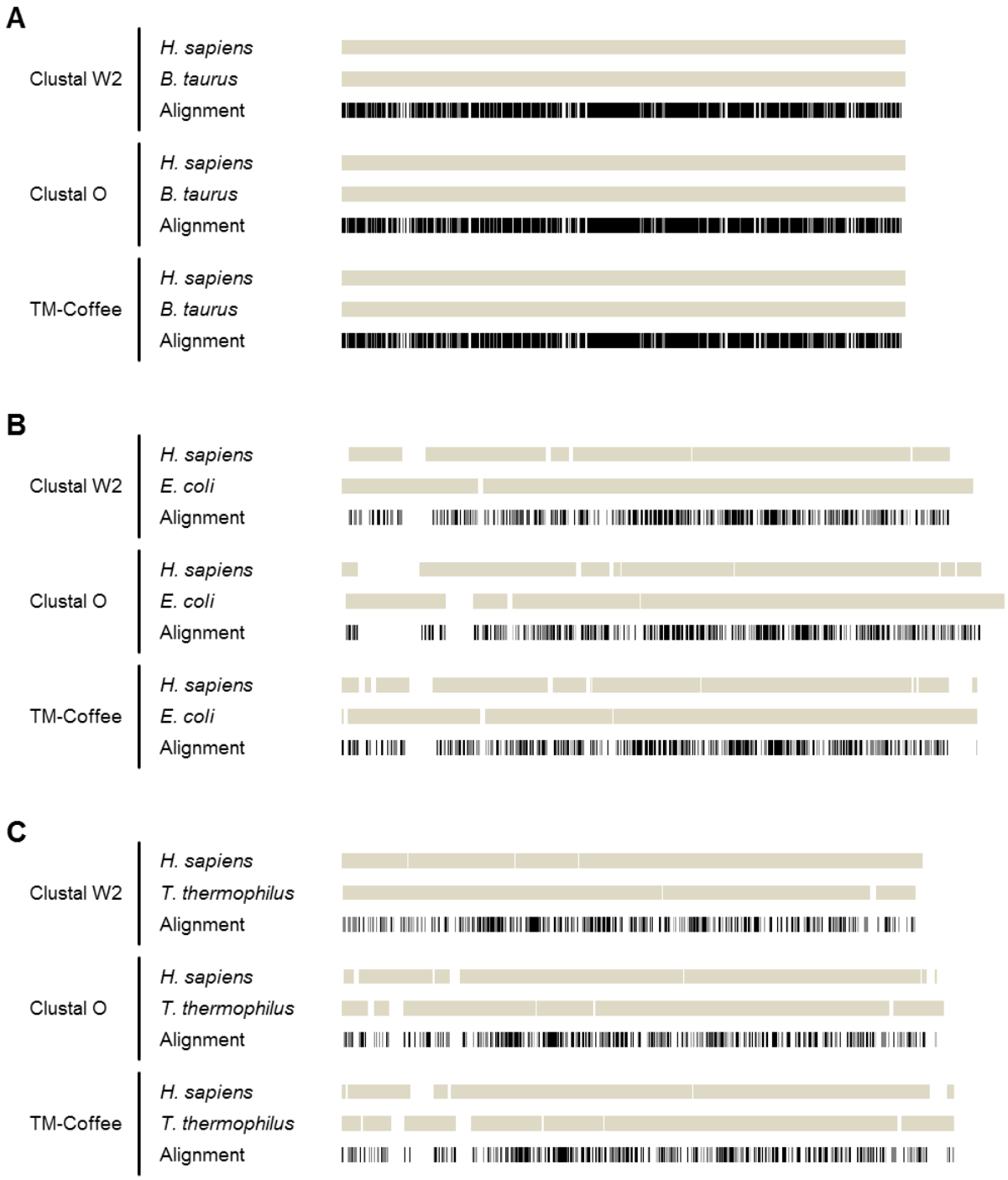

Figure 11 – Alignment of ND4 homologues. Alignment of *Homo sapiens* ND4 and (**A**) *Bos taurus* ND4, (**B**) *Escherichia coli* NuoM, or (**C**) *Thermus thermophilus* Nqo13 using diverse protein sequence alignment servers. The brown segments represent the aligned sequences and the blank spaces represent alignment gaps. Alignment scores are coloured from low (white) to high (black).

As expected, the results of the alignments present ND4 from *Bos taurus* as the most similar to the human homologue (Figure 11 A). *Thermus thermophilus* presents smaller and shorter alignment gaps than *Escherichia coli*. So, *Thermus thermophilus* seems to be a better model for ND4 than *Escherichia coli* since there are fewer differences in the primary structure.

However, comparison of the primary structure is not sufficient to determine which organism represents the best structural model available. In order to study the structure of the *Thermus thermophilus* and *Escherichia coli* ND4 subunit, the structure of complex I and the microenvironment of the residues homologue to *Homo sapiens* Arg^{340} were obtained from atomic resolution coordinates (Figure 12).

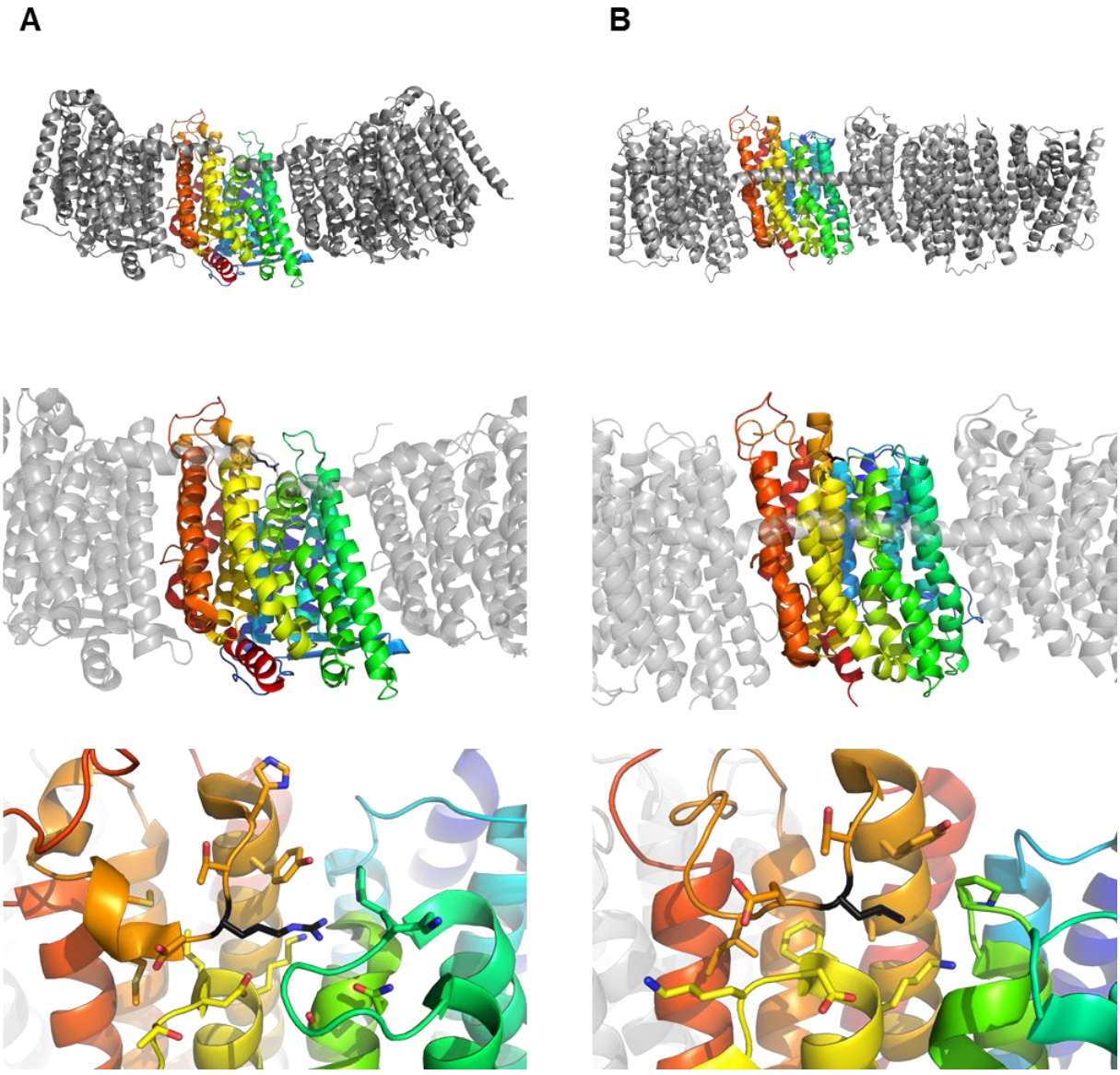

Figure 12 – Spatial characterization of Arg^{340}. (**A**) Using the crystal structure of the membrane portion of *Escherichia coli* complex I (PDB 3RKO (Efremov and Sazanov, 2011)), the ND4 subunit is spatially contextualized as well as residue Arg^{369} (correspondent to *Homo sapiens* Arg^{340}). (**B**) Comparison with the *Thermus thermophilus* structure (PDB 4HE8 (Baradaran *et al.*, 2013)), locating the corresponding residue Leu^{339}. The residues corresponding to *Homo sapiens* Arg^{340} are coloured black. The side chain of residues within 5 Å of the Arg^{340} homologues are presented as sticks.

As concluded before (section 4.1.), the *Thermus thermophilus* homologue of *Homo sapiens* Arg^{340} is Leu^{339}. Despite the chemical differences, the microenvironment of the homologue residues is similar (Figure 12 A bottom, B bottom), possibly indicating a functional role for this region of the subunit.

Taking into consideration the findings in the prokaryote complex I and in order to better understand the context of the amino acid substitution and its impact on the protein structure and stability in the human homologue, diverse *in silico* tools were used to predict secondary structure and topology, and to identify and assess the known SNPs of the *Homo sapiens* ND4 (Figure 13).

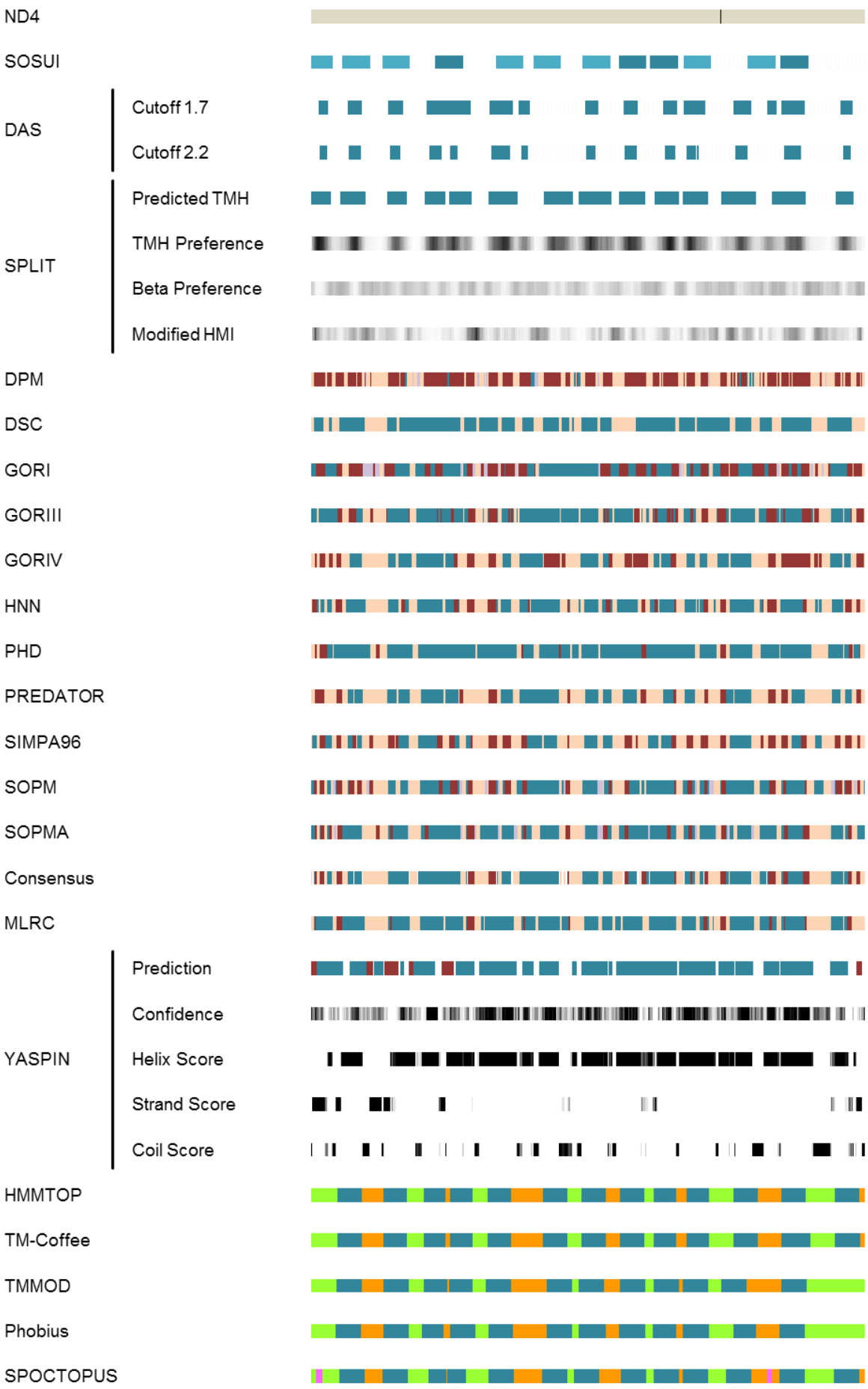
ND4
SOSUI
DAS
Cutoff 1.7
Cutoff 2.2
SPLIT
Predicted TMH
TMH Preference
Beta Preference
Modified HMI
DPM
DSC
GORI
GORIII
GORIV
HNN
PHD
PREDATOR
SIMPA96
SOPM
SOPMA
Consensus
MLRC
YASPIN
Prediction
Confidence
Helix Score
Strand Score
Coil Score
HMMTOP
TM-Coffee
TMMOD
Phobius
SPOCTOPUS

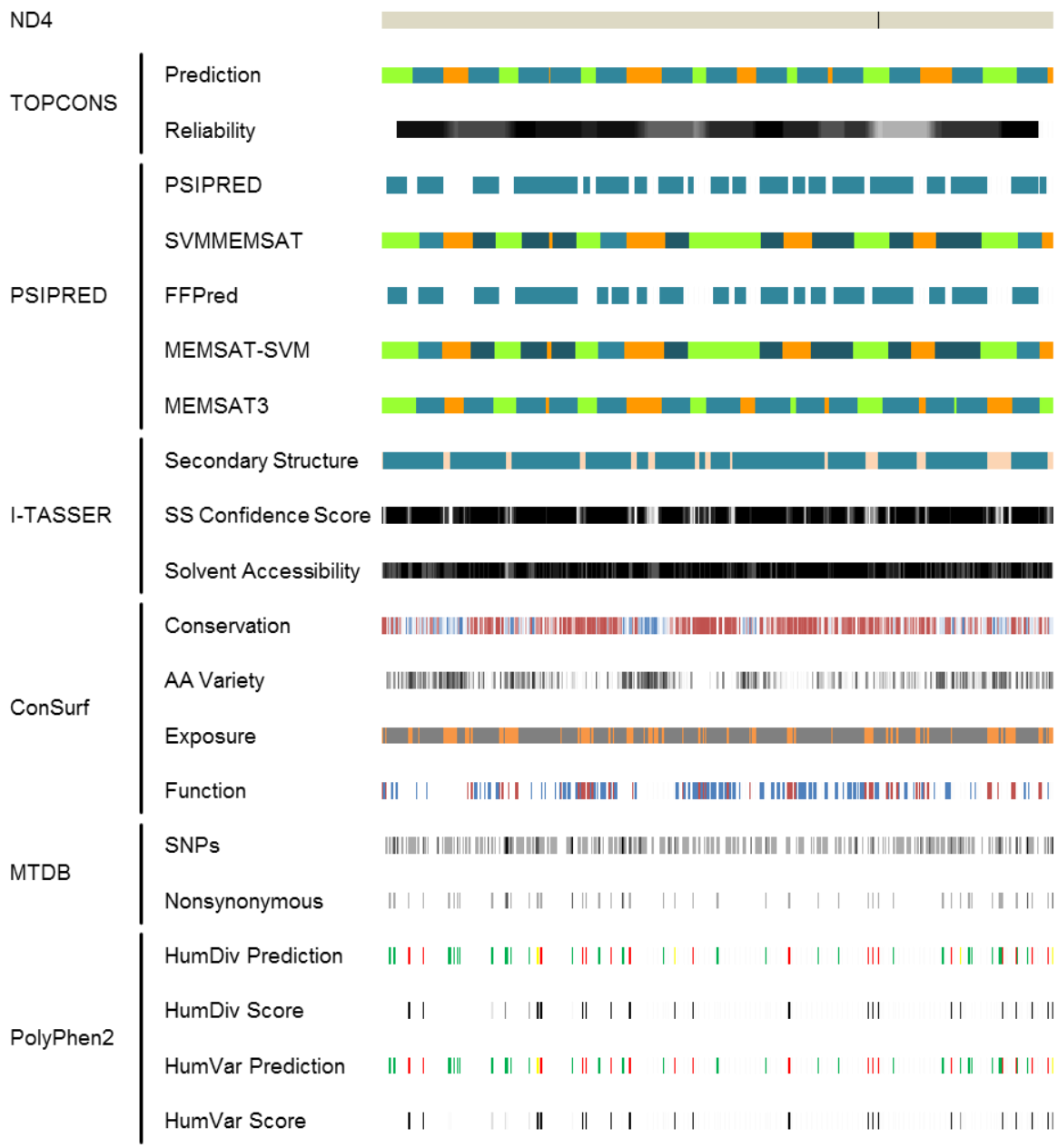

Figure 13 – *In silico* study of *Homo sapiens* ND4 structure. SOSUI: primary TMH (dark blue); secondary TMH (light blue). DAS: transmembrane region (blue). SPLIT: TMH (blue). DPM, DSC, GOR1, GOR3, GOR4, HNNC, PHD, Predator, SIMPA96, SOPM, SOPMA, Consensus, MLRC, YASPIN: coiled (light orange); helix (blue); strand (red); turn (purple). HMMTOP, TM-Coffee, TMMOD, Phobius, SPOCTOPUS, TOPCONS, PSIPRED: intracellular (green); extracellular (orange); TMH (blue); re-entrant/dip region (pink). PSIPRED: intracellular (green); extracellular (orange); TMH (blue); pore lining helix (dark blue). I-TASSER: coiled (light orange); helix (blue). ConSurf: Conservation: highly conserved (red), poorly conserved (blue); Exposure: solvent exposed region (orange), buried (grey); Function: structural role (blue), functional role (red). PolyPhen2: benign (green); possibly damaging (yellow); probably damaging (red). Quantitative scores are coloured in greyscale from the minimum value (white) to the maximum (black). Position 340 is denoted by a black line in the ND4 diagram. Further information on the servers can be obtained in Table 5.

Predictions of secondary structure by several servers localize the Arg^{340} residue in the loop between helixes XI and XII. Furthermore, topology prediction classify that loop as intracellular; since these servers assume that the protein is located in the cell membrane and ND4 localizes to the IMM, the intra- and extracellular predictions can be transposed to MM and IMS, respectively.

These results are in accordance with the structure of the prokaryotic complex I, where residues Arg^{369} (*Escherichia coli*) and Leu^{339} (*Thermus thermophilus*) localize in a loop exposed to the MM. This further validates the usage of the prokaryotic atomic resolution structures of complex I as a model for the human homologue.

The fact that there is low confidence associated to the predictions for residue 340 is indicatory of a disordered region, which is in accordance with the prediction of that being a loop.

Despite the observed topology consensus, it was not possible to obtain a consensus from the servers both in terms of the number and location of the helixes. For this may contribute diverse factors such as the differences between the *in silco* and the *in vivo* media and the variance across the algorithms used for prediction. Further and careful *in silico* analysis must be performed in order to estimate the secondary structure of ND4. However, there are considerations that can help analysing the results.

Diverse predictions, and the crystallographic structure of prokaryotic complex I, revealed that ND4 presents 14 transmembrane segments. Note that the three N-terminal helixes of subunit ND2 from fungi, bacteria and lower eukaryotes are not present in bilaterian complex I (e.g. mammals). This truncation may indicate that these helixes are not essential to the function of ND2. The low conservation observed in the three N-terminal helixes of subunits ND4 and ND5 plus the high structural and functional may also indicate that these segments are not functionally relevant (Bridges *et al.*, 2011).

ConSurf predicts that residue 340 has a structural role, is buried and highly conserved. Furthermore, it is located in a region characterized by low incidence of SNPs, as observed in the distribution of SNPs deposited in the MRDB. A remarkable aspect of ND4 is that nsSNPs which are predicted to be benign are clustered in its N-terminus.

In order to determine the impact of the R340H substitution in structural terms, mutational analysis was performed using atomic resolution structures of the prokaryotic complex I and a structure prediction model of the human complex I (Figure 14).

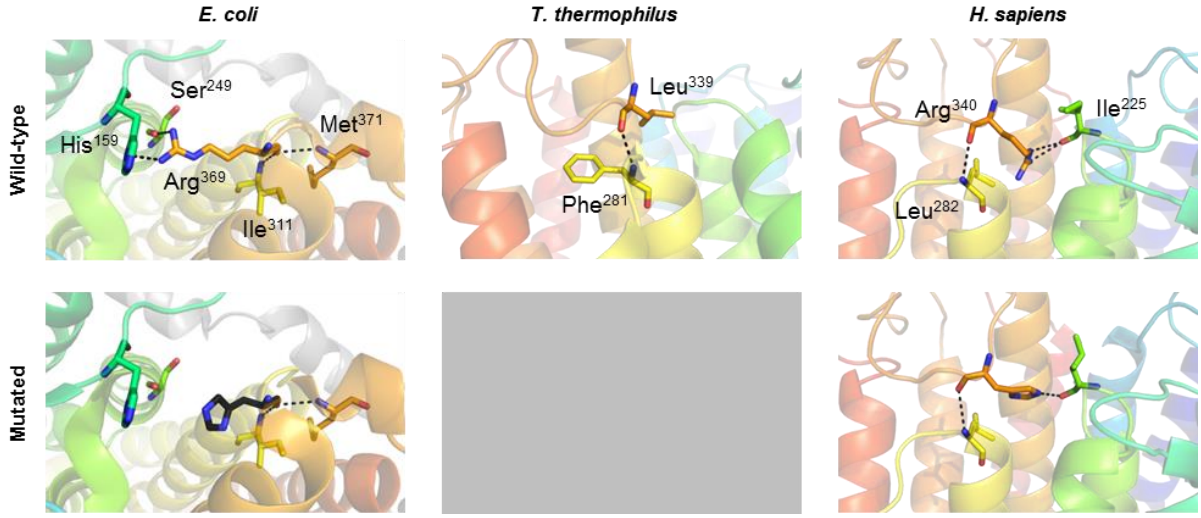

Figure 14 – Structural and mutational study on residue Arg^{340} and its microenvironment. Residue Arg^{369}, Leu^{339} and Arg^{340} of the ND4 subunit of *Escherichia coli* (PDB 3RKO (Efremov and Sazanov, 2011)), *Thermus thermophilus* (PDB 4HE8 (Baradaran *et al.*, 2013)) and *Homo sapiens* (model) are presented as well as the hydrogen bonds they establish with the neighbouring residues (top row). After mutation to histidine residues, the polar contacts were determined in the resulting structure. The *Homo sapiens* ND4 wild-type and mutated structures were generated by I-TASSER from the amino acid sequence.

In the *Escherichia coli* complex I, the most approximate to the human homologue, Arg^{340} is involved in four hydrogen bonds, two of them of the main chain-main chain type, one of the side chain-main chain type and one of the side chain-side chain type. The former are established between the H^+ acceptor carbonyl group of Arg^{369} with the H^+ donor amine group of residues Ile^{311} (Leu^{282} of *Homo sapiens* ND4) and Met^{371} (Met^{342} of *Homo sapiens*). The H^+ donor guanidinium group of Arg^{369} establishes hydrogen bonds with the carbonyl group of Ser^{249} (Val^{221} of *Homo sapiens*) and the H^+ acceptor N_π atom of His^{159} (Asn^{138} of *Hono sapiens*); this way both $N_{\eta1}$ and $N_{\eta2}$ groups of residue Arg^{369} establish interactions, creating a symmetric geometry. Substitution of the Arg^{369} residue to histidine in the ND4 subunit of *Escherichia coli* complex I disrupts the hydrogen bonds established by the $N_{\eta1}$ and $N_{\eta2}$ groups or arginine, possibly affecting the structure.

In the *Homo sapiens* model, residue 340 in the wild-type and R340H mutant establish hydrogen bonds with the same residues: the side chain interacts with the carbonyl group of Ile^{225} while the main chain interacts with the amine group of Leu^{282}.

Although the homologous residue of Arg^{340} in *Thermus thermophilus* is Leu^{339}, the same study was performed in the wild-type structure, presenting a single interaction with the amine group of Phe^{281}, which corresponds to Leu^{282} in *Homo sapiens*. Since the residue that corresponds to Arg^{340} in this prokaryote presents distinct characteristics, namely polarity, size and capacity to form hydrogen bonds, *in silico* mutagenesis was not performed. However, the vicinity of Leu^{339} was analysed to detect possible hydrophobic interactions; residues Lys^{282} (Lys^{283} in *Homo sapiens*), Ala^{329} (Ala^{330} in *Homo sapiens*) and Tyr^{333} (Lys^{334} in *Homo sapiens*) may establish interactions with the hydrophobic side chain of Leu^{339}.

Preservation and consistent prediction of the interactions between residue Arg^{340} and residue Leu^{282} is remarkable, which may be indicative of the structural role predicted previously (Figure 14).

Despite lacking definite evidence on the human ND4 protein structure, diverse data obtained by human protein prediction and prokaryotic modelling support that the m.11778G>A sequence variation produces a destabilization of unknown magnitude and nature at the protein level.

4.3. Assessment of the m.11778G>A heteroplasmy level

The analysis of the family is invaluable in most genetic investigations. This also applies to the field of mitochondrial genetics, with a special impact on the maternal lineage of the family since the mitochondrial genome exhibits maternal inheritance.

Certain mutations in the mitochondrial DNA have been associated with LHON. However, no biochemical or structural sense has been uncovered so that a clear genotype-to-phenotype correlation can be obtained. Further observations were reported and the mutations commonly associated with LHON, which were known as the primary cause of the disease until recently, have been put through scrutiny.

A case where one of the LHON-causing mutations underwent further analysis is herein described. In this case, the proband is the only family member exhibiting the clinical manifestations of LHON while 72% of the individuals from the maternal lineage are homoplasmic for the m.11778G>A variation and 100% are carriers but do not present LHON symptoms (Figure 15).

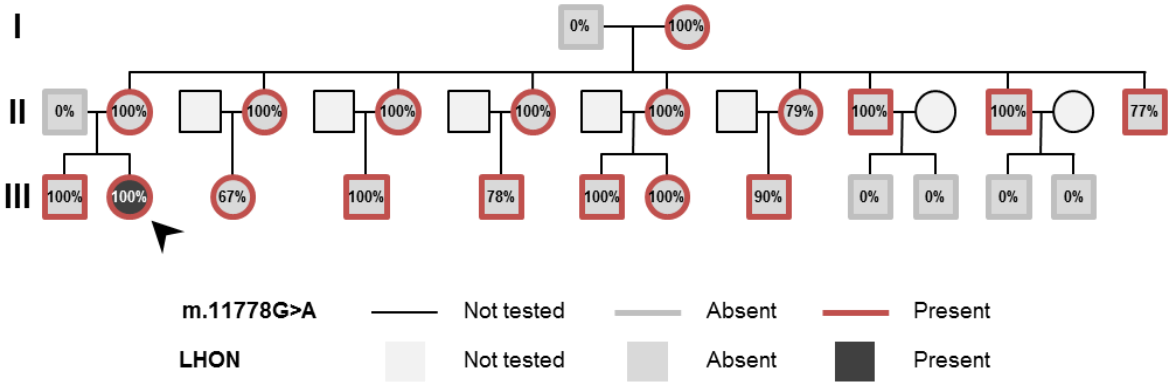

Figure 15 – Genealogic composition of the proband's family. Each individual is classified according to genotype (contour) and phenotype (filling). Data from PCR-RFLP used to determine the heteroplasmy is also presented (see below).

Careful investigation on the proband was carried out, and she was diagnosed with LHON-*plus* due to additional neurological findings previous to this work (Grazina *et al.*, 2007).

Peripheral blood was collected from family members and DNA was extracted. The portion of the *MT-ND4* gene containing nucleotide 11778 was amplified by PCR. After that, the resulting DNA molecules were digested with an endonuclease which cleavage activity is specific for the np 11778 (Figure 16 A); if there is a guanine nucleotide in this position, the DNA molecule is kept intact while if

the position is occupied by an adenine nucleotide, the molecule is cleaved originating fragments with differing molecular weights (Figure 16 B, C). These results were obtained at LBG, prior to the present work, in the context of diagnostic investigation. These results are shown with permission of Professor Manuela Grazina.

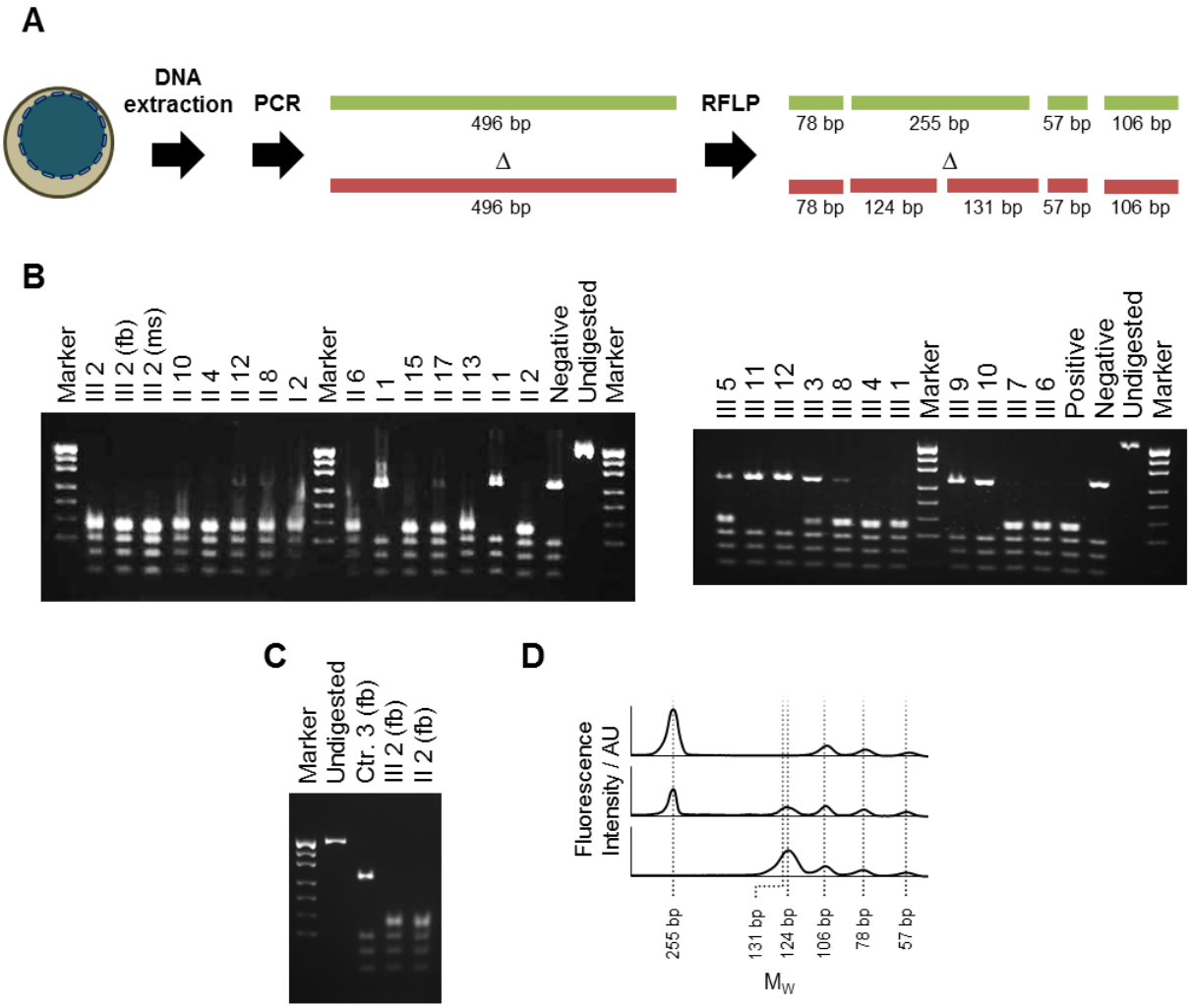

Figure 16 – Genetic screening of the m.11778G>A mutation by PCR-RFLP. (**A**) Schematic representation of the PCR-RFLP procedure for the m.11778G>A mutation. Restriction map shows position of the *MaeIII* site created at np 11774 only when the G to A mutation is present at np 11778. (**B**) PCR-RFLP electrophoresis results of the proband's family members. The digested fragments were run in an agarose gel electrophoresis resulting in band distributions which were used to perform the genetic screening for the m.11778G>A mutation and heteroplasmy levels. Negative and positive controls were loaded as well as the undigested PCR product. João Pratas and Manuela Grazina's personal communication. (**C**) PCR-RFLP electrophoresis results of Ctr. 3, Patient-20yo and her mother for the m.11778G>A mutation. (**D**) Profile of PCR-RFLP products from ethidium bromide stained agarose gel: 11778G homoplasmic (top), 67% 11778A heteroplasmic (middle), and 11778A homoplasmic (bottom). DNA was extracted from lymphocytes, fibroblasts (fb) or muscle (ms) samples.

Quantification of the PCR-RFLP products was carried out in order to determine heteroplasmy. All individuals of the maternal lineage present the m.11778G>A sequence variant, being the grandmother the first carrier ancestor identified.

As homozygotic alleles, homoplasmic variations that have a big impact on the normal function of the cell are less likely to be observed since they decrease the fitness of the carriers. This way, pathogenic sequence variations are more likely to be presented in heteroplasmy and the more damaging, the lower their representativeness in the overall mtDNA pool. As observed before, the majority of individuals of the maternal lineage are homoplasmic and still do not express the phenotype associated to LHON.

So, this case questions the role of the m.11778G>A variation as a unique cause in the pathogenesis of LHON.

4.4. Assessment of the mtDNA copy number

In contrast to the nuclear genome, the mitochondrial genome is characterized by a remarkable flexibility in terms of the number of copies present in each mitochondria and in each cell.

Depletion of the mitochondrial genome translates into very low or even null mtDNA copy number and is characterized by typical clinical manifestations, namely profound weakness, encephalopathy and liver failure – mitochondrial depletion syndromes –, being the most frequent cause of multisystemic mitochondrial disease (Venegas *et al.*, 2011). Postmitotic tissues as the liver, brain and muscle are the main tissues affected by this condition and the depletion may be restricted to them (Schaller *et al.*, 2011). However, it is not possible to perform diagnostic methodologies in some cases such as brain, and liver in new-borns. So, different tissues that can be accessed more easily as blood and skin are commonly used as indicators of mtDNA depletion. However blood and the hematopoietic system are not commonly affected by this type of depletion, decrease in the mtDNA copy number in this tissue is a strong indicator of mitochondrial depletion syndrome; the reverse is not applicable: if no depletion is observed in blood cells, depletion in liver, brain and/or muscle may or may not be presented (Dimmock *et al.*, 2010). On the other hand, fibroblasts are relatively easy to obtain by skin biopsy and, due to the shared embryonic origin (ectoderm) with the central nervous system, they can be more informative of brain-related conditions, at least in theory.

The most broadly used method to quantify the mtDNA copy number is qPCR. The assay uses a primer that specifically binds to the mtDNA and another that targets the nuclear low-polymorphic single-copy *B2M* gene, which encodes β-microglobulin 2. Since the mtDNA is far more abundant than the nDNA in terms of copy number (~4000 versus 1) (Venegas *et al.*, 2011), the amplification product of the mtDNA primer reaches higher concentrations in early cycles while the nuclear product is detected in such levels further in the amplification cycles. After finishing the protocol, values of the cycle in which the concentration of the amplified products exceed a given threshold are obtained and translated into copy number values by normalizing with the product arising from the *B2M* gene, which is the endogenous normalizing control of the experiment.

Diverse chemistries can be used in the assay in order to quantify the resulting amplification products. SYBR Green is an intercalating agent which fluorescence is considerably enhanced upon binding to double-stranded DNA. TaqMan probes are modified DNA primers bearing a fluorophore in one 3'-end and a quencher in the 5'-end; as DNA polymerase proceeds to form the new DNA strand, its 5'-3' exonuclease activity removes the 3' nucleotides of the primer along with the fluorophore which fluorescence increases considerably since it is free from the quencher.

Quantification of the mtDNA copy number was performed using DNA extracted from fibroblasts and lymphocytes of the individuals included in this study (Figure 17).

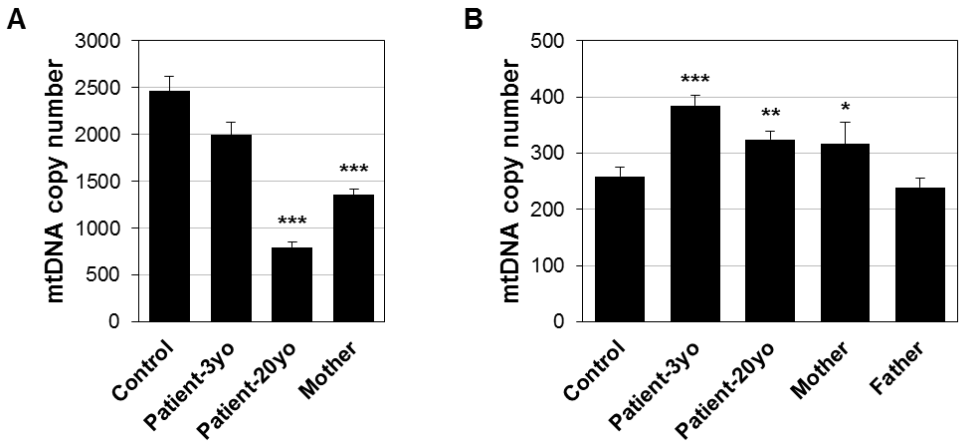

Figure 17 – Results of the mtDNA copy number quantification by qPCR. The analysis was carried out on total genomic DNA extracted from different tissues: (**A**) cultured primary skin fibroblasts from skin biopsy, (**B**) lymphocytes isolated from peripheral blood. Values are presented as the mean of two triplicated experiments, with standard error bars. Patient-3yo denotes biological material from the first harvest and Patient-20yo denotes biological material from the second harvest.

A decrease in the mtDNA content in leukocytes and an increase in fibroblasts throughout aging have been reported (Dimmock *et al.*, 2010; Venegas *et al.*, 2011). Furthermore, different tissues present distinct dependency on mitochondria both for energetic and signalling purposes. So, mtDNA copy number varies accordingly to tissue and age, results are validated by comparison with tissue- and age-matched controls.

The decrease observed between the patient's first and second skin biopsies is significant and may be the result of oxidative damage accumulated throughout the years which damages the mtDNA impairing its replication and consequent maintenance. Moreover, the patient's mother also presents a significantly low mtDNA copy number, which may also be explained by oxidative damage (Figure 17 A).

As mentioned before, lymphocytes are not good indicators of mitochondrial disorders. This may explain the smaller variations observed in the mtDNA copy number quantification using lymphocytes (Figure 17 B). The patent father's lymphocytes present a mtDNA copy number similar to that in control individuals, indicating that the maternal lineage present modifications, which may include the m.11778G>A variation, that account to the phenotype of the proband; however, it is worth to mention that the absence of unusual findings in the father's cells is not indicative of a non-contribution to the same phenotype.

4.5. Study of the activity of the MRC complexes

Evaluation of the catalytic activity of the MRC complexes is an invaluable tool to diagnose and identify mitochondrial cytopathies. It can be performed by spectrophotometry using compounds that are oxidized or reduced, producing a variation in the absorbance of the solution which can be measured at a given wavelength.

In order to investigate the activity state of the MRC complexes, primary fibroblasts were used (Figure 18). The possibility of studying the patient at two distinct time points (3 and 20 years old) provides information on the development of the disease and the transformations that occurred during the aging process.

When the patient was diagnosed with LHON (Grazina *et al.*, 2007), the activity of complex I was decreased by ~40% (Figure 18 A), which is in accordance with previous studies (Majander *et al.*, 1991; Carelli *et al.*, 2002). Furthermore, complex I presents increased activity, which may arise from a compensation mechanism. The relatively high activity of complex III may also contribute to the higher efficiency of electron transport from all the available substrates, which are imputed mainly at complex II.

In the fibroblasts collected when the patient was 20 years old (Figure 18 B), a completely different MRC activity pattern is observed. First of all, the activity of complex I (which was decreased at the age of 3 years old) is now increased by more than 30% compared to the control values. Also, the activity of complex II (which was increased at the age of 3 years old) is decreased by more than 20% from the reference value. Complex III presents a shift in the activity, being decreased, while complex IV is now more active.

Remarkable findings of the MRC analysis using the patient's mother fibroblasts (Figure 18 C) include a decrease in the activity of complex II by ~70% and that of complex III.

Segments (I+III) and (II+III) measure the combined activity of complex I or II and complex III, respectively. This is, complex I or II substrates are added to the reaction mixture and the activity of complex III is measured. Since the mobile electron transporter ubiquinone is not added, the activity of complex III depends not only on the capacity of complex I or II to oxidize their substrates and transfer the withdrawn electrons to ubiquinone, but also on the quantity of this mobile electron transporter. While segment (I+III) presented low activity in the fibroblasts collected when the patient was 3 years old due to a decrease in complex I (Figure 18 A), the same segment presents the same qualitative variation in the fibroblasts from the 20 years old patient (Figure 18 B) and her mother (Figure 18 C) due to low complex III activity, which also impacts on the (II+III) segment.

Altogether these results may indicate that the MRC transited between two stress scenarios. First, at 3 years old, when the clinical symptoms of LHON were started to express (i.e. LHON onset), the MRC adapted to the decreased activity of complex I by increasing the activity of complex II to allow an equilibrated input of electrons, and also by increasing the activity of complex III to ensure that there is

a constant electron flow through the downstream complexes of the MRC. At the age of 20 years, when the patient's condition is more stable, an increase in the NADH dehydrogenase activity of complex I conjugated to the decreased activity of complex II and complex III most likely represents a recovery of complex I, thus reducing the need for the compensatory effect.

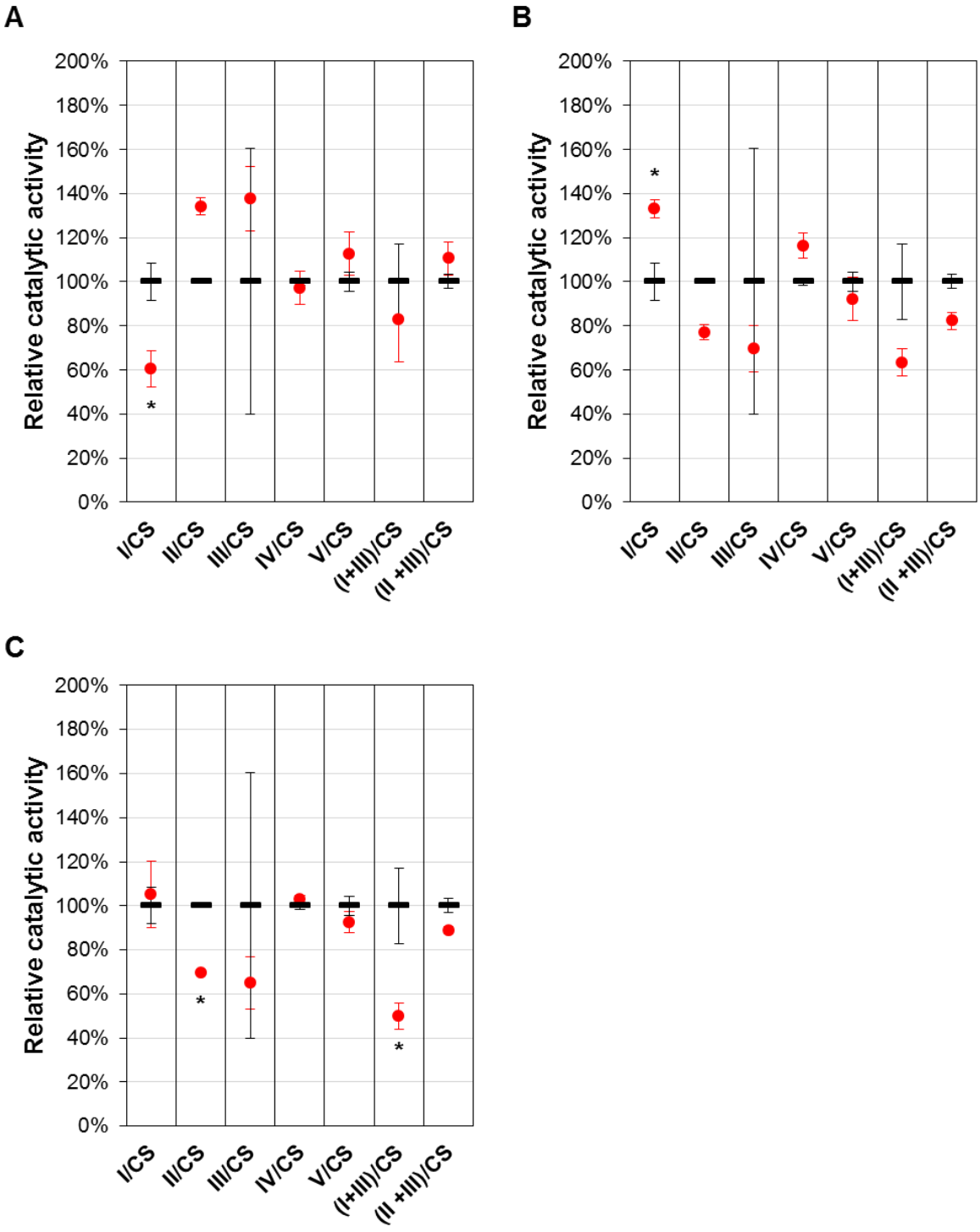

Figure 18 – Spectrophotometric determination of the MRC catalytic activities in fibroblasts. (**A**) Patient-3yo, (**B**) Patient-20yo, (**C**) mother. Values were normalized to an endogenous control (CS: citrate synthase) and are presented as the mean of at least three experiments (Control 1: n=5; Control 2: n=5; Control 3: n=3 (III/CS: n=2); Patient-3yo: n=3 (III/CS: n=2); Patient-20yo: n=3 (III/CS, (I+III)/CS: n=2); Mother: n=3 (III/CS: n=2)), with standard error bars. Values of the controls are presented as black bars and those from individuals in study are represented as red circles. Patient-3yo denotes fibroblasts from the first harvest and Patient-20yo denotes fibroblasts from the second harvest.

Complex I and complex III represent major production sites of mitochondrial and both mitochondrial and cytoplasmic ROS, respectively; so, the contribution of an electron leak factor in the (I+III) and (II+III) segments must not to be disregarded, especially in the former. Moreover, ubiquinone can function as a source of ROS once reduced to the ubisemiquinone state, which validates the previous consideration.

In order to unmask MRC deficiencies, an alternative approached was used. For this assay, fibroblasts were cultured in different conditions: one in which the main carbon source is glucose and another where is is galactose. While glucose can be promptly phosphorylated, being directed to glycolysis, galacose requires further preparatory transformations so that it can also be inputted to glycolysis. Those steps involve a set of enzymes (D-galactose 1-epimerase, galactokinase, galactose-1-phosphate uridylyl transferase, UDP-glucose:hexose-1-phosphate uridylyl transferase and UDP-glucose 4-epimerase). While glycolytic pyruvate production from glucose yields 2 ATP, its production from glucose yields no net ATP. This shifts the ATP production to a higher dependency on OxPhos, enhancing mitochondrial metabolism (e.g. higher respiration rate, lower lactate production). At the same time, cells will be more susceptible to mitochondrial toxins and defects on mitochondrial proteins that are involved in energy production (e.g. MRC complexes) (Aguer *et al.*, 2011).

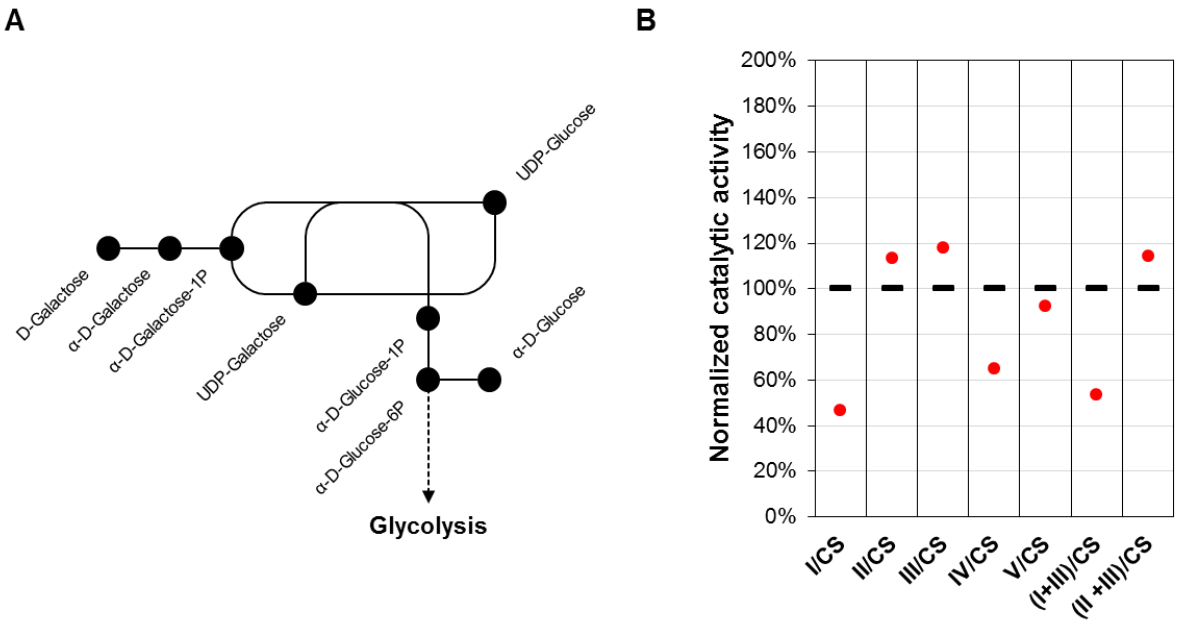

Figure 19 – Spectrophotometric determination of the MRC catalytic activities in fibroblasts from the galactose assay. (**A**) Schematic representation of the transformations of galactose and glucose in order to be inputted to glycolysis. Adapted from Kegg pathway (Kanehisa *et al.*, 2014) (**B**) Results of the spectrophotometric evaluation of the activity of the MRC complexes using fibroblasts from a control (black bars; n=1) and Patient-20yo (red circles; n=1). Values are presented as the ratio between the results obtained in the glucose and galactose treatment. Values of the controls are presented as black bars and those from individuals in study are represented as red circles.

Galactose treatment results in a decrease in the activity of complex I and complex IV. Furthermore, segment (I+III) also presents lower activity, which may be explained by low complex I activity.

These results show that, despite the increased activity of complex I observed in normal culture conditions (Figure 19 B), this MRC component is unable to withstand stress and fails to maintain its activity in this condition, as expected. Due to time limitations, the number of experiments is too small to draw major conclusions, so these data have to be considered as preliminary.

In order to gain further insight on the function of isolated MRC complexes, normalization of the measured catalytic activity for the quantity of each complex could be performed. This way, individual complexes could be studied, reducing the impact of additional factors and increasing the relevance of mutations and other direct implications (e.g. assembly state) in the results.

As mentioned before, there are several modifications that occur with aging, especially in the mitochondria where the oxidative damage shapes the landscape of the system at a considerable rate. Besides modifications in the mtDNA copy number, aging also impacts on the proficiency of the MRC. A decline in the overall mitochondrial function was observed in aged rat hearts, translating in a decrease in complex I and complex V activities, respiratory capacity and ATP production (Preston *et al.*, 2008).

Furthermore, several small molecules may modulate the function of the MRC. So, pharmacologic treatments may impose an additional veil to the results.

4.6. Analysis of MRC protein stability

Cell components are constantly subjected to stress and damage. In order to avoid collateral damages due to the failure of these components, they are constantly being recycled. For instance, more stable proteins (e.g. histones) present low turnover rates while highly dynamic proteins (e.g. tubulin) or those being subjected to oxidative damage are quickly recycled.

Catalytic activity and quantity are commonly associated since greater quantities a given enzyme present more capacity to conduce the reaction they catalyse in non-saturated conditions. However, in cases where enzymes are modified, different activity-to-quantity ratios may arise.

In order to determine whether the catalytic activity of the MRC complexes presented previously (section 4.5.) correlates with changes in the quantity of those complexes, western blot was employed (Figure 20 A, B). Furthermore, immunodetection of the complex I subunit ND4 was also carried out to inspect the stability of this protein in fibroblasts from individuals carrying the m.11778G>A sequence variation (Figure 20 C).

Evaluation of the UQCRC2 band was only possible in one experiment. The proximity of its band and that corresponding to the α subunit of complex V (ATP5A), and the high intensity of the last, hamper the detection and quantification process. Furthermore, it was impossible to detect the band of the complex I subunit NDUFB8 in all experiments, which precluded its quantification.

COXII presents the main difference between the proband and her mother. While this complex IV subunit is severely down-regulated in the affected individual (~20 %), it is only slightly deviated from the control's values in the carrier (> 80 %).

There is a slight increase in the quantity of MRC subunits when comparing the patient's samples from the first and second biopsy, which may represent a stabilization/amelioration of the phenotype.

In order to determine whether the ND4 subunits is destabilized in individuals bearing the m.11778G>A sequence variation, western blot for this complex I subunit was also carried out.

Due to the fact that ND4 is both a membrane protein and is mitochondrially encoded, the production of antibodies is more difficult, resulting in low-specificity and high background during detection. Nonetheless, it was possible to detect and quantify the ND4 subunit in all samples.

The observed decrease in ND4 protein quantity may be indicative of the loss of stability due to the p.R340H substitution which was predicted by *in silico* tools (section 4.1.). Destabilization of this protein may also impact on complex I assembly and disruption of intra-complex protein-protein interactions.

Summing up, both proband and her mother present a significant decrease in the quantity of the complex I subunit ND4. However, while the proband presents a marked decrease in complex IV subunit COXII, a trait not shared by her mother who presents values similar to control.

However, it is necessary to increase the number of experiments to draw more detailed conclusions and confirm these preliminary results.

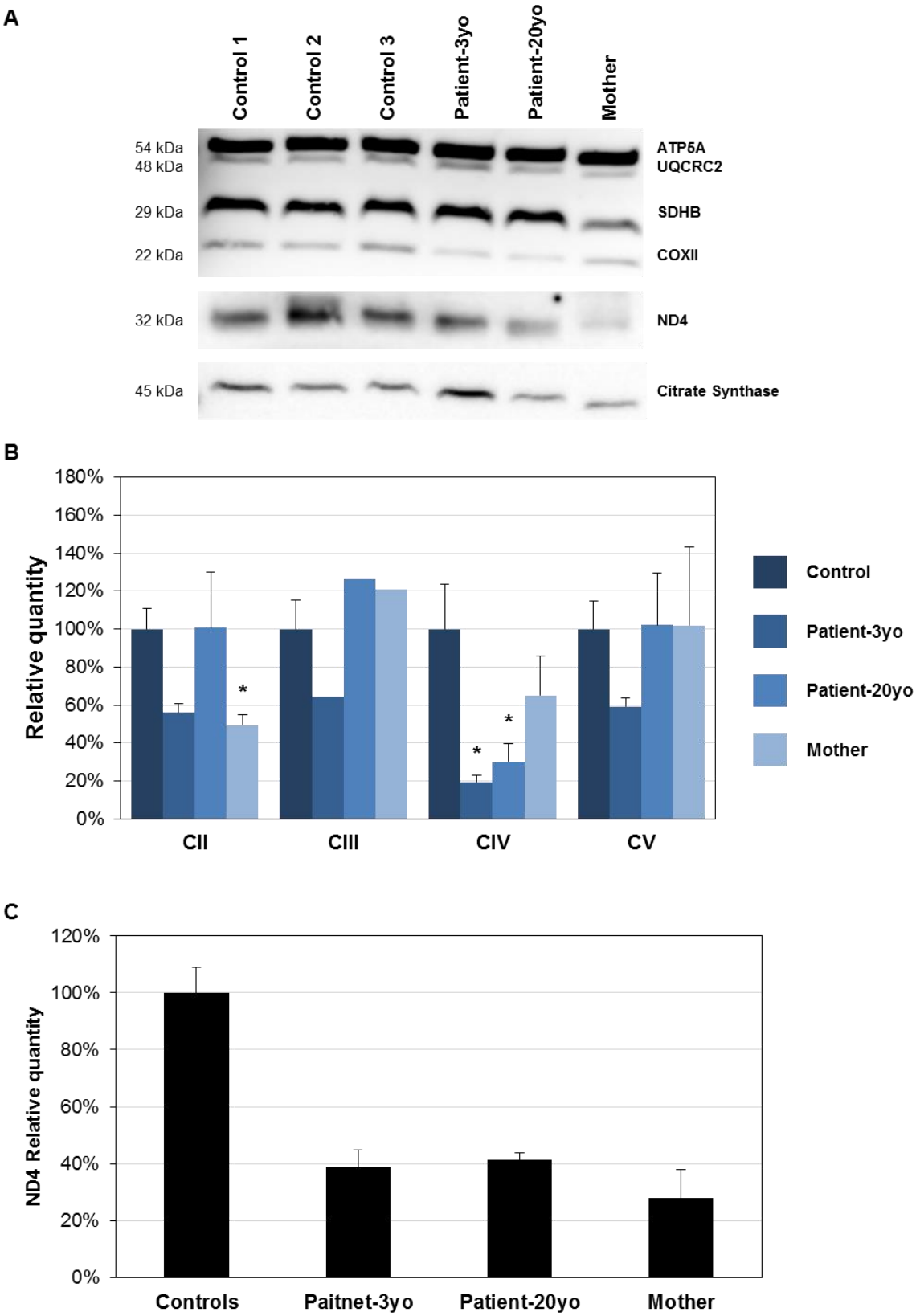

Figure 20 – Evaluation of the MRC composition by western blot. (**A**) Western blots analysis of extracts from cultured primary fibroblasts by immunostaining with an antibody cocktail against diverse MRC subunits (complex II: SDHB; complex III: UQCRC2; complex IV: COXII; complex V: ATP5A) and an antibody against ND4. (**B**) Quantification of the MRC profile. (**C**) Quantification of the ND4 subunit. Values were normalized to an endogenous control (CS: citrate synthase) and are presented as the mean of three experiments (CIII: n=1; ND4: n=2), with standard error bars. Patient-3yo denotes fibroblasts from the first harvest and Patient-20yo denotes fibroblasts from the second harvest.

4.7. Study of the assembly of MRC complexes

Cellular machinery regulates the expression of its components according to their function. For instance, proteins that are vital to the cell are under a tight regulation where the slightest dysfunction can lead to their degradation so that harmful effects are prevented. However, if alternative pathways exist or the function is not severely affected, up-regulation may compensate for the low-activity.

It is accepted that the MRC is highly flexible both in quantitative and qualitative terms. Mitochondrial ATP production is carried out at a cost, ROS production. So, the MRC needs to adapt to the overall cellular status. This regulation extends to the level of the individual components.

Considering the case where the electron flow through the MRC is low, adaptative changes will transform the composition of the chain to decrease the activity and quantity of the final interveners, especially complex IV since it catalyses the final electron transference of the chain. The overall gain of this adaptation is the decreased production of ROS in a MRC dysfunction scenario, avoiding further cellular damage.

After electrophoretic separation of proteins by BN-PAGE and Coomassie staining, MRC complexes can be visualized and analysed both in terms of quality and quantity. Whole lymphocytes were used in this analysis since samples with higher protein content can be easily obtained. Optic densitometry of bands corresponding to complexes I-V was performed (Figure 21).

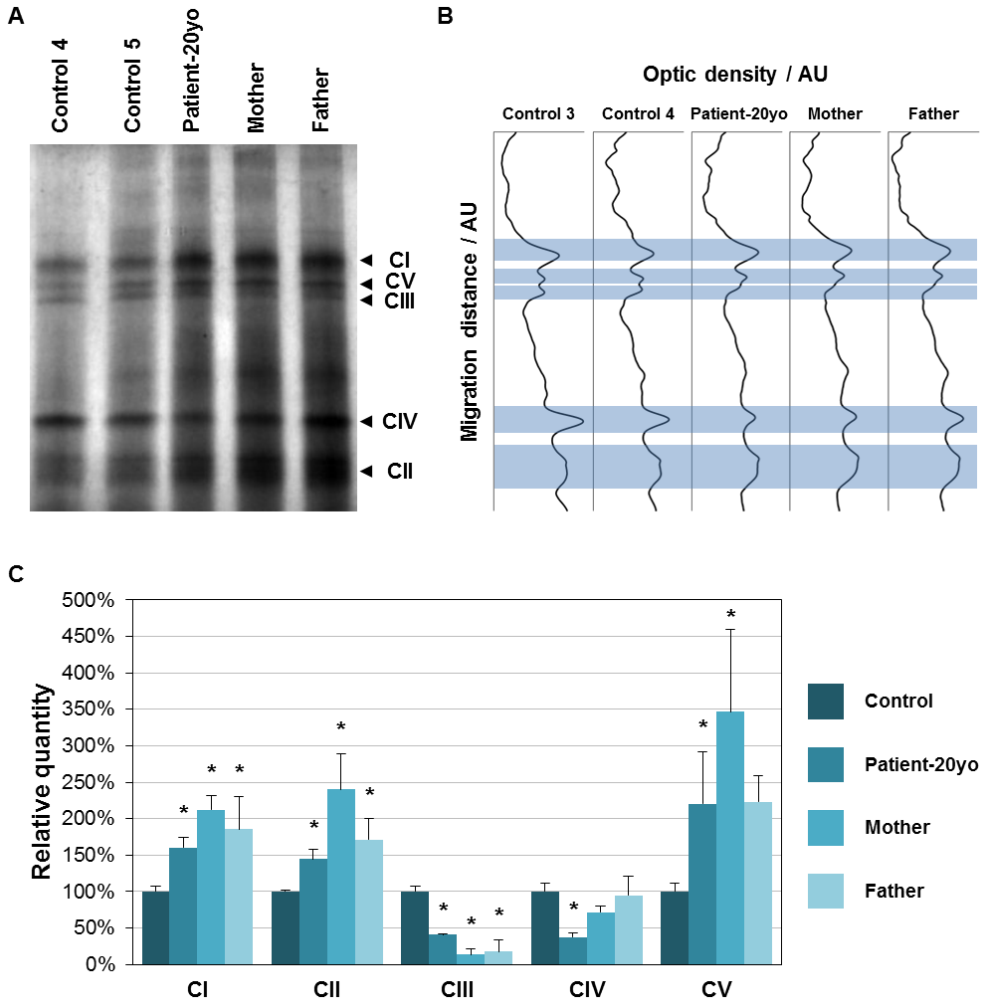

Figure 21 – Qualitative and quantitative study of MRC complexes by BN-PAGE. (**A**) Example of a BN-PAGE gel of lymphocyte samples after Coomassie staining. Arrowheads indicate the position of the bands that correspond to MRC complexes. Mitochondria derived from whole lymphocytes were used and 60 µg of total protein were loaded per lane. (**B**) Optic densitometry results of the presented gel. Regions corresponding to the MRC complexes' peaks are highlighted by blue boxes. (**C**) Quantification of the assembled MRC complexes by BN-PAGE. Values are presented as the mean of three experiments, with standard error bars. Patient-20yo denotes lymphocytes from the second harvest.

As with most macroscopic gel electrophoresis, molecular weight can only be estimated. This is also the case of native electrophoresis. However, native electrophoresis of membrane proteins poses an additional problem to molecular weight determination since the only commercially available molecular weight standards are composed solely by soluble proteins, which migration pattern differs significantly relatively to hydrophobic proteins (Wittig *et al.*, 2010). Diverse strategies can be used, such as the production of native mitochondrial extracts from bovine heart, but no other standard is best than that of the same species and tissue. Accordingly, the qualitative evaluation of MRC complexes was performed by comparison of the migration patterns of subjects and controls' samples. Since no significant deviations of protein migration were observed in the subjects' samples, it can be concluded that the complexes are correctly assembled or, at least, no significant perturbations in the composition exist. Note that native gels are used to separate proteins and complexes with high molecular weights (~0.5 MDa) and band shifts due to lack of low molecular weight accessory subunits can be unnoticeable using this technique.

Further consolidation of the qualitative analysis can be done by mass spectrometry characterization of isolated complexes (e.g. eluted from bands excised from the native gel).

In qualitative terms, diverse aspects are target for discussion.

Firstly, the quantity of complex I is significantly increased both in the most recent patient and mother's lymphocytes samples. This may correlate with the dysfunction of this complex, probably caused by the ND4 p.R340H substitution, and the cell's attempt to restore the normal activity of complex I by its up-regulation. Although not significantly, the quantity of complex II is slightly increased. This may also constitute a strategy to bypass the dysfunctional complex I allowing a normal input of substrates into the MRC. Complex III, to which the electrons from complexes I and II converge, is significantly down-regulated in the patient, the mother and the father's samples, which may indicate a low flow of electrons through the MRC. This is corroborated by the down-regulation of complex IV in the patient and mother's samples.

Quantification of complex IV subunits by SDS-PAGE/western blot of mitochondria-rich fractions obtained from cultured fibroblasts (Figure 20 B) is in accordance with the decreased quantity of assembled complexes. Furthermore, the use of BN-PAGE may indicate an assembly defect of complex III (Figure 21 B).

From the combination of these findings (activity and quantity of assembled complex), it can be perceived that the production of ROS by complex I may be considerable since both its quantity and activity are increased but it is not followed by an increase in quantity or activity of complex III.

Altogether, these findings are in accordance with a MRC stress panel caused by complex I dysfunction in the patient and her mother, and further suggests complex IV dysfunction as a distinctive factor that distinguishes affected and carrier individuals.

4.8. Evaluation of the autophagic function

Degradation of faulty cellular components is vital to maintain homeostasis. For instance, membrane proteins and long-lived proteins are degraded in lysosomes as a result of autophagy. The same applies to large structures such as mitochondria.

As mentioned before (section 1.5.3.), mitochondria in which membrane potential is disrupted are targeted for destruction by specialized machinery. The late stages of mitophagy overlap with the autophagic pathway, sharing some interveners such as LC3 and p62.

Accumulation of defective mitochondria may catalyse the onset of mitochondria-related disorders by exceeding the threshold. The balance between mitochondrial biogenesis and mitophagy is essential to maintain mutation burdens as low as possible. Defects on either pathways compromise mitochondrial homeostasis.

In order to determine whether alterations on the autophagic pathway may intervene in the proband's phenotype, functional immunofluorescence studies were carried out (Figure 22).

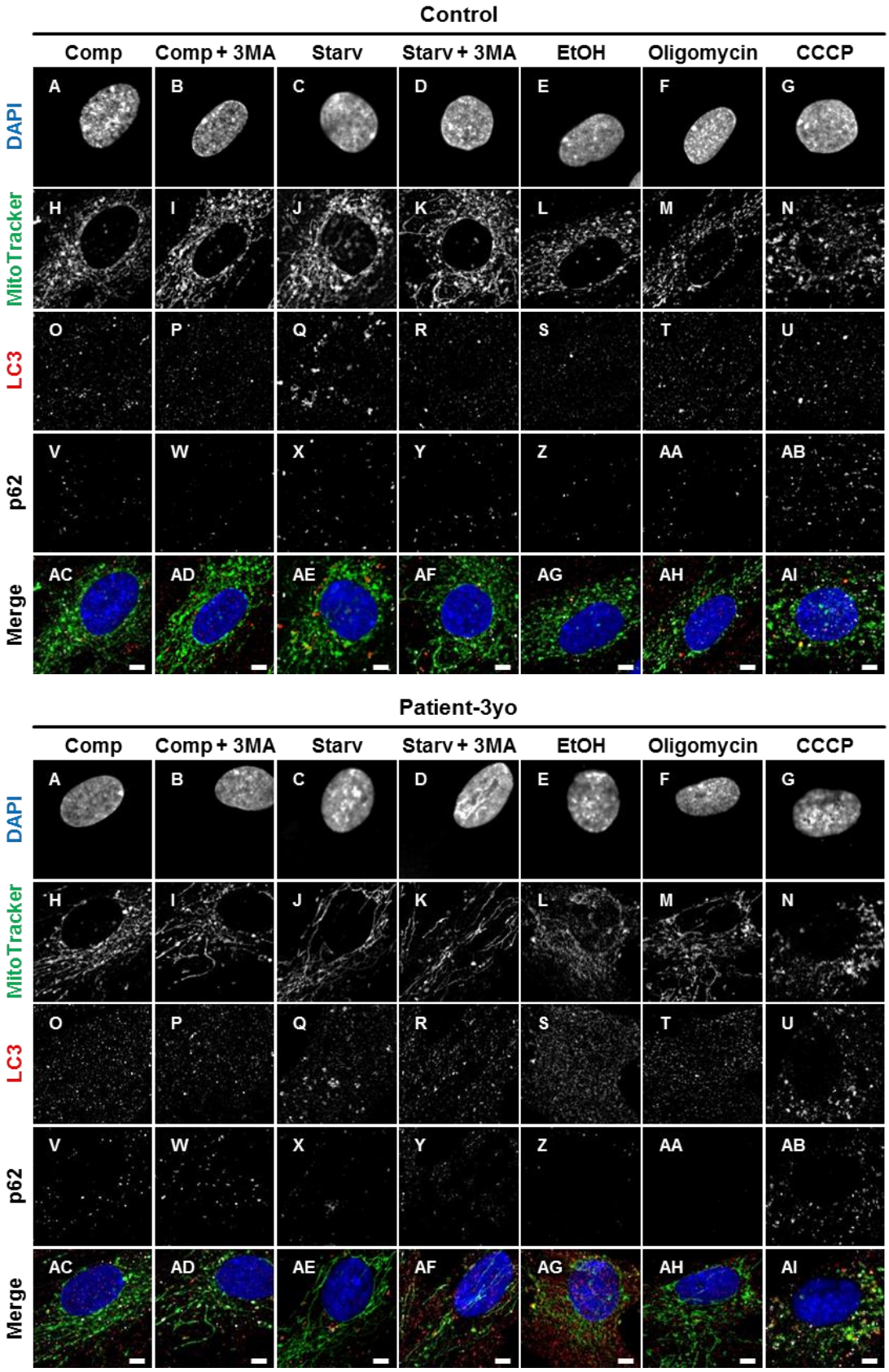
Control
Comp
Comp + 3MA
Starv
Starv + 3MA
EtOH
Oligomycin
CCCP
DAPI
MitoTracker
LC3
p62
Merge
A
B
C
D
E
F
G
H
I
J
K
L
M
N
O
P
Q
R
S
T
U
V
W
X
Y
Z
AA
AB
AC
AD
AE
AF
AG
AH
AI
Patient-3yo
Comp
Comp + 3MA
Starv
Starv + 3MA
EtOH
Oligomycin
CCCP
DAPI
MitoTracker
LC3
p62
Merge
A
B
C
D
E
F
G
H
I
J
K
L
M
N
O
P
Q
R
S
T
U
V
W
X
Y
Z
AA
AB
AC
AD
AE
AF
AG
AH
AI

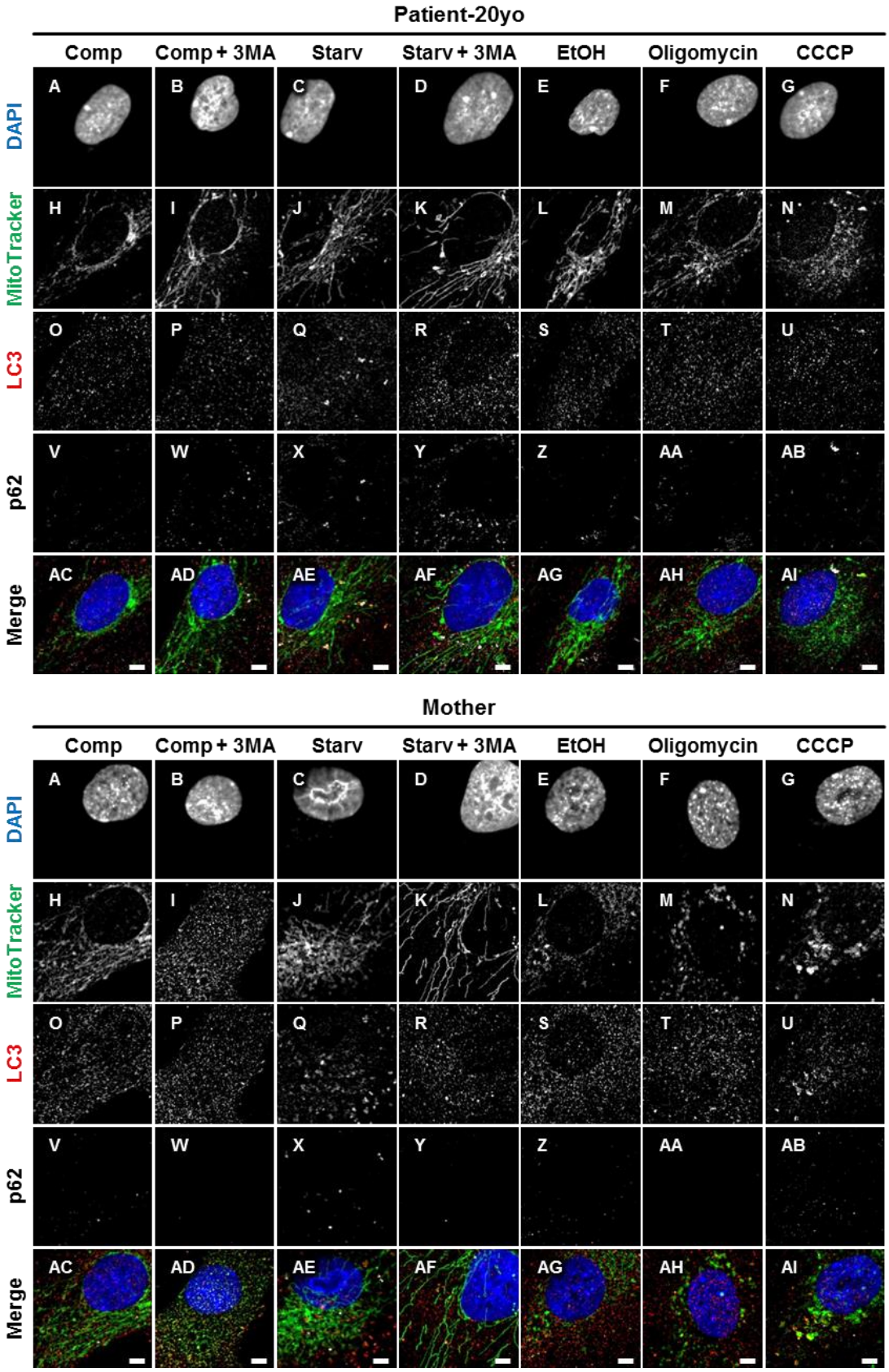

Figure 22 – Immunofluorescence study of autophagy in primary fibroblasts. Control, patient and her mother's fibroblasts were subjected to four conditions to functionally assess autophagy in terms of LC3 puncta and p62 accumulation. Patient-3yo denotes fibroblasts from the first harvest and Patient-20yo denotes fibroblasts from the second harvest. Comp: complete medium; Comp+3MA: complete medium supplemented with 3MA; Starv: serum-free medium; Starv+3MA: serum-free medium supplemented with 3MA. Mitochondria and nuclei were stained using MitoTracker Green and DAPI, respectively. Scale bar: 5 µm.

The assessment of a pathway gains depth and robustness by implementing a functional assay where cells are challenged by different stimuli and respond according to the machinery they possess.

Since this study intends to assess autophagy, cells were challenged with an inhibitor (3MA) and a trigger (starvation) of this pathway.

Mitochondria form a dense network of tubular filaments. In order to degrade mitochondria, the network needs to be broken down, segregating small mitochondria that can be readily processed by the autophagic machinery. So, mitochondrial fragmentation is an indicator of degradation of these organelles.

However, to analyse the function of autophagy, other indicators must also be used. In this study, LC3 and p62 were used to complement the results from the morphological analysis of mitochondria and to provide further insight on the activity of general autophagy.

Autophagy is a constitutive process, which means that it occurs in normal conditions at a basal level. This can be observed by discrete LC3 (Figure 22 Control O) and p62 puncta (Figure 22 Control V). When autophagy is pharmacologically inhibited, a considerable decrease in the number of LC3 puncta is observed (Figure 22 Control P) as well as an almost absolute dissipation of the p62 signal (Figure 22 Control W).

Serum constitutes a vital source of nutrients to culture cells; when cells are deprived from this constituent, autophagy mechanisms are up-regulated in order to provide basic components that can be used in vital processes. This up-regulation involves the increase of LC3 puncta both in number and size (Figure 22 Control Q) as well as more p62 to gather ubiquitinated proteins that are targeted for recycling (Figure 22 Control X).

Incubation of cells in serum-free medium with concomitant 3MA treatment was employed to provide evidences that the conditions used to trigger autophagy are specific, as a basal-like rate of autophagy are observed (Figure 22 Control R, Y).

In this analysis, no considerable deviations from the expected behaviour were observed in the patient and the mother's fibroblasts.

However, an accumulation of p62 puncta upon autophagy inhibition was observed in the patient's fibroblasts collected in both skin biopsies (Figure 22 Patient-3yo W, Patient-20yo W). This accumulation was even more notorious when 3MA was added in starvation conditions (Figure 22 Patient-3yo Y, Patient-20yo Y).

In order to induce mitophagy, cells were treated with CCCP, which is a protonophore which decouples the mitochondrial electrochemical potential by equilibrating H^+ across the IMM. Oligomycin was used to inspect changes in autophagy upon mitochondria hyperpolarization by inhibition of the decoupling activity of complex V. Since CCCP and oligomycin were solubilized in ethanol, a solvent control was also analysed.

To start with, no changes were observed between the basal conditions and the solvent control in all samples (Figure 22 E, L, S, Z, AG). Despite altering mitochondrial morphology, which became more spherical and less mesh-like, oligomycin treatment did not produce changes in the autophagy flow of the fibroblasts (Figure 22 F, M, T, AA, AH). Upon mitochondrial uncoupling, a starvation-like scenario was observed, including increase in the number and size of LC3 puncta (Figure 22 U) and p62 (Figure 22 AB); mitochondrial morphology was clearly affected by this treatment, with disassembly of the network and formation of mitochondrial aggregates (Figure 22 N).

Since the labelled proteins are shared downstream effectors of diverse pathways and a pharmacological approach was used to modulate the degradation of cell components, the presented results can be used to assess the general status of degradation mechanisms.

Mitophagy-directed studies using PINK1 and Parkin labelling must be carried out in order to conclude about the status of the mitochondria-selective degradation pathway. Furthermore, these studies can be complemented with protein quantification and gene expression analysis.

4.9. Ultrastructural and morphological study

The detail needed to understand cellular processes depends on the type and aims of the studies.

However, one has to bear in mind that great resolution is commonly associated with high noise-to-signal ratios, which can mask results and hinder the advance of the study.

Mitochondrial morphology can be indicative of the status of this organelle and the cell's metabolism. For instance, defects mitochondrial fusion and fission machinery and even in the mtDNA copy number produce significant alterations in mitochondrial morphology mainly in terms of size and cristae organization.

Ultrastructural studies on LHON patients using ocular tissue confirmed optic nerve atrophy and some reported the observation of electron-dense, double-membrane-bound, calcium-rich inclusions (Kerrison *et al.*, 1995; Yu *et al.*, 2012). Still, a characteristic more defined cellular phenotype still remains to be determined.

In order to study the ultrastructure of cells bearing the m.11778G>A mutation, culture fibroblasts from controls, the patient and her mother were processed so that they could be analysed by transmission electron microscopy (Figure 23).

Since fibroblasts present long extensions, they are presented as thin sections upon the required preparation for the observation under the electron microscope.

A common feature observed in most of the samples is the presence of a great number of vesicles both intracellular and connected to the cell membrane, which is in accordance with the secreting role of these cells.

Mitochondrial morphology was well preserved in all samples, no paracristaline inclusions or pyrophosphate granules were observed, and mitochondrial cristae and both the OMM and the IMM could be easily identified. No changes in mitochondrial morphology were detected.

When analysing the patient's fibroblasts (Figure 23 C), it was common to find several multilamelar cisternae-like structures which may correspond to dictiosomes or smooth ER; however, the characteristic spatial organization of the cisternae and the presence of surrounding vesicles are strong indicatives of the former.

The sample of the proband's mother (Figure 23 D) presents an unusually low cytoplasmic density with disperse structures and further studies are needed.

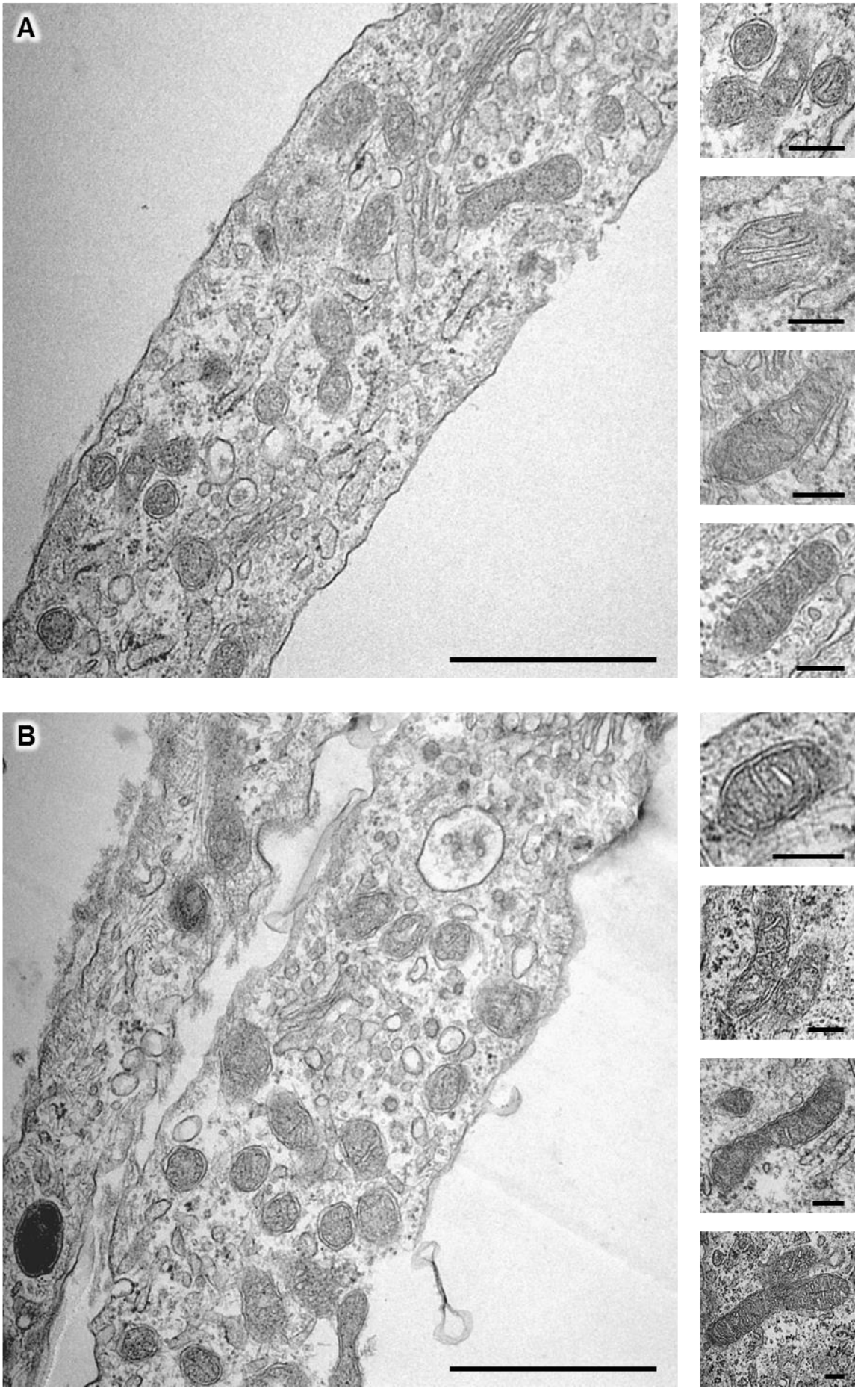
A
B

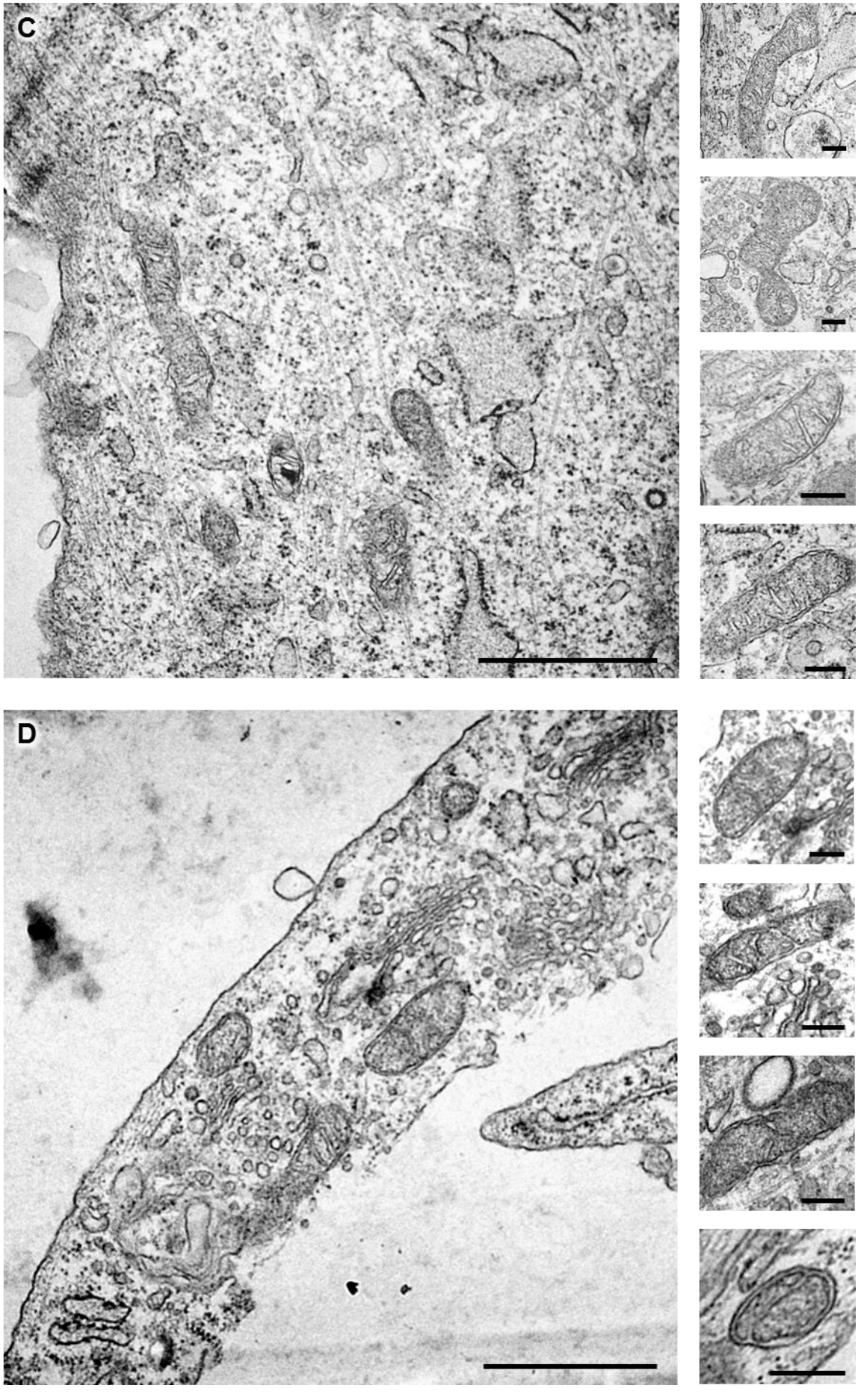
C
D

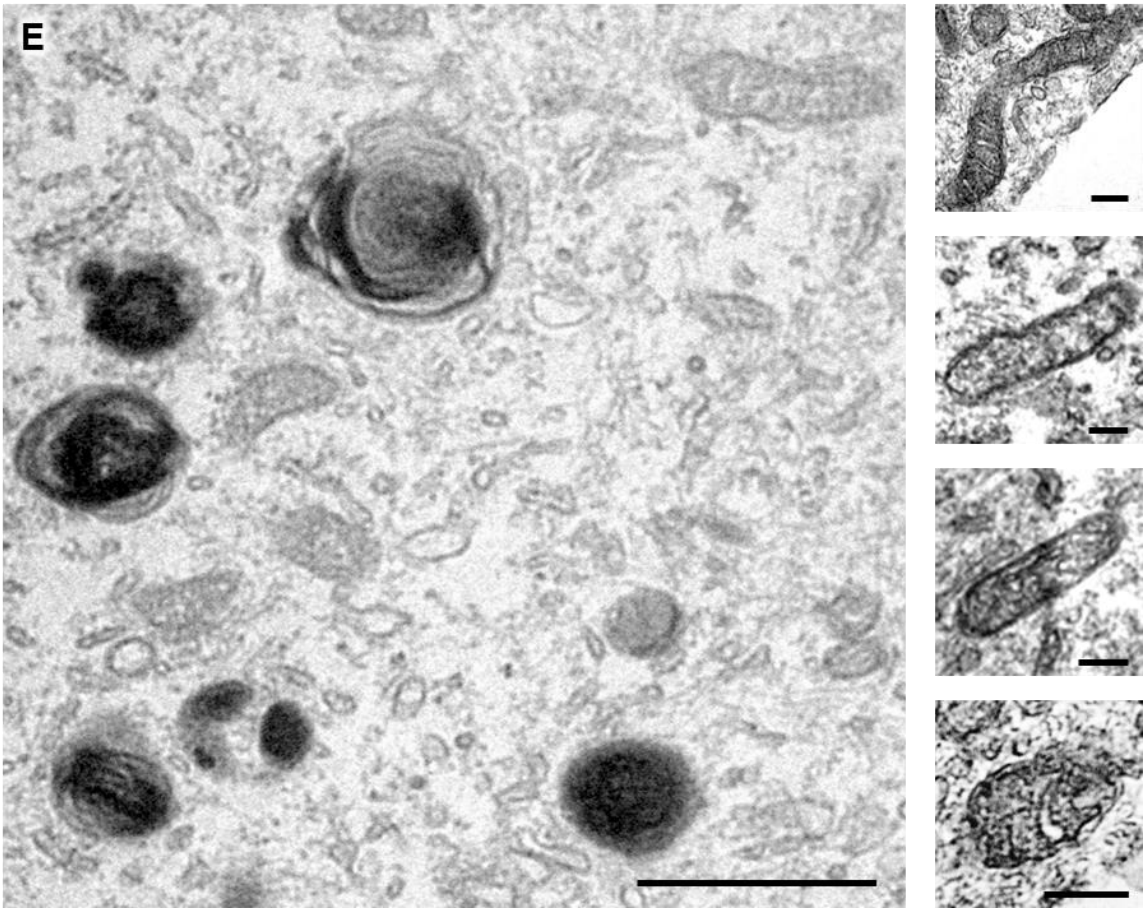

Figure 23 – Transmission electron microscopy morphological study of primary fibroblasts. Ultrastructural aspect of primary fibroblasts from (**A**) control 1, (**B**) control 2, (**C**) control 3, (**D**) patient-20yo and (**E**) patient's mother. Scale bar: 1 μm (left), 200 nm (right).

4.10. Morphological study of the Golgi apparatus

The processing of samples for electron microscopy involves steps that may produce artefacts. Since samples are analysed at high magnifications, the presence of artefacts is more notorious, which can impact negatively on the quality of the conclusions.

In order to confirm the findings observed in the patient's fibroblasts under the transmission electron microscope related to the Golgi apparatus morphology, primary fibroblasts were transfected with the YFP-PH fusion protein by an adenoviral vector and subjected to inspection by confocal live imaging (Figure 24).

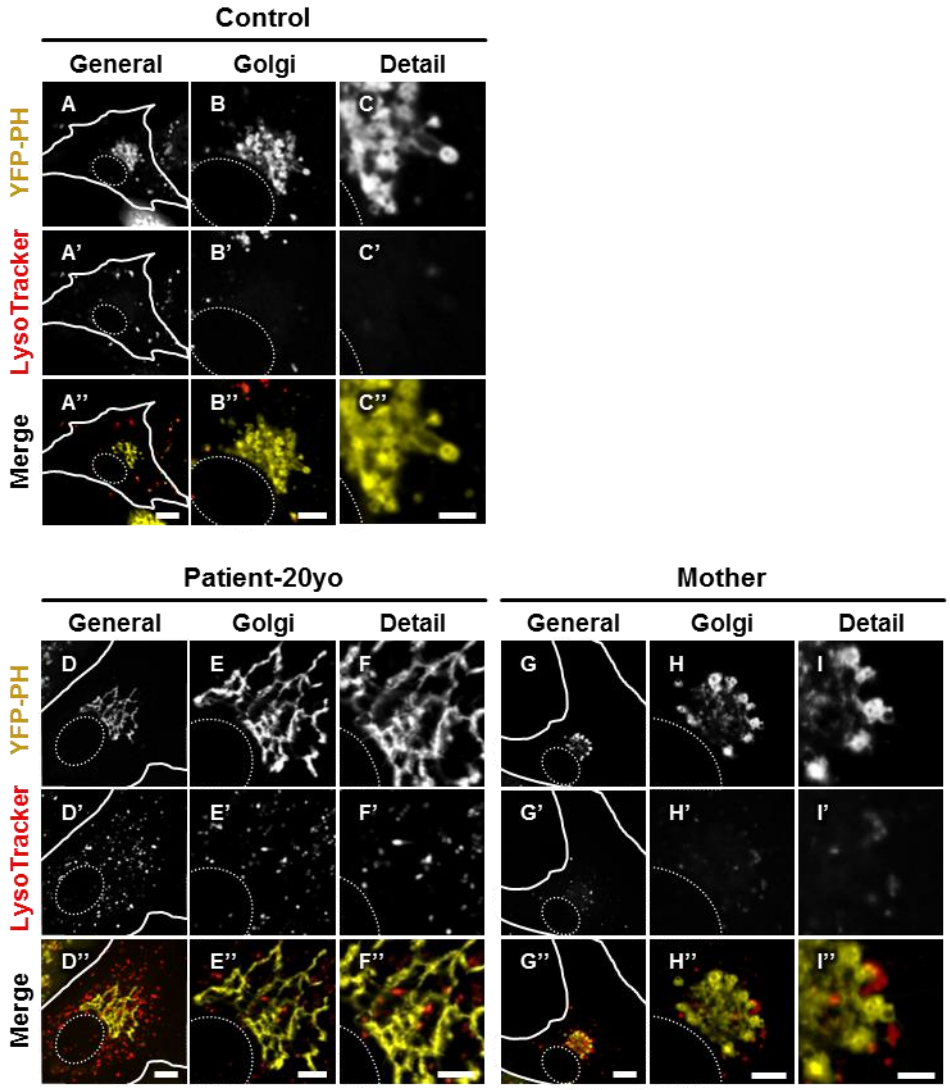

Figure 24 – Confocal microscopy images of the YFP-PH transfected primary fibroblasts. Control, patient and her mother's fibroblasts were transfected with the Golgi apparatus marker YFP-PH and stained with LysoTracker to locate acidic compartments. Images with diverse magnifications were collected in order to present the whole cell (general), the Golgi apparatus (Golgi) and details of the cisternae (detail). The cell limits are represented by full white contours and nuclei by dashed elipsoids. Scale bar: 10 μm (top row), 5 μm (middle row), 2.5 μm (bottom row).

The fusion protein used in this study is composed by a fluorescent moiety (YFP) and a PI(4)P-binding moiety (PH). Since PI(4)P is the main phosphoinositide in the Golgi apparatus, the fusion protein labels specifically this cellular structure, enabling its location as well as the study of its dynamics. The pH probe LysoTracker labels acidic compartments, including lysosomes.

Expression of the YFP-PH construct in control cells presented the Golgi apparatus as a perinuclear mass with foamy aspect due to vesicle traffic. The same aspect was obtained with fibroblasts of patient's mother. However, the patient's fibroblasts presented a distinct morphology of the Golgi apparatus, which was less condensed, despite preserving the perinuclear location. Furthermore, low YFP-positive vesicle-like structures were identified in the vicinity of the Golgi apparatus and the overall morphology of the organelle was also altered to a tubulated wide mesh (Figure 24 E).

Another unusual finding was observed when acquiring time lapse images of the same sample. Very thin YFP-positive strands were observed extending and retracting from the Golgi apparatus (Figure 25).

The nature of these projections remains to be clarified by posterior studies. However, the probable cause of this phenotype may be related with defects in the formation of vesicles from the Golgi apparatus (i.e. pinching off).

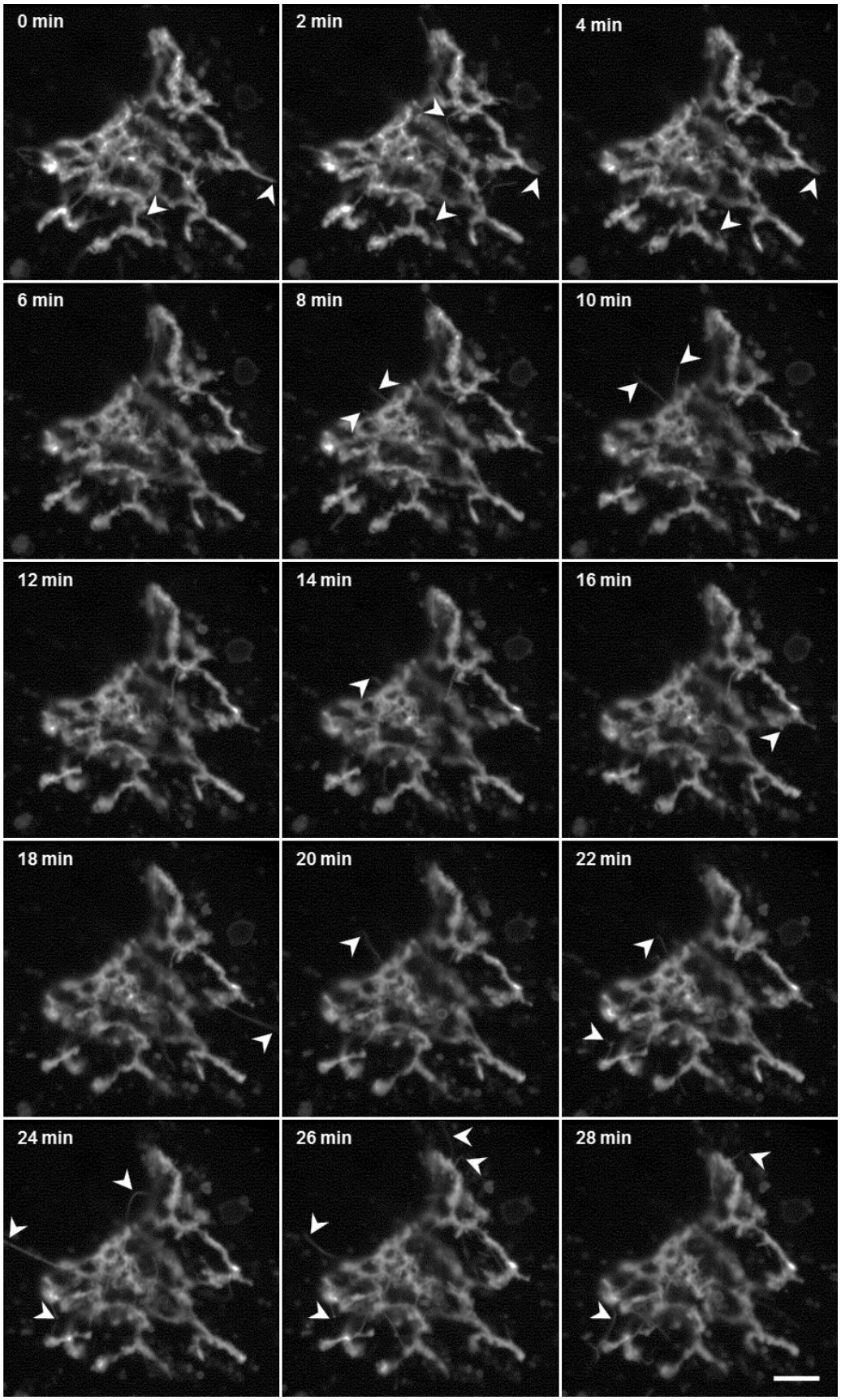

Figure 25 – Time lapse images of the YFP-PH transfected patient's primary fibroblasts. Images of the patient's fibroblasts (from the second harvest) were collected every 2 minutes and the YFP-PH signal is presented in grayscale. Arrowheads localize dynamic ends of projections from the Golgi apparatus. The nucleus is located in the top left corner of each image and its representation was omitted for the sake of image clarity. Scale bar: 5 μm.

CHAPTER 5

CONCLUSIVE REMARKS

5. CONCLUSIVE REMARKS

The herein presented study represents an advance in the understanding of mitochondrial cytopathies caused by alterations in the mitochondrial genome, although some data have to be considered as preliminary.

The use of *in silico* tools may contribute to the establishment of the pathogenic role of sequence variations but the critical analysis of their results is vital as well as complementation by functional studies.

This study presents aspects that may function as seeds for further research. For instance, the morphological changes observed in the Golgi apparatus can be studied using a more functional approach in order to determine the basis of the cross-talk between this organelle and mitochondria.

The existence of SNPs that can be synergistic by enhancing the defects caused by the currently accepted primary LHON mutations is not to be disregarded. Since the mitochondrially-encoded subunits of the MRC complexes present tight intra-complex interactions, the association of different alterations may produce effects that are, so far, unpredictable. Moreover, since MRC complexes interact with each other to form supercomplexes, there may be destabilizing effects arising from a point mutation.

Besides variations in the mitochondrial genome (including those which define the human haplogroups), when inspecting their effect on the cell homeostasis, the nuclear background is also to consider due to the intense cross-talk between these organelles. Furthermore, the effect of pharmacological treatments must also be considered in all the analysis performed since they have the potential to alter cellular processes which involve mitochondrial components.

The complex I subunit ND2 has been found in a complex with the Src kinase and the NMDA receptor at synaptic membranes in the brain (Bridges *et al.*, 2011). This information is of utmost importance since it opens new hypothesis such as mitochondrial export and moonlighting activity of mitochondrialy-encoded proteins. Since ND4 and ND2 share remarkable structural and functional similarity, the hypothesis of extramitochondrial roles of ND4 assumes an unexpected relevance not only in homeostasis but also in pathological contexts.

Further insights on the primary causes of LHON can be provided by analysis of a larger number of individuals. Also, a more powerful approach such as next generation sequencing can be useful in order to simultaneously detect candidates that may be related to the aetiology of LHON (Figure 26). This approach is being performed in the broader project in which the work of the present thesis is included (PTDC/DTP-EPI/0929/2012 - Translational Bigenomics Investigation in Leber´s Hereditary Optic Neuropathy: Genotype-Phenotype Correlation; PI - Professor Manuela Grazina).

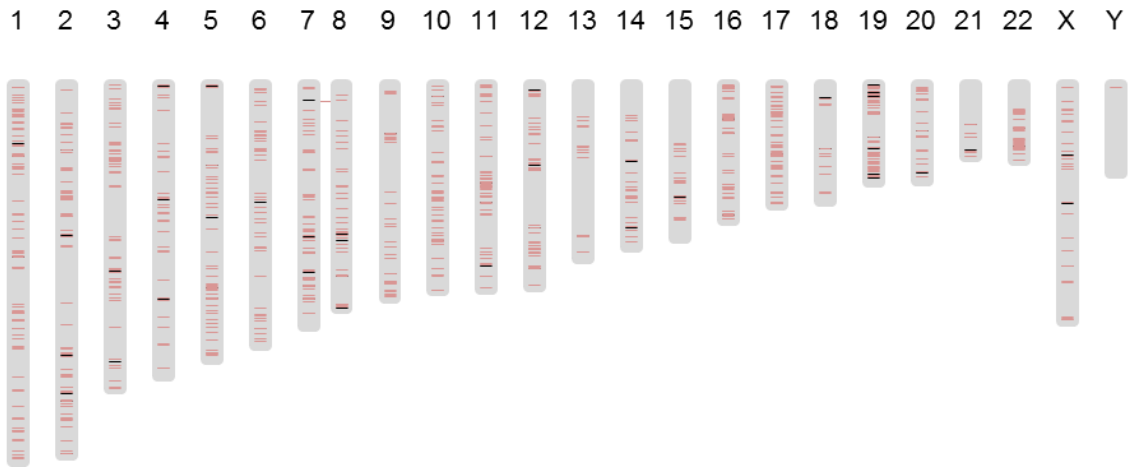

Figure 26 – Distribution of mitochondria-related genes in the *Homo sapiens* karyogram. Each chromosome is proportionally represented by a grey bar. Genes coding proteins that compose the MRC are coloured black and other mitochondria-related genes are coloured light red.

However, the major contributions which will provide invaluable help to decipher the role of alterations affecting complex I are those related to the clarification of its structure and the interactions between its subunits.

In conclusion, a special caution must be taken when analysing genetic data and defining the primary causes of diseases since the complex and intricate network of the cells' components produce phenotypes which are, to date, not fully understood.

CHAPTER 6

REFERENCES

6. REFERENCES

Abzhanov A, Protas M, Grant BR, Grant PR, Tabin CJ. Bmp4 and morphological variation of beaks in Darwin's finches. Science. 2004; 305(5689):1462-5.

Acín-Pérez R, Bayona-Bafaluy MP, Fernández-Silva P, Moreno-Loshuertos R, Pérez-Martos A, Bruno C, Moraes CT, Enríquez JA. Respiratory complex III is required to maintain complex I in mammalian mitochondria. Mol Cell. 2004; 13(6):805-15.

Adzhubei I, Jordan DM, Sunyaev SR. Predicting functional effect of human missense mutations using PolyPhen-2. Curr Protoc Hum Genet. 2013; Chapter 7:Unit7.20.

Adzhubei IA, Schmidt S, Peshkin L, Ramensky VE, Gerasimova A, Bork P, Kondrashov AS, Sunyaev SR. A method and server for predicting damaging missense mutations. Nat Methods. 2010; 7(4):248-9.

Aguer C, Gambarotta D, Mailloux RJ, Moffat C, Dent R, McPherson R, Harper ME. Galactose enhances oxidative metabolism and reveals mitochondrial dysfunction in human primary muscle cells. PLoS One. 2011; 6(12):e28536.

Arnold S, Kadenbach B. Cell respiration is controlled by ATP, an allosteric inhibitor of cytochrome-c oxidase. Eur J Biochem. 1997; 249(1):350-4.

Ashrafi and Schuarz. The pathways of mitophagy for quality control and clearance of mitochondria. Cell Death Differ. 2013; 20(1):31-42.

Baradaran R, Berrisford JM, Minhas GS, Sazanov LA. Crystal structure of the entire respiratory complex I. Nature. 2013; 494(7438):443-8.

Bernsel A, Viklund H, Hennerdal A, Elofsson A. TOPCONS: consensus prediction of membrane protein topology. Nucleic Acids Res. 2009; 37(Web Server issue):W465-8.

Bernstein FC, Koetzle TF, Williams GJ, Meyer EF Jr, Brice MD, Rodgers JR, Kennard O, Shimanouchi T, Tasumi M. J Mol Biol. 1977; 112(3):535-42.

Blakely EL, Mitchell AL, Fisher N, Meunier B, Nijtmans LG, Schaefer AM, Jackson MJ, Turnbull DM, Taylor RW. A mitochondrial cytochrome b mutation causing severe respiratory chain enzyme deficiency in humans and yeast. FEBS J. 2005; 272(14):3583-92.

Bradford MM. A rapid and sensitive method for the quantitation of microgram quantities of protein utilizing the principle of protein-dye binding. Anal Biochem. 1976; 72:248-54

Bridges HR, Birrell JA, Hirst J. The mitochondrial-encoded subunits of respiratory complex I (NADH:ubiquinone oxidoreductase): identifying residues important in mechanism and disease. Biochem Soc Trans. 2011; 39(3):799-806.

Calabrese R, Capriotti E, Fariselli P, Martelli PL, Casadio R. Functional annotations improve the predictive score of human disease-related mutations in proteins. Hum Mutat. 2009; 30(8):1237-44.

Calvo S, Jain M, Xie X, Sheth SA, Chang B, Goldberger OA, Spinazzola A, Zeviani M, Carr SA, Mootha VK. Systematic identification of human mitochondrial disease genes through integrative genomics. Nat Genet. 2006; 38(5):576-82.

Carelli V, Ross-Cisneros FN, Sadun AA. Optic nerve degeneration and mitochondrial dysfunction: genetic and acquired optic neuropathies. Neurochem Int. 2002; 40(6):573-84.

Carroll J, Fearnley IM, Shannon RJ, Hirst J, Walker JE. Analysis of the subunit composition of complex I from bovine heart mitochondria. Mol Cell Proteomics. 2003; 2(2):117-26.

Carroll J, Fearnley IM, Skehel JM, Shannon RJ, Hirst J, Walker JE. Bovine complex I is a complex of 45 different subunits. J Biol Chem. 2006; 281(43):32724-7.

Celniker G, Nimrod G, Ashkenazy H, Glaser F, Martz E, Mayrose I, Pupko T, Ben-Tal, N. ConSurf: Using Evolutionary Data to Raise Testable Hypotheses about Protein Function. Isr. J. Chem. Volume 53, Issue 3-4, pages 199–206, 2013.

Chance B, Williams GR. A method for the localization of sites for oxidative phosphorylation. Nature. 1955; 176(4475):250-4.

Choi Y, Sims GE, Murphy S, Miller JR, Chan AP. Predicting the functional effect of amino acid substitutions and indels. PLoS One. 2012; 7(10):e46688.

Clason T, Ruiz T, Schägger H, Peng G, Zickermann V, Brandt U, Michel H, Radermacher M. The structure of eukaryotic and prokaryotic complex I. J Struct Biol. 2010; 169(1):81-8.

Cleeter MW, Banister SH, Ragan CI. Chemical cross-linking of mitochondrial NADH dehydrogenase from bovine heart. Biochem J. 1985; 227(2):467-74.

Cserzö M, Wallin E, Simon I, von Heijne G, Elofsson A. Prediction of transmembrane alpha-helices in prokaryotic membrane proteins: the dense alignment surface method. Protein Eng. 1997; 10(6):673-6.

Darwin C. (1988) The Voyage of the Beagle. New York: New American Library.
Deléage G, Roux B. An algorithm for protein secondary structure prediction based on class prediction. Protein Eng. 1987; 1(4):289-94.
Diaz F, Fukui H, Garcia S, Moraes CT. Cytochrome c oxidase is required for the assembly/stability of respiratory complex I in mouse fibroblasts Mol Cell Biol. 2006; 26(13):4872-81.
Dieteren CE, Koopman WJ, Swarts HG, Peters JG, Maczuga P, van Gemst JJ, Masereeuw R, Smeitink JA, Nijtmans LG, Willems PH. Subunit-specific incorporation efficiency and kinetics in mitochondrial complex I homeostasis. J Biol Chem. 2012; 287(50):41851-60.
Dimmock D, Tang LY, Schmitt ES, Wong LJ. Quantitative evaluation of the mitochondrial DNA depletion syndrome. Clin Chem. 2010; 56(7):1119-27.
Dodson M, Darley-Usmar V, Zhang J. Cellular metabolic and autophagic pathways: traffic control by redox signaling. Free Radic Biol Med. 2013; 63:207-21.
Efremov RG, Baradaran R, Sazanov LA. The architecture of respiratory complex I. Nature. 2010; 465(7297):441-5.
Efremov RG, Sazanov LA. Structure of the membrane domain of respiratory complex I. Nature. 2011; 476(7361):414-20.
Fader, C. M.; Colombo, M. I. Autophagy and multivesicular bodies: two closely related partners. Cell Death Differ. 2009; 16(1):70-8.
Fearnley IM, Carroll J, Shannon RJ, Runswick MJ, Walker JE, Hirst J. GRIM-19, a cell death regulatory gene product, is a subunit of bovine mitochondrial NADH:ubiquinone oxidoreductase (complex I). J Biol Chem. 2001; 276(42):38345-8.
Frishman D, Argos P. Incorporation of non-local interactions in protein secondary structure prediction from the amino acid sequence. Protein Eng. 1996; 9(2):133-42.
Garnier J, Gibrat JF, Robson B. GOR method for predicting protein secondary structure from amino acid sequence. Methods Enzymol. 1996; 266:540-53.
Garnier J, Osguthorpe DJ, Robson B. Analysis of the accuracy and implications of simple methods for predicting the secondary structure of globular proteins. J Mol Biol. 1978; 120(1):97-120.
Geourjon C, Deléage G. SOPM: a self-optimized method for protein secondary structure prediction. Protein Eng. 1994; 7(2):157-64.
Geourjon C, Deléage G. SOPMA: significant improvements in protein secondary structure prediction by consensus prediction from multiple alignments. Comput Appl Biosci. 1995; 11(6):681-4.
Gibrat JF, Garnier J, Robson B. Further developments of protein secondary structure prediction using information theory. New parameters and consideration of residue pairs. J Mol Biol. 1987; 198(3):425-43.
Gilkerson RW, Selker JM, Capaldi RA. The cristal membrane of mitochondria is the principal site of oxidative phosphorylation. FEBS Lett. 2003; 546(2-3):355-8.
Giordano C, Iommarini L, Giordano L, Maresca A, Pisano A, Valentino ML, Caporali L, Liguori R, Deceglie S, Roberti M, Fanelli F, Fracasso F, Ross-Cisneros FN, D'Adamo P, Hudson G, Pyle A, Yu-Wai-Man P, Chinnery PF, Zeviani M, Salomao SR, Berezovsky A, Belfort R Jr, Ventura DF, Moraes M, Moraes Filho M, Barboni P, Sadun F, De Negri A, Sadun AA, Tancredi A, Mancini M, d'Amati G, Loguercio Polosa P, Cantatore P, Carelli V. Efficient mitochondrial biogenesis drives incomplete penetrance in Leber's hereditary optic neuropathy. Brain. 2014; 137(Pt 2):335-53.
Grantham, R. Amino acid difference formula to help explain protein evolution. Science 1974; 185(4154), 862-4.
Grazina MM (2012). Mitochondrial Respiratory Chain: Biochemical analysis and criterion for deficiency in diagnosis. Methods Mol Biol, 837:73-91.
Grazina MM, Diogo LM, Garcia PC, Silva ED, Garcia TD, Robalo CB, Oliveira CR. Atypical presentation of Leber's hereditary optic neuropathy associated to mtDNA 11778G>A point mutation – A case report. Eur J Paediatr Neurol. 2007; 11(2):115-8.
Guermeur Y, Geourjon C, Gallinari P, Deléage G. Improved performance in protein secondary structure prediction by inhomogeneous score combination. Bioinformatics. 1999; 15(5):413-21.
Hackenbrock CR, Chazotte B, Gupte SS. The random collision model and a critical assessment of diffusion and collision in mitochondrial electron transport. J Bioenerg Biomembr. 1986; 18(5):331-68.
Haines TH, Dencher NA. Cardiolipin: a proton trap for oxidative phosphorylation. FEBS Lett. 2002; 528(1-3):35-9.
Hirokawa T, Boon-Chieng S, Mitaku S. SOSUI: classification and secondary structure prediction system for membrane proteins. Bioinformatics. 1998; 14(4):378-9.
Hirst J, Carroll J, Fearnley IM, Shannon RJ, Walker JE. The nuclear encoded subunits of complex I from bovine heart mitochondria. Biochim Biophys Acta. 2003; 1604(3):135-50.

Hoepken HH, Gispert S, Morales B, Wingerter O, Del Turco D, Mülsch A, Nussbaum RL, Müller K, Dröse S, Brandt U, Deller T, Wirth B, Kudin AP, Kunz WS, Auburger G. Mitochondrial dysfunction, peroxidation damage and changes in glutathione metabolism in PARK6. Neurobiol Dis. 2007; 25(2):401-11.

Hofmann S, Bauer MF. Mitochondrial Disorders. eLS. 2006.

Huang X, Holden HM, Raushel FM. Channeling of substrates and intermediates in enzyme-catalyzed reactions. Annu Rev Biochem. 2001; 70:149-80.

Ingman M, Gyllensten U. mtDB: Human Mitochondrial Genome Database, a resource for population genetics and medical sciences. Nucleic Acids Res. 2006; 34(Database issue):D749-51.

Iverson TM1, Maklashina E, Cecchini G. Structural basis for malfunction in complex II. J Biol Chem. 2012; 287(42):35430-8.

Jonckheere AI, Smeitink JA, Rodenburg RJ. Mitochondrial ATP synthase: architecture, function and pathology. J Inherit Metab Dis. 2012; 35(2):211-25.

Jones DT. Protein secondary structure prediction based on position-specific scoring matrices. J Mol Biol. 1999; 292(2):195-202.

Juretić D, Zoranić L, Zucić D. Basic charge clusters and predictions of membrane protein topology. J Chem Inf Comput Sci. 2002; 42(3):620-32.

Kahsay RY, Gao G, Liao L. An improved hidden Markov model for transmembrane protein detection and topology prediction and its applications to complete genomes. Bioinformatics. 2005; 21(9):1853-8.

Käll L, Krogh A, Sonnhammer EL. A combined transmembrane topology and signal peptide prediction method. J Mol Biol. 2004; 338(5):1027-36.

Kanehisa M, Goto S, Sato Y, Kawashima M, Furumichi M, Tanabe M. Data, information, knowledge and principle: back to metabolism in KEGG. Nucleic Acids Res. 2014; 42(Database issue):D199-205.

Kerrison JB, Howell N, Miller NR, Hirst L, Green WR. Leber hereditary optic neuropathy. Electron microscopy and molecular genetic analysis of a case. Ophthalmology. 1995; 102(10):1509-16.

King RD, Sternberg MJ. Identification and application of the concepts important for accurate and reliable protein secondary structure prediction. Protein Sci. 1996; 5(11):2298-310.

Klionsky, D. J. and Deretic, V. Autophagy: molecular mechanisms and disease outcomes Nature Reviews Molecular Cell Biology. 2010. http://www.nature.com/nrm/posters/autophagy

Koh H, Chung J. PINK1 as a molecular checkpoint in the maintenance of mitochondrial function and integrity. Mol Cells. 2012; 34(1):7-13.

Laemmli UK. Cleavage of structural proteins during the assembly of the head of bacteriophage T4. Nature. 1970; 227(5259):680-5.

Larkin MA, Blackshields G, Brown NP, Chenna R, McGettigan PA, McWilliam H, Valentin F, Wallace IM, Wilm A, Lopez R, Thompson JD, Gibson TJ, Higgins DG. Clustal W and Clustal X version 2.0. Bioinformatics. 2007; 23(21):2947-8.

Lenaz G, Baracca A, Barbero G, Bergamini C, Dalmonte ME, Del Sole M, Faccioli M, Falasca A, Fato R, Genova ML, Sgarbi G, Solaini G. Mitochondrial respiratory chain super-complex I-III in physiology and pathology. Biochim Biophys Acta. 2010; 1797(6-7):633-40.

Lenaz G, Genova ML. Kinetics of integrated electron transfer in the mitochondrial respiratory chain: random collisions vs. solid state electron channeling. Am J Physiol Cell Physiol. 2007; 292(4):C1221-39.

Levin JM. Exploring the limits of nearest neighbour secondary structure prediction. Protein Eng. 1997; 10(7):771-6.

Li B, Krishnan VG, Mort ME, Xin F, Kamati KK, Cooper DN, Mooney SD, Radivojac P. Automated inference of molecular mechanisms of disease from amino acid substitutions. Bioinformatics. 2009; 25(21):2744-50.

Lin K, Simossis VA, Taylor WR, Heringa J. A simple and fast secondary structure prediction method using hidden neural networks. Bioinformatics. 2005; 21(2):152-9.

Lloyd RE, McGeehan JE. Structural analysis of mitochondrial mutations reveals a role for bigenomic protein interactions in human disease. PLoS One. 2013; 8(7):e69003.

Lodish H, Berk A, Matsudaira P, Kaiser C, Krieger M, Scott M, Zipursky SL, Darnell J. (2003). Molecular Cell Biology (5th ed.), pp. 163-165. New York: W.H. Freeman and Company.

Majander A, Huoponen K, Savontaus ML, Nikoskelainen E, Wikström M. Electron transfer properties of NADH:ubiquinone reductase in the ND1/3460 and the ND4/11778 mutations of the Leber hereditary optic neuroretinopathy (LHON). FEBS Lett. 1991; 292(1-2):289-92.

Mannella CA. The relevance of mitochondrial membrane topology to mitochondrial function. Biochim Biophys Acta. 2006; 1762(2):140-7.

McKenzie M, Lazarou M, Thorburn DR, Ryan MT. Mitochondrial respiratory chain supercomplexes are destabilized in Barth Syndrome patients. J Mol Biol. 2006; 361(3):462-9.
Miles EW, Rhee S, Davies DR. The molecular basis of substrate channeling. J Biol Chem. 1999; 274(18):12193-6.
Mitchell P. Chemiosmotic coupling in oxidative and photosynthetic phosphorylation. 1966. Biochim Biophys Acta. 2011; 1807(12):1507-38. doi: 10.1016/j.bbabio.2011.09.018.
MITOMAP: A Human Mitochondrial Genome Database. http://www.mitomap.org, 2013.
Moore D, Strauss WM, Richards E, Reichardt M, Rogers S, Willson K, Fineey M, Chory J, Ribaudo RK, Baldwin Jr AS, Brown T, Ellington A, Green R, Richards EJ, Budelier K, Schorr J. Preparation and Analysis of DNA. in: Current Protocols inn Molecular Biology. Ausubel FM, Brent R, Kingston RE, Moore DD, Seidman JG, Smith JA, Struhl K (eds), John Wiley & Sons, 1997, Chapter 2: pp 2.0.1-2.14.8.
Napiwotzki J, Kadenbach B. Extramitochondrial ATP/ADP-ratios regulate cytochrome c oxidase activity via binding to the cytosolic domain of subunit IV. Biol Chem. 1998 Mar; 379(3):335-9.
Nass MM, Nass S. Intramitochondrial fibers with DNA characteristics. I. Fixation and electron staining reactions. J Cell Biol. 1963; 19:593-611.
Nass S, Nass MM. Intramitochondrial fibers with DNA characteristics. II. Enzymatic and other hydrolytic treatments. J Cell Biol. 1963; 19:613-29.
Nelson DL, Cox. (2008) Lehninger Principles of Biochemistry (5th ed.), pp. 1100-1109. New York: W.H. Freeman and Company.
Ng PC, Henikoff S. SIFT: Predicting amino acid changes that affect protein function. Nucleic Acids Res. 2003; 31(13):3812-4.
Nikoskelainen EK, Savontaus ML, Huoponen K, Antila K, Hartiala J. Pre-excitation syndrome in Leber's hereditary optic neuropathy. Lancet. 1994; 344(8926):857-8.
Noda NN, Fujioka Y, Hanada T, Ohsumi Y, Inagaki F. Structure of the Atg12-Atg5 conjugate reveals a platform for stimulating Atg8-PE conjugation. EMBO Rep. 2013; 14(2):206-11.
Notredame C, Higgins DG, Heringa J. T-Coffee: A novel method for fast and accurate multiple sequence alignment. J Mol Biol. 2000; 302(1):205-17.
Pagliarini DJ, Calvo SE, Chang B, Sheth SA, Vafai SB, Ong SE, Walford GA, Sugiana C, Boneh A, Chen WK, Hill DE, Vidal M, Evans JG, Thorburn DR, Carr SA, Mootha VK. A mitochondrial protein compendium elucidates complex I disease biology. Cell. 2008; 134(1):112-23.
Pagliarini DJ, Dixon JE. Mitochondrial modulation: reversible phosphorylation takes center stage? Trends Biochem Sci. 2006; 31(1):26-34.
Patel SD, Cleeter MW, Ragan CI. Transmembrane organization of mitochondrial NADH dehydrogenase as revealed by radiochemical labelling and cross-linking. Biochem J. 1988; 256(2):529-35.
Patel SD, Ragan CI. Structural studies on mitochondrial NADH dehydrogenase using chemical cross-linking. Biochem J. 1988; 256(2):521-8.
Pfeiffer K, Gohil V, Stuart RA, Hunte C, Brandt U, Greenberg ML, Schägger H. Cardiolipin stabilizes respiratory chain supercomplexes. J Biol Chem. 2003; 278(52):52873-80.
Phasukkijwatana N, Kunhapan B, Stankovich J, Chuenkongkaew WL, Thomson R, Thornton T, Bahlo M, Mushiroda T, Nakamura Y, Mahasirimongkol S, Tun AW, Srisawat C, Limwongse C, Peerapittayamongkol C, Sura T, Suthammarak W, Lertrit P. Genome-wide linkage scan and association study of PARL to the expression of LHON families in Thailand. Hum Genet. 2010; 128(1):39-49.
Preston CC, Oberlin AS, Holmuhamedov EL, Gupta A, Sagar S, Syed RH, Siddiqui SA, Raghavakaimal S, Terzic A, Jahangir A. Aging-induced alterations in gene transcripts and functional activity of mitochondrial oxidative phosphorylation complexes in the heart. Mech Ageing Dev. 2008; 129(6):304-12.
Ramensky V, Bork P, Sunyaev S. Human non-synonymous SNPs: server and survey. Nucleic Acids Res. 2002; 30(17):3894-900.
Randow F, Youle RJ. Self and Nonself: How Autophagy Targets Mitochondria and Bacteria. Cell Host Microbe. 2014; 15(4):403-411.
Rellos P, Pike AC, Niesen FH, Salah E, Lee WH, von Delft F, Knapp S. Structure of the CaMKIIdelta/calmodulin complex reveals the molecular mechanism of CaMKII kinase activation. PLoS Biol. 2010; 8(7):e1000426.
Reva B, Antipin Y, Sander C. Predicting the functional impact of protein mutations: application to cancer genomics. Nucleic Acids Res. 2011; 39(17):e118.
Riley BE, Lougheed JC, Callaway K, Velasquez M, Brecht E, Nguyen L, Shaler T, Walker D, Yang Y, Regnstrom K, Diep L, Zhang Z, Chiou S, Bova M, Artis DR, Yao N, Baker J, Yednock T, Johnston

JA. Structure and function of Parkin E3 ubiquitin ligase reveals aspects of RING and HECT ligases. Nat Commun. 2013; 4:1982.
Rost B, Sander C. Improved prediction of protein secondary structure by use of sequence profiles and neural networks. Proc Natl Acad Sci U S A. 1993; 90(16):7558-62.
Roy A, Kucukural A, Zhang Y. I-TASSER: a unified platform for automated protein structure and function prediction. Nat Protoc. 2010; 5(4):725-38.
Ryan MT, Hoogenraad NJ. Mitochondrial-nuclear communications. Annu Rev Biochem. 2007; 76:701-22.
Sagan L. On the origin of mitosing cells. J Theor Biol. 1967; 14(3):255-74.
Sambrook J, Fritch EF, Maniatis T. Isolation of High Molecular Weight DNA from Mammalian Cells. in: Molecular Cloning – A Laboratory Manual. Irwin N, Ford N, Ferguson M, Ockler M (eds), 2nd edition, New York, Cold Spring Harbor Laboratory Press, 1987, Chapter 9: pp 9.14-9.22.
Schägger H, Pfeiffer K. The ratio of oxidative phosphorylation complexes I-V in bovine heart mitochondria and the composition of respiratory chain supercomplexes. J Biol Chem. 2001; 276(41):37861-7.
Schägger H. Tricine-SDS-PAGE. Nat Protoc. 2006; 1(1):16-22.
Schaller A, Hahn D, Jackson CB, Kern I, Chardot C, Belli DC, Gallati S, Nuoffer JM. Molecular and biochemical characterisation of a novel mutation in POLG associated with Alpers syndrome. BMC Neurol. 2011; 11:4.
Sievers F, Wilm A, Dineen D, Gibson TJ, Karplus K, Li W, Lopez R, McWilliam H, Remmert M, Söding J, Thompson JD, Higgins DG. Fast, scalable generation of high-quality protein multiple sequence alignments using Clustal Omega. Mol Syst Biol. 2011; 7:539.
Sparks CA, Guertin DA. Targeting mTOR: prospects for mTOR complex 2 inhibitors in cancer therapy. Oncogene. 2010; 29(26):3733-44.
Th. Leber. Ueber hereditäre und congenital-angelegte Sehnervenleiden. Albrecht von Graefes Archiv für Ophthalmologie 1871, Volume 17, Issue 2, pp 249-291.
Thomas PD, Campbell MJ, Kejariwal A, Mi H, Karlak B, Daverman R, Diemer K, Muruganujan A, Narechania A. PANTHER: a library of protein families and subfamilies indexed by function. Genome Res. 2003; 13(9):2129-41.
Tomoike F, Wakamatsu T, Nakagawa N, Kuramitsu S, Masui R. Crystal structure of the conserved hypothetical protein TTHA1606 from Thermus thermophilus HB8. Proteins. 2009; 76(1):244-8.
Trempe JF, Fon EA. Structure and Function of Parkin, PINK1, and DJ-1, the Three Musketeers of Neuroprotection. Front Neurol. 2013; 4:38.
Trounce, I.A., Kim, Y.L., Jun, A.S. and Wallace, D.C. (1996) Assessment of mitochondrial oxidative phosphorylation in patient muscle biopsies, lymphoblasts, and transmitochondrial cell lines. Methods Enzymol., 264, 484–509.
Tusnády GE, Simon I. The HMMTOP transmembrane topology prediction server. Bioinformatics. 2001; 17(9):849-50.
Ugalde C, Vogel R, Huijbens R, Van Den Heuvel B, Smeitink J, Nijtmans L. Human mitochondrial complex I assembles through the combination of evolutionary conserved modules: a framework to interpret complex I deficiencies. Hum Mol Genet. 2004; 13(20):2461-72.
UniProt Consortium. Activities at the Universal Protein Resource (UniProt). Nucleic Acids Res. 2014; 42(Database issue):D191-8.
Venegas V, Wang J, Dimmock D, Wong LJ. Real-time quantitative PCR analysis of mitochondrial DNA content. Curr Protoc Hum Genet. 2011; Chapter 19:Unit 19.7.
Vieira OV, Verkade P, Manninen A, Simons K. FAPP2 is involved in the transport of apical cargo in polarized MDCK cells. J Cell Biol. 2005; 170(4):521-6.
Viklund H, Bernsel A, Skwark M, Elofsson A. SPOCTOPUS: a combined predictor of signal peptides and membrane protein topology. Bioinformatics. 2008; 24(24):2928-9.
Voet D, Voet JG. (2011) Biochemistry (4th ed.). Massachusetts: John Wiley & Sons.
Wauer T, Komander D. Structure of the human Parkin ligase domain in an autoinhibited state. EMBO J. 2013; 32(15):2099-112.
Wauer T, Komander D. Structure of the human Parkin ligase domain in an autoinhibited state. EMBO J. 2013; 32(15):2099-112.
Wilkinson, K. D. Regulation of ubiquitin-dependent processes by deubiquitinating enzymes. FASEB J 1997; 11(14); 1245-1256.
Wittig I, Beckhaus T, Wumaier Z, Karas M, Schägger H. Mass estimation of native proteins by blue native electrophoresis: principles and practical hints. Mol Cell Proteomics. 2010; 9(10):2149-61.
Wittig I, Braun HP, Schägger H. Blue native PAGE. Nat Protoc. 2006; 1(1):418-28.

Wittig I, Karas M, Schägger H. High resolution clear native electrophoresis for in-gel functional assays and fluorescence studies of membrane protein complexes. Mol Cell Proteomics. 2007; 6(7):1215-25.

Wu Z, Sawada T, Shiba K, Liu S, Kanao T, Takahashi R, Hattori N, Imai Y, Lu B. Tricornered/NDR kinase signaling mediates PINK1-directed mitochondrial quality control and tissue maintenance. Genes Dev. 2013; 27(2):157-62.

Yano T, Chu SS, Sled' VD, Ohnishi T, Yagi T. The proton-translocating NADH-quinone oxidoreductase (NDH-1) of thermophilic bacterium Thermus thermophilus HB-8. Complete DNA sequence of the gene cluster and thermostable properties of the expressed NQO2 subunit. J Biol Chem. 1997; 272(7):4201-11.

Yu H, Ozdemir SS, Koilkonda RD, Chou TH, Porciatti V, Chiodo V, Boye SL, Hauswirth WW, Lewin AS, Guy J. Mutant NADH dehydrogenase subunit 4 gene delivery to mitochondria by targeting sequence-modified adeno-associated virus induces visual loss and optic atrophy in mice. Mol Vis. 2012; 18:1668-83.

Zoncu R, Efeyan A, Sabatini DM. mTOR: from growth signal integration to cancer, diabetes and ageing. Nat Rev Mol Cell Biol. 2011; 12(1):21-35.